HELSINGIN YLIOPISTO
HELSINGFORS UNIVERSITET
UNIVERSITY OF HELSINKI

Pro gradu -tutkielma
Geologia
Kallioperä- ja taloudellisen geologian linja

The Kuohatti mafic layered intrusion, it petrology structure and petrogenesis

Joona Sorsa

2017

Ohjaaja(t):
Tapani Rämö ja Tapio Halkoaho

HELSINGIN YLIOPISTO
MATEMAATTIS-LUONNONTIETEELLINEN TIEDEKUNTA
GEOTIETEIDEN JA MAANTIETEEN LAITOS
MAANTIEDE

PL 64 (Gustaf Hällströmin katu 2)
00014 Helsingin yliopisto

Tiedekunta/Osasto Fakultet/Sektion – Faculty	Laitos/Institution– Department
Matemaattis- luonnontieteellinen tiedekunta	Geotieteiden ja maantieteen laitos

Tekijä/Författare – Author

Joona Antton Sorsa

Työn nimi / Arbetets titel – Title

Kuohattijärven mafisen kerrosintruusion petrologia, rakenne ja petrogenesis

Oppiaine /Läroämne – Subject

Geologia

Työn laji/Arbetets art – Level	Aika/Datum – Month and year	Sivumäärä/ Sidoantal – Number of pages
Pro gradu -tutkielma	20.05.2017	111

Tiivistelmä/Referat – Abstract

Kuohattijärven mafinen kerrosintruusio sijaitsee 150 kilometriä Nurmeksesta koilliseen. Se kuuluu Geologian tutkimuskeskuksen kallioperäkartoituksissa määriteltyyn Kuohattijärven seurueeseen. Tämä 100 m x 2 km kerrosintruusio havaittiin ensimmäisen kerran Kuohattijärven ja sen ympäristön kallioperägeologisessa kartoituksessa. Nykyisellä eroosiopinnalla havaitut plagioklaasihajarakeiden täyttämät gabrot ja nykyään talkki-kloriitti -pitoisiksi liuskeiksi muuttuneet mafiset kivet herättivät jatkotutkimuksia, joiden pohjalta myös tämä työ on laadittu. Koko intruusion alueella havaittavat plagioklaasihajarakeet kertovat todennäköisesti niiden adkumulaatiosta ja magmojen differentiaatiosta. Metamorfoituneet mafiset kivet puolestaan ovat jäänteitä intruusion peridotiittisesta pohjasta. Intruusio on jaettu useaan kerrokseen, mafisen pohjan, gabroidisten kivien ja plagioklaasihajarakeista rikkaiden gabrojen (leukokraattiset gabrot) mukaan. Intruusio on kauttaaltaan jyrkässä kulmassa (70-90°), mikä on seurausta alueen granuliittifasieksen metamorfoosista. Intruusiota myös leikkaavat useat diabaasijuonet. Kokokivikoostumus antaa viitteitä mahdollisesta anortiittirikkaiden plagioklaasikiteiden ($An_{80–90}$) vajoamisesta intruusion pohjalle, samalla kun kevyemmät ja huomattavasti anortiitista köyhemmät ($An_{40–70}$) kiteet kohosivat ylös kohti kehittyvää gabroidista sulaa. Intruusion sivukivestä ja leukokraattisesta gabrosta analysoitiin U-Pb isotooppeja useista zirkonikiteistä ja näiden pohjalta lasketut kiteytymisiät ovat väliltä 2,72–2,88 mrd. v.. Talkki-kloriitti liuskeesta analysoidut monatsiittien U-Pb isotooppikoostumukset jakautuvat kolmelle selkeälle aikajaksolle: 2,68, 2,42 ja 1,90 mrd. v., mikä sopii yhteen alueen metamorfisten tapahtumien ja sieltä analysoitujen diabaasijuonien kanssa. Analysoidut kiteet ovat tekstuuristaan päätellen perittyjä ja kertovat intruusiota ympäröivien kivien vaiheista. Tarkkaa kerrosintruusion kiteytymisajankohtaa ei saatavilla olevan isotooppiaineiston pohjalta ole mahdollista määrittää, mutta todennäköisesti kiteytymisajankohta on välillä 1.9–2.41 mrd. v.. Alueelta on aikaisemmin tutkittu useita Proterotsooisia kerrosintruusioita, mikä viittaa sivukivistä saatujen tulosten yhteydessä siihen että Kuohatin mafinen kerrosintruusio on todennäköisesti iältään Proterotsooinen, eikä Arkeeinen kuten alun perin ajateltiin. Intruusio on tällä hetkellä asettunut biotiittiparagneissin ja Arkeeisen tonaliitin väliin ja jos intruusio on iältään Proterotsooinen, sen on täytynyt kiilautua näiden väliin.

Avainsanat – Nyckelord – Keywords

Kuohattijärvi, mafinen, kerrosintruusio, plagioklaasihajarakeet, Kuohatti

Säilytyspaikka – Förvaringställe – Where deposited

Muita tietoja – Övriga uppgifter – Additional information

Tiedekunta/Osasto Fakultet/Sektion – Faculty	Laitos/Institution– Department
Faculty of Science	Department of Geosciences and Geography

Tekijä/Författare – Author

Joona Antton Sorsa

Työn nimi / Arbetets titel – Title

The Kuohatti mafic layered intrusion, its petrology, structure and petrogenesis

Oppiaine /Läroämne – Subject

Geology

Työn laji/Arbetets art – Level	Aika/Datum – Month and year	Sivumäärä/ Sidoantal – Number of pages
Master's Thesis	20.05.2017	111

Tiivistelmä/Referat – Abstract

The Kuohatti mafic layered intrusion is located 150 kilometers northeast from the city of Nurmes. It is a part of the Kuohattijärvi suite determined earlier by the Geological Survey of Finland. The 100 meters wide and 2 kilometers long intrusion was found during the bedrock mapping related to Kuohattijärvi and its surrounding areas. Gabbros with abundant plagioclase phenocrysts and metamorphosed mafic rocks, now seen as talc-chlorite schists on the current erosion level led to this study. The plagioclase phenocrysts are visible throughout the whole intrusion and are signals of plagioclase floating - a typical feature in layered intrusions caused my magmatic differentiation. The metamorphosed mafic rocks are remnants of the peridotitic bottom of the intrusion. The intrusion is divided into multiple layers, a mafic bottom, anorthosites, gabbroic rocks and plagioclase phenocryst –rich gabbros, here abbreviated as leucocratic gabbros. The intrusion is currently thoroughly tilted 70–90 degrees, cut by diabase dykes and metamorphosed in the granulite facies. Rock compositions suggest that during the formation of the mafic bottom and the gabbroic rocks, some amounts of calcic plagioclase (An_{80-90}) crystals subsided to the lower parts of the intrusion, whereas lighter and notably less calcic (An_{40-70}) crystals floated upwards into the evolving gabbroic melt. Zircons from a country-rock (talc-chlorite schist) and a leucocratic gabbro from intrusion were analyzed for U-Pb isotopes. All these yield U-Pb age groups at ca. 2.72 Ga and 2.88 Ga. Monazite grains show three distinctive age groups at 2.68 Ga, 2.42 Ga and 1.90 Ga, indicating strong correlation with the formation of the diabase dykes and metamorphic events in the area. The analyses are likely from an inherited source, indicating the actual age of the surroundings. The exact crystallization age of the intrusion is possibly between 2.4 and 1.9 Ga. This would correlate with the Proterozoic layered intrusions surrounding the area and suggest that the Kuohatti layered intrusion is actually of Proterozoic rather than Archean origin. The intrusion is now located between a biotite paragneiss and an Archean tonalite, which might show a tilted lithology for the intrusions surroundings during and after its settling.

Avainsanat – Nyckelord – Keywords

Kuohattijärvi, mafic, layered intrusion, plagioclase phenocrysts, Kuohatti, gabbroic, anorthositic

Säilytyspaikka – Förvaringställe – Where deposited

Muita tietoja – Övriga uppgifter – Additional information

1. INTRODUCTION

The Kuohatti mafic layered intrusion was first discovered during bedrock- and aeromagnetic mapping of the mostly Archean Nurmes area. Distinctive plagioclase phenocrysts and strongly foliated tremolite-talc schists on outcrops suggested plausible mineralization and structure known in layered intrusion. To support this, an hourglass shaped anomaly in magnetometric maps and multiple drill cores led to the hypothesis of the anomaly being related to a layered intrusion, possibly of Archean origin. In this study petrography, mineralogy, structure, and petrogenesis of the Kuohatti intrusion is are discussed. An attempt was also made to constrain the age of the intrusion.

2. MATERIALS AND METHODS

Lithology and the major rock classification of the intrusion is based on six 89–203 meter long diamond drill holes (Appendix 12.1), each drilled in an angle of 45° that gradually decreases to 35° as the drill core depth increases. Drill cores are labeled with drill core prefix (DH) and labeled from 7–12. The drill cores are stored at the Finnish Geological Survey's (GTK) core archive in Loppi.

Thin sections were prepared from the drill core samples at selected locations and so that they represent enough rock types necessary for the lithological classification and modelling of the intrusion. Petrographic study and photography of these thin sections were conducted with a Nikon OPTIPHOT-POL polarizing microscope at the Department of Geosciences and Geography at the University of Helsinki.

Bulk rock compositions were prepared from samples cut from the drill core at the desired depth. Sample preparations and analyses were ordered from Labtium Oy by the GTK. Samples were prepared by first exhausting the sample at 70 °C, crushed with a jaw crusher made of manganese-steel and then milled in a steel cup with a plate mill. Samples are then made into a bricket and analyzed with a wavelength dispersive x-ray fluorescence method (WD-XRF). Trace-elements other than Co, Sc, V, Y, Zr are also

analyzed with ICP-MS, and the latter with ICP-OES from a hydrogenfluoride-perchloride acid dissolution and melt. PGEs are measured with ICP-OES from a Fire assay enriched 50 gram subsample or ICP-MS for some samples. Sulfur was analyzed with sulfur analyzer and carbon with a carbon analyzer. Bulk-rock compositions were plotted with GCDkit (Janousek et al. 2006) and CIPW-normative compositions calculated with windows excel spreadsheet made by Kurt Hollocher (2004).

The composition of minerals was measured from 10 carbon-coated thin sections in a electron-microprobe standard analysis with a JEOL JXA-8600 Superprobe at the Department of Geosciences and Geography at the University of Helsinki. Used standards for each mineral are listed among the results in the appendix (12.5.1). Beam current of 15 nA and an acceleration voltage of 15 kV were used for the measurements.

U-Pb isotope composition of selected zircon and monazite grains was determined using a single collector laser ablation inductively coupled plasma mass spectrometer (SC-LA-ICP-MS) at the GTK. Desired grains are separated from milled drill core samples with heavy-liquid and magnetic separation and then hand-picked and mounted onto an epoxy resin. Back-scattered electron images (BSE) were then prepared from of these grains to verify their condition and possible metallic or sulfuric inclusions. Analysis was conducted with Nu AttoM SC-LA-ICP-MS connected to a Photon Machine Analyte G2 laser ablation system, in which the samples are ablated into a helium gas with HelEx ablation cell (Müller et al. 2009) and then transmitted into the plasma in a mix with argon gas. Beam diameter of 25 μm, pulse frequency of 5 Hz and a beam energy density of 2 J/cm^2 are used during the measurements. Samples are also pre-ablated for 10 s to remove possible excess common lead and then ablated for 30 s for the measurements. Two zircon and one monazite samples from GTK are used for control at the start, between and in the end of measurements and two GTK's zircon samples (A382 and A1772) are used for standards. After measurements the U-Pb ages were calculated with protocols of Andersen et al. (2004) and Jackson et al. (2004) from the U-Pb isotope ratios and plotted to concordia with Isoplot/Ex 4.1 (Ludwig 2003).

3. KUOHATTIJÄRVI AREA

Tonalities, leucocratic granitoids, leucogranites and sanukitoids in Eastern Finland are results of multiple periods of magmatism in the Neoarchean (Käpyaho et al. 2006). Kuhmo district tonalites formed in three periods during 2.81–2.74 Ga and are a part of the most extensive period of Karelian cratons growth and create the Kuhmo-Suomussalmi greenstone belt. After this a series of high scale metamorphic events on the Karelian craton took place 2.67–2.63 Ga and 2.72–2.70 Ga (Kontinen et al. 2007, Käpyaho 2007). Metamorphic rocks are abundant in the area and the Neoarchean plutonic rocks also show signs of metamorphism.

The Kuohattijärvi suite, located on the western part of the Karelia and first described by Mikkola et al. (2013) is considered as the 8 km long fractured rock suite consisting of gabbro and amphibolite and going through Kuohattijärvi (Figs 1 and 2). On the Kuohattijärvi suite a 40 km^2 tonalitic bedrock is surrounded by granitic rocks and migmatitic TTG-gneisses, amphibolite and 2.74–3.31 Ga old biotite paragneisses that deposited during the back- or intra-arc period of the Neoarchean (Kontinen et al. 2007). The biotite paragneisses are also the most dominant rocks within the Kuhmo and Nurmes suites (Kontinen et al. 2007, Mikkola 2008 Mikkola et al. 2013). The surrounding area of Kuohattijärvi is a strongly deformed greenstone belt that consists of at least 2.7 Ga old amphibolized ultramafic volcanic rocks and foliated biotite paragneisses, of which the former consists of komatiitic serpentinites, basalts and basaltic andesites. The volcanic rocks and biotite paragneisses have a tectonic contact with granitoids in the west (Mikkola et al 2013).

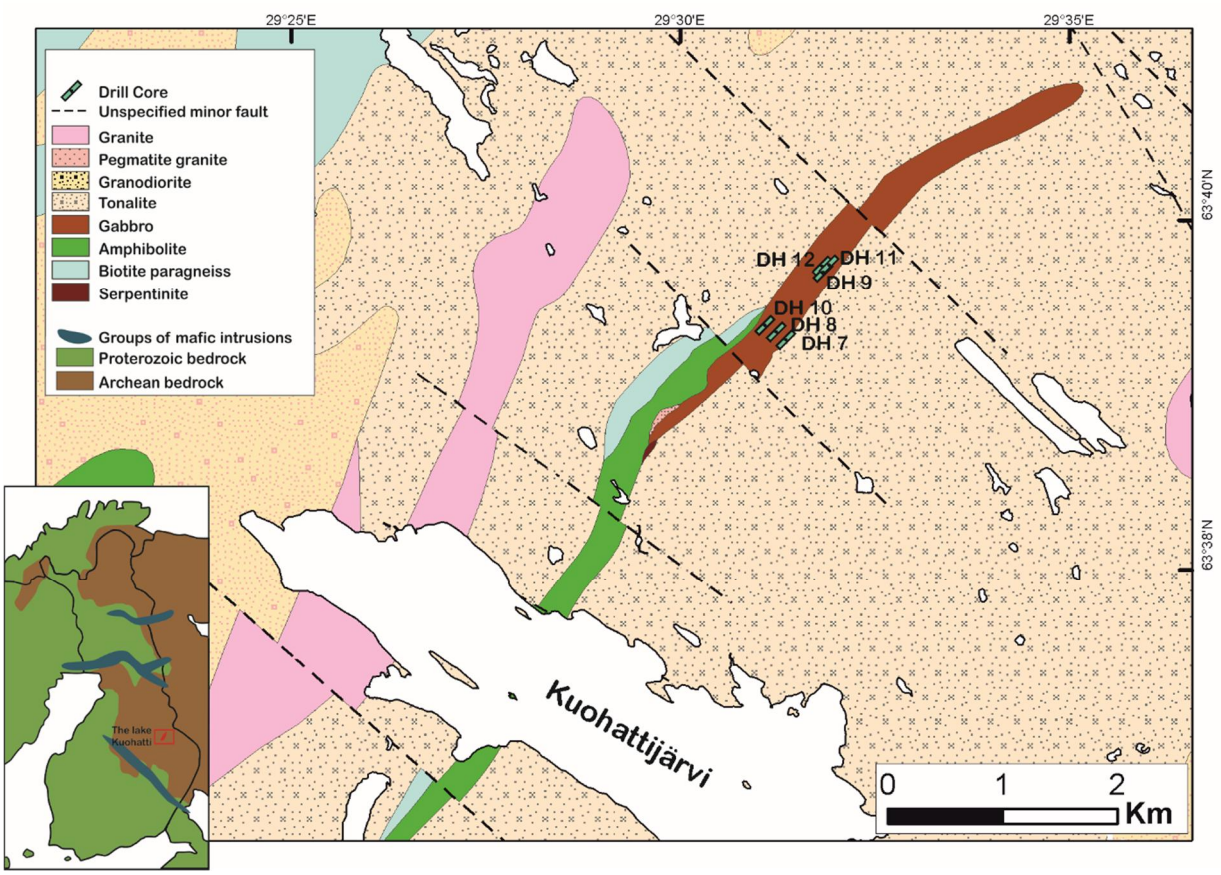

Figure 1. Geological map of the Kuohattijärvi area, rock suites next to the presumed intrusion and the studied diamond drill holes (DH). Index map given in lower left corner.

Multiple Proterozoic nickel- and copper-rich mafic-ultramafic intrusion of the Kotalahti nickel belt are located roughly about 150 km south-west-west of the Kuohatti area (Makkonen and Huhma 2007, Hanski et al. 2010). A group of know early Proterozoic (2.44 Ga) mafic layered intrusions is located roughly about 250 km north in the Koillismaa area (Lauri and Mänttäri 2002) and more further on the area along Proterozoic and Archean collision boundary (Alapieti et al. 1990). The Junttilanniemi intrusion is the nearest individual intrusion of this age group and located in Paltamo, 120 km NW from the Kuohattijärvi area (Halkoaho and Niskanen 2012).

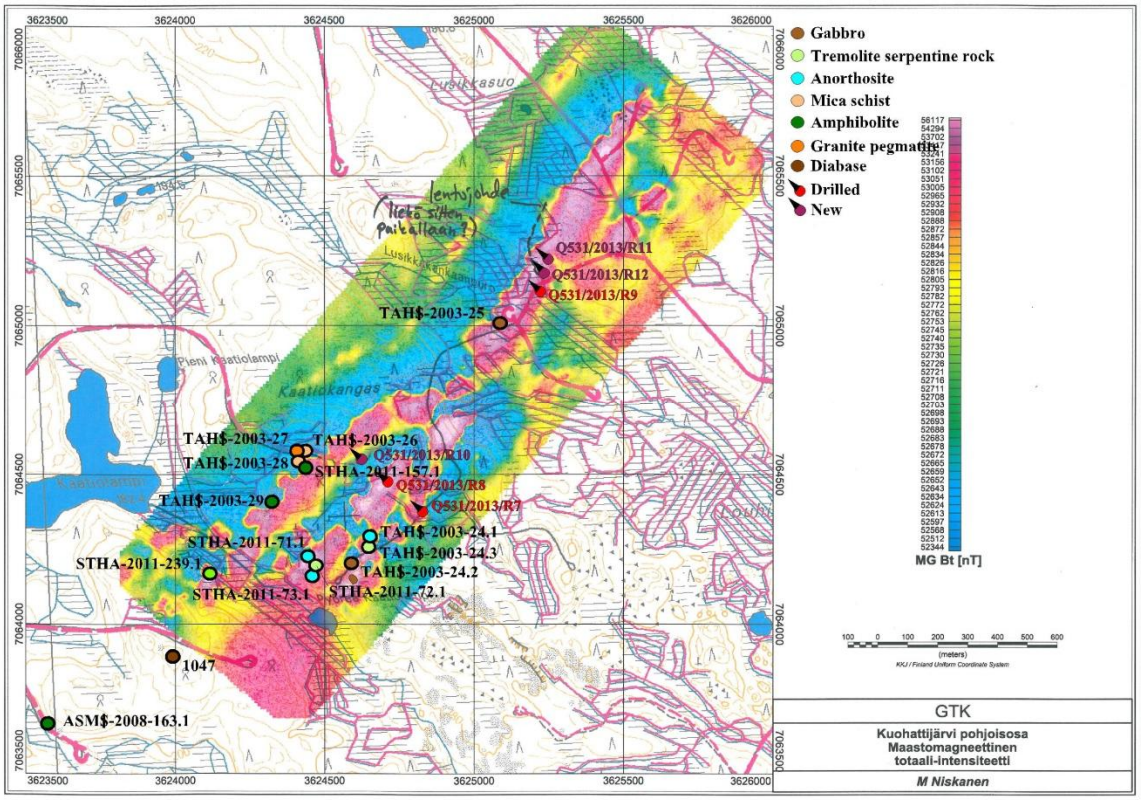

Figure 2. Ground magnetic total intensity map of the Kuohattijärvi area. Drill cores are marked on the map to clarify the possible shape and area of the intrusion. Photo courtesy of Tapio Halkoaho in Mikkola et al. (2013).

The Kuohattijärvi layered intrusion is located about 20 kilometers northeast from the city of Nurmes, Eastern Finland on the northern part of Kuohattijärvi suite, between Hyrynsalmi (Mikkola 2008) and Lieksa (Mikkola et al. 2013) complexes on the Archean side of the Finnish bedrock and 3 km north of the Kuohattijärvi. It was first noted during bedrock mapping of Eastern Finland (Mikkola et al. 2013), which lead to the further study in this work. The intrusion is located on a north-eastbound 0.5 km wide line consisting of gabbro, greenstone and biotite paragneisses lying in the middle of this tonalite unit. A few pegmatitic granites and serpentinite rocks are exposed in the transition zone between the gabbro and amphibolite. All these rocks are cut by 2.7 Ga old leucogranitoids (Mikkola et al. 2013) and multiple minor faults in a southeast-bound direction.

4. LITHOLOGIC ASSEMBLAGE AND PETROGRAPHY OF THE KUOHATTI INTRUSION

4.1. Drill core observations and inferred structure of the Kuohatti Intrusion

The intrusion is surrounded by three distinctive rock types: metamorphosed igneous rocks, veins cutting the intrusion and rocks on the boundaries of the intrusions. Rocks along the intrusion boundaries are granitic gneiss, tonalite and biotite paragneiss. Less than 0.5 m thick veins are often sulfide- or amphibole-rich, but there are also some granitic pegmatite and syenitic veins. Igneous rock types within the intrusion are gabbro, leucocratic gabbro, anorthosite, pyroxenite and peridotite (Fig. 3), which are occasionally cut by granitic, amphibolite or diabase dikes in addition with scattered metamorphic amphibolitic veins. The metamorphic rocks in the area are metapyroxenites, mica- and amphibole schists and variations of tremolite, chlorite and talc-based rocks. Due to the high level of metamorphosis in the intrusion, its rocks are here considered metamorphic, yet when considering the layering of the intrusion in the discussion section their photoliths are used. The rock-type classification presented here is based on thin section samples and drill core logs.

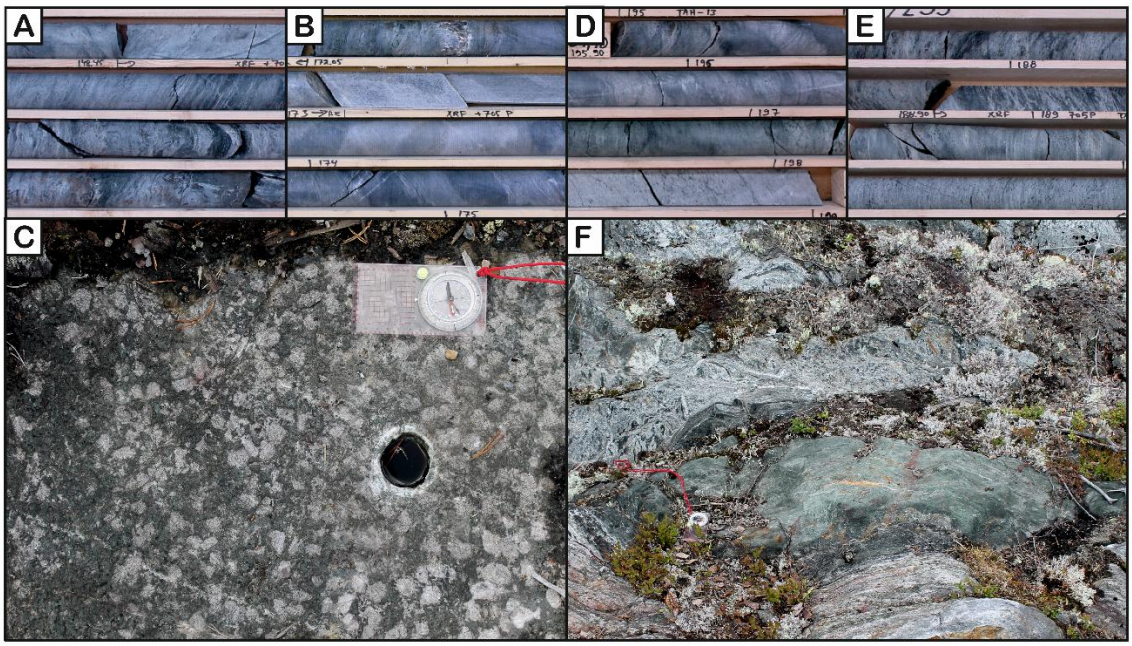

Figure 3. A) Leucocratic gabbro from DH 7, B) Anorthosite from DH 7, C) Plagioclase phenocryst filled gabbro (leucocratic gabbro in drill cores) on an outcrop on the Kuohatti suite, D) Pyroxenite from DH 7, E) Peridotite from DH 7 and F) Tremolite-chlorite schist contacting a gabbro on an outcrop on the Kuohatti suite. Photos C and F courtesy of Tapio Halkoaho in Mikkola et al. (2013).

4.1.1. Drill core 7

Drill core 7 (DH 7) is located on the southern part of the intrusion, east of DH 8 and DH 10 (Figs 1,2 and 4). The first 70 m consist of granitic gneiss and tonalite, with a couple granitic pegmatite veins cutting the gneiss and an amphibolite layer between them. The intrusion starts at 72.50 m with a gabbroic unit, cut by amphibolite and small sulfuric dikes. After 76 m the gabbroic unit is in a sharp contact with a tremolite-talc schist and turns into a more leucocratic gabbro (Fig. 3A and 3C). After this the gabbroic layers alternate and are occasionally alternated into tremolite-talc schist (Fig. 3F) units until the depth of 115.35 m. After this, anorthositic layers start showing up and alternate with the gabbroic layers. Two thick anorthositic layers are found at depths of 131.15 and 172.90 m (Fig. 3B). At the depth of 184.00 m leucocratic gabbro is followed by a pyroxenitic layer (Fig. 3D). This pyroxenite transforms into an amphibolite that is followed by a 5 meter thick peridotite (Fig. 3E) and again followed by another amphibolite. After 10 m of gabbroic and leucogabbroic rocks another pyroxenitic layer with a thickness of 3.75 m is present. The drill core ends with a gabbro that likely represents the middle of the intrusion.

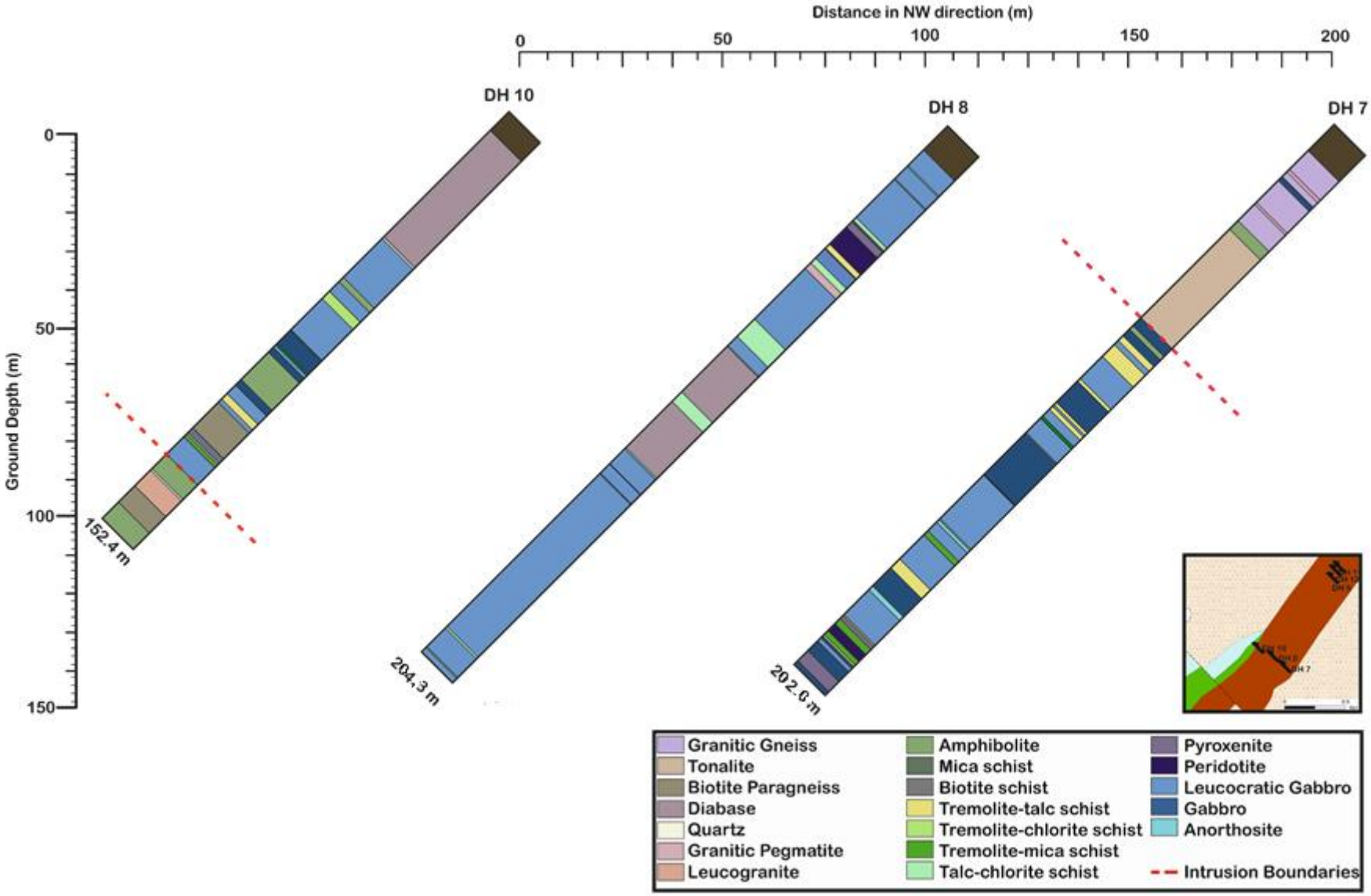

Figure 4. Lithological assemblages for the southern samples of Kuohattijärvi intrusion.

4.1.2. Drill Core 8

Drill core 8 (DH 8) is located in the southern part of the intrusion, between drill cores 10 and 7. DH 8 has a 45 m thick leucogabbroic layer at the beginning (Fig. 4). The layer has multiple small anorthositic layers and veins in it during the first 20 m. This is followed by a pyroxenite through a tremolite-talc rock. A 10 m thick peridotitic layer ending in an amphibolite layer is present right after the pyroxenite. After this a five meter thick anorthositic layer turns into a leucocratic gabbro through tremolite talc-rock cut by a granitic vein. This is cut by multiple amphibolitic dikes and a layer before it is cut by a diorite at the depth of 77 m. This diorite is likely an intrusive layer formed after the intrusions emplacement and it turns into a leucogabbro through a sharp contact with a thin anorthositic layer. This leucogabbro is cut by multiple anorthositic dikes at a shallow depth as well as many amphibolite and sulfide veins on the bottom until the drill core ends at 195.40 m.

4.1.3 Drill Core 10

Drill core 10 (DH 10) is located in the southern part of the intrusion, west of DH 8 and DH 7. The first 46.90 m (Fig. 4) cut homogeneous and evenly grained diorite followed by a 0.5 m thick granitic part. This contact consists of multiple amphibolitic veins. This is followed by a leucocratic gabbro, occasionally cut by amphibolite at 63.00–63.50 m and multiple amphibolitic and anorthositic dikes. A 1.80 m thick gabbroic part starts at 88.35 m, which then turns into a leucocratic gabbro through amphibolite. This leucocratic gabbro is cut by a 30 cm granitic pegmatite. After this it is followed by a thin amphibolite layer followed by a gabbroic layer. The intrusion is then cut by a biotite paragneiss at 108.90 m. This otherwise homogeneous rock is cut by a 1.70 meters thick gabbroic rock at 118.50 m. After 121.80 m comes a layer of leucocratic gabbro, followed by a biotite paragneiss at 134.30 m. The first instance of biotite paragneiss is again followed by a gabbro cut by multiple tremolitic veins. This layer is followed by a leucocratic gabbro including multiple thin amphibolitic veins and cut by a quartz-feldspar dike right before it is followed by a biotite paragneiss. The rock type continues as an amphibolite from 146.30 m onward and the drill core ends at 152.35 m.

4.1.4. Drill Core 9

Drill core 9 (DH 9) is located in the northern part of the intrusion, south of DH 12 and DH 11 (Figs 1,2 and 5). The rock types in the northern drill holes all show quite high amounts of alteration, especially at shallower depths and are quite rich in amphibolitic and sulfidic veins compared to their southern counterparts. This is also clearly visible in the whole-rock geochemistry of these drill cores as elements such as Zn, V and Ni show a huge rise in their amounts towards the bottom. DH 9 starts with a gabbroic part similar to the one at 72.50 m in DH 7 (Figs 4 and 5). This gabbroic part transforms with a sharp contact into a tonalitic rock at 21.50 m. This tonalitic rock then fades into a tremolite-talc schist. This is followed by a leucocratic gabbro at 30.00 m that transforms into an amphibolite at 38.35 m. This amphibolite is cut with sharp contacts by a leucocratic gabbro at 43.90–44.75 m and is followed by a leucocratic gabbro at 46.65 m, yet roughly the first meter is cut by multiple amphibolitic veins. At 65.60 m it turns into a tonalitic rock. The tonalitic rock is cut sharply by a tremolite vein at 67.80–67.90 m and after this its grain size turns from fine to coarse until it ends at 74.90 m. It turns into a leucocratic gabbro that sharply turns into a more mafic one at 77.20 m. This is followed by a tremolite-talc schist at 81.60 m that turns into a fine-grained talc schist at 92.05 m. The amount of sulfides in this talc schist highly rises at 92.60 m and is followed by an amphibolized biotite schist at 94.10 m and is filled with sulfides. This biotite schist is cut by an amphibolite at 100.30 m that composes the rest of the drill core till 100.50 m.

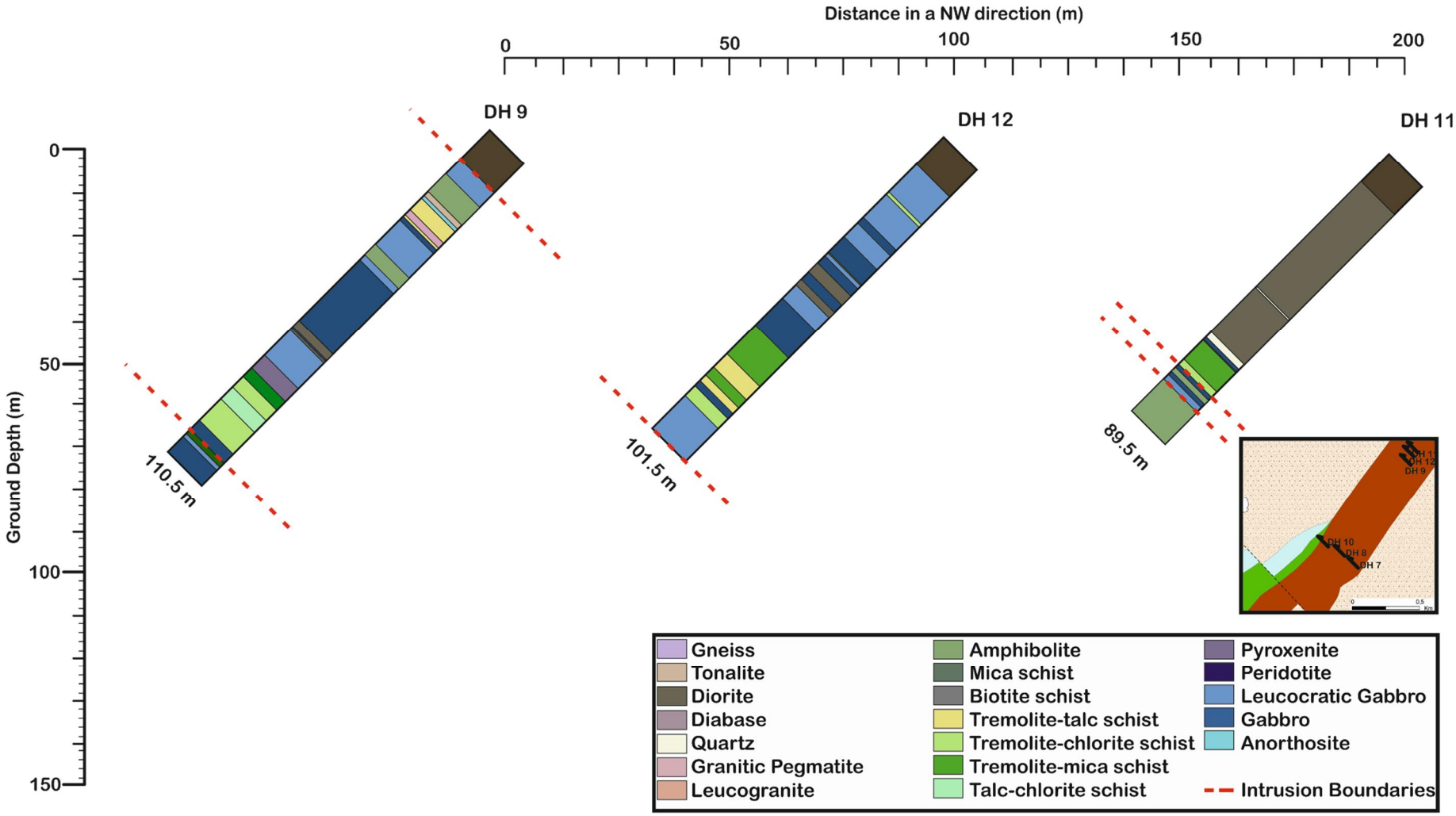

Figure 5. Lithological assemblages for the northern samples of the Kuohattijärvi intrusion.

4.1.5. Drill Core 12

Drill core 12 (DH 12) is located in the northern part of the intrusion, between DH 9 and DH 11. It starts with half a meter of tonalitic rock that turns into a leucocratic gabbro at 10.50 m (Fig. 5). This leucocratic gabbro is cut by multiple anorthositic dikes, amphibolitic, and sulfide veins. The amount of tremolite in the rock rises after 16.80 m before a sharp tremolite-rich contact with a tonalitic rock at 28.85 m. It then turns back into a leucocratic gabbro at 30.05 m, which alternates with an amphibolite until 41.40 m. The contacts with amphibolite and leucocratic gabbro are filled with tremolite and sulfide mineralizations and followed by multiple anorthositic dikes. After this another tonalitic rock is followed with a gabbro filled with sulfide mineralizations and anorthositic dikes at 44.40 m. This gabbro is cut by a tonalite filled with multiple amphibolitic veins until 53.65 m and changes to a sulfide-rich tremolite-talc rock at 65.60 m. As with DH 9, this tremolite-talc rock turns into a sulfide-rich biotite schist at 75.55 m and the biotite schist turns back into tremolite-talc rock at 82.95 m. This is cut by a gabbro at 85.75–85.60 m. The amount of sulfides sharply decreases at 91.30 m and switches into an amphibolite that continues till the end of the drill core at 101.50 m.

4.1.6. Drill Core 11

Drill core 11 (DH 11) is located 100 m north of DH 12. It starts with a diabase that continues until 61.95 meters with a feldspar vein at 46.05–46.50 (Fig. 5). At 61.95 this biotite paragneiss has a sharp contact with a quartz vein that has a 50 cm thick gabbroic unit with pyrite mineralization in it. At 64.85 m this vein turns into a tremolite-talc schist full of sulfides as in DH 9 and DH 12. This is cut by an anorthositic dike and a biotite schist at 71.80–73.30. The tremolite-talc schist alters into an amphibolite at 75.75 m. This continues till the end of drill core at 89.50 meters.

4.2. Petrography of the Intrusion

4.2.1. Gabbro and gabbronorite

Gabbro (Fig. 6) and gabbronorite are met in contacts or transition zones between leucocratic gabbro and amphibolite. They are found on the top and bottom of the intrusion as well as in its inner parts. The color of gabbro varies from greenish grey to

lightly dark grey. They are even-grained and have ranging values of amphibole. Susceptibility varies from 10 to 100 x10^{-5} κ. Gabbros are often foliated to some extent and also show marks of pressure solution on quartz as well as subgrains of feldspars and quartz. Plagioclase has quite a small grain size, yet some subgrains are likely past remnants of larger grains. Accessory minerals are mostly quartz, biotite, chlorite, sulfides, zircon and carbonate.

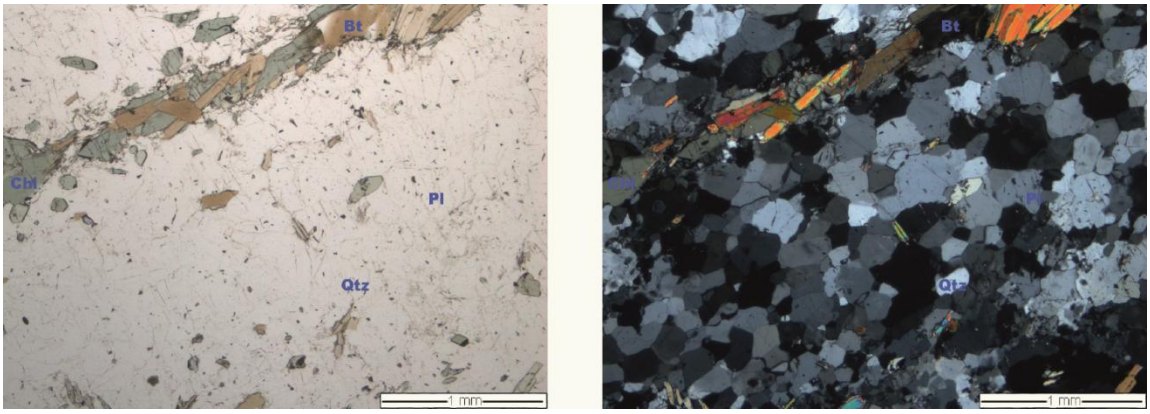

Figure 6. Gabbroic sample from DH 7 at 194.80 m. Photograph on the left is taken in straight light and the one on the right with crossed polarizers. Mineral abbreviations are as follows: Chl = chlorite, Pl = plagioclase and Qtz = quartz.

4.2.2. Leucocratic gabbro

Leucocratic gabbros are the most common rocks of the intrusion. They are also more common in the southern parts of the intrusion. The color and composition of them are closer to the more leucocratic end of gabbroic rocks although no more than 65 % euhedral plagioclase is present which does not make them traditional leucogabbros although they are given the prefix leucocratic. They also have a distinguishable texture especially in the topmost layers that have multiple centimeters thick plagioclase phenocrysts. Their color is mostly light grey, but some layers of the intrusion have a more light greenish shade of grey. They are even-grained, but the texture varies from homogeneous to heterogeneous and the amount of amphiboles and sulfides varies substantially. Susceptibility varies from 15 to 80 x10^{-5} κ. Leucocratic gabbros have 45–65 % plagioclase, 35 % amphiboles and 9–10 % K-feldspar (Fig. 7). Accessory minerals are mostly quartz, biotite, chlorite, sulfides, zircon and carbonate. Structural deformation caused by the metamorphosis is visible on quartz and plagioclase grains, yet one thin section from DH 8 (Fig. 7 lower panel) has some well-preserved plagioclase phenocrysts.

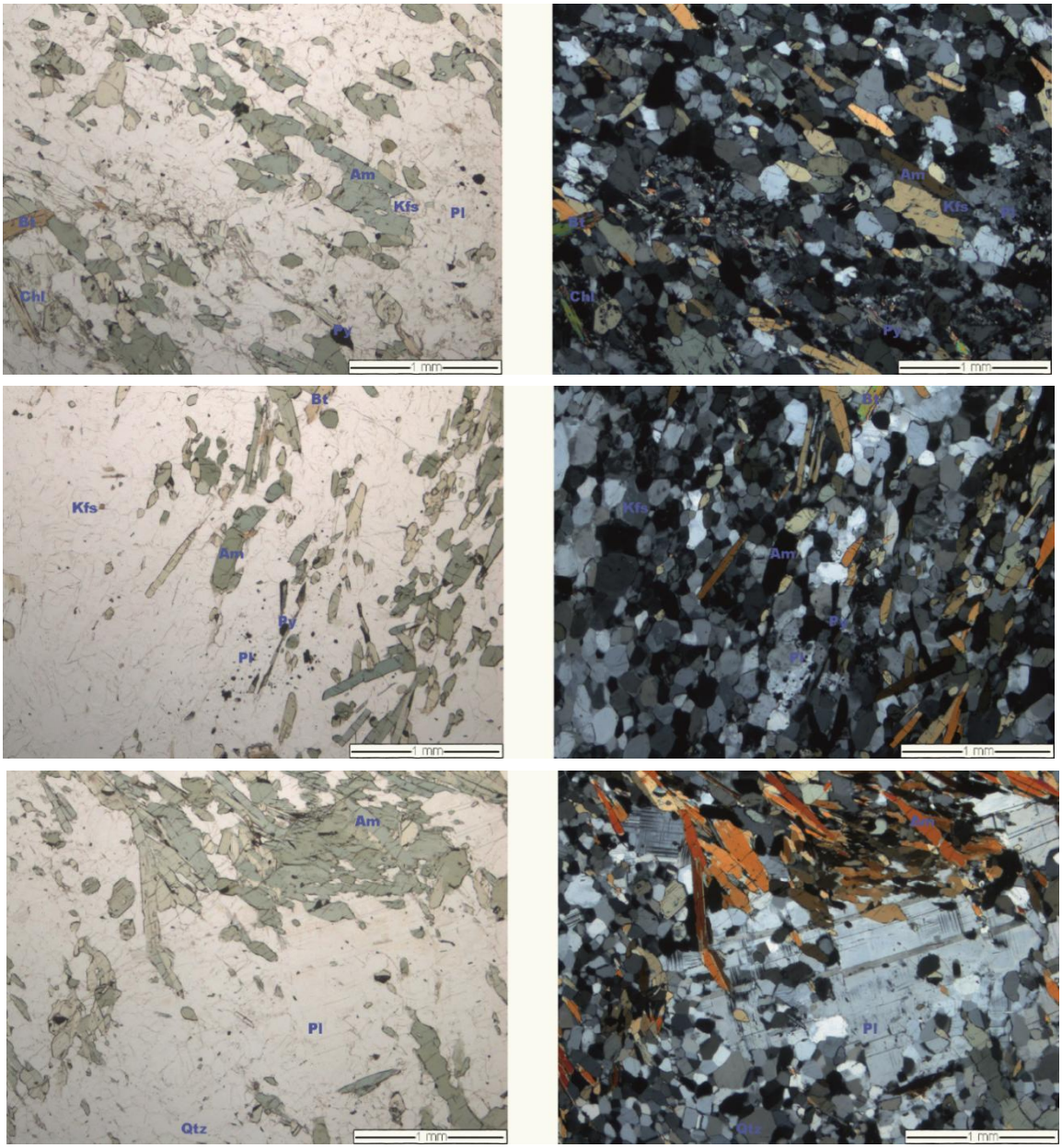

Figure 7. Leucocratic gabbros samples from DH 7 at drill core depths of 78.50 m (upper) and 82.15 m (middle) and DH 8 at the depth of 54.05 m (lower). Photographs on the left are taken in straight light and the ones on the right with crossed polarizers. Mineral abbreviations are as follows: Chl = chlorite, Bt = biotite, Am = amphibole, Kfs = K-feldspar, Pl = plagioclase and Qtz = quartz.

4.2.3. Anorthosite

Anorthosite appears mostly as 5–20 cm layers, yet a few individual layers exceed several meters in thickness. Homogeneous anorthosite ranges from bluish white grey to whitish grey, is evenly grained and usually very amphibole-poor compared to the other rocks in the intrusion. Anorthosites have 38–58 % clinozoisite and 35–49 % plagioclase (Fig. 8). Samples from DH 7 from the depth of 173.00 m (Fig. 8 lower panel) show 10–15 % apatite, some accessory amounts of iron-rich variation of clinozoisite as well as

accessory amounts of pyroxene from 31–49 % and 0–4 % respectively to the bottom of the sample. Sample at the depth of 148.95 m (Fig. 8 upper panels) has in addition sulfides, titanite and talc as accessory minerals.

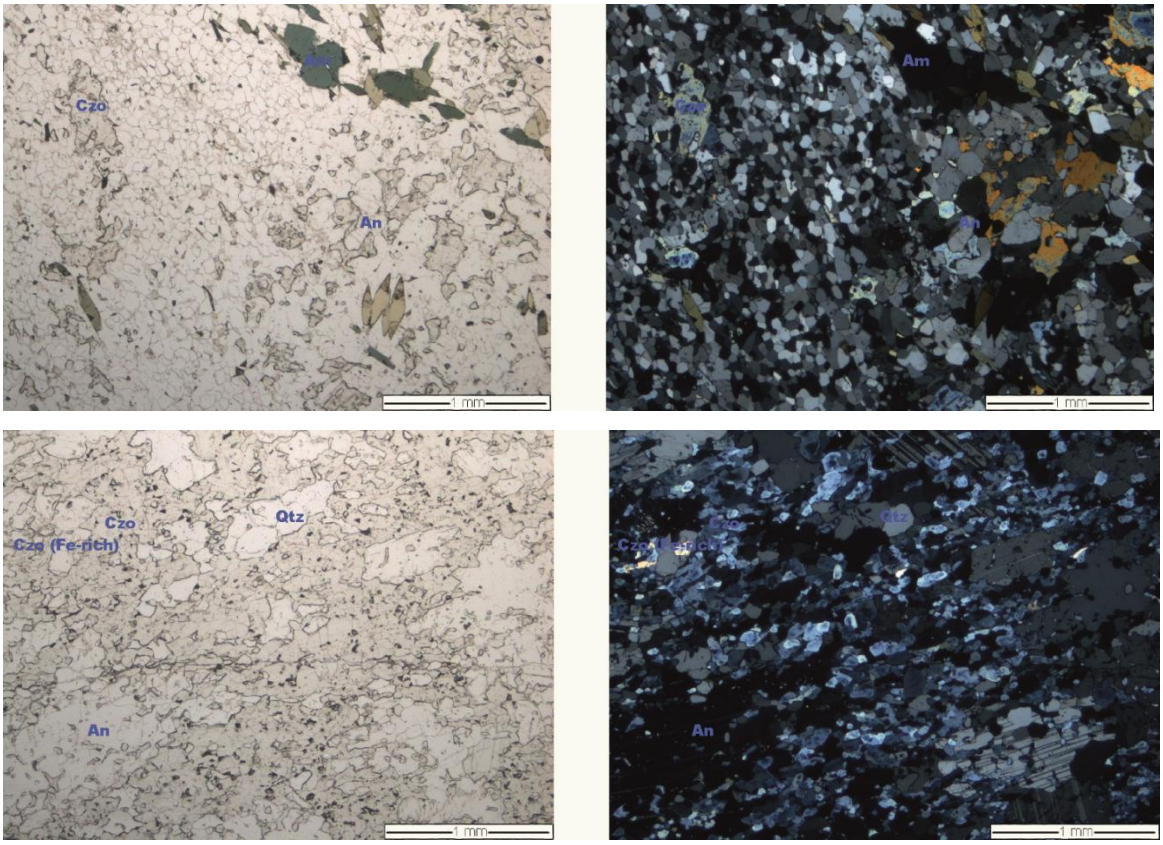

Figure 8. Anorthosites from DH 7 at the depths of 148.95 m (upper) and 173.00 m (lower). Photographs on the left are taken in straight light and the ones on the right with crossed polarizers. Mineral abbreviations are as follows: Czo = clinozoisite, An = anorthosite, A, = amphibole and Qtz = quartz.

4.2.4. Pyroxenite

Pyroxenite appears right underneath the anorthositic layers. On the bottom it is in contact with a thin gabbroic layer followed by a peridotite Pyroxenites have a color ranging from light greenish grey to whitish grey and are homogeneous in texture. They are even-grained and amphibole-rich. Individual pyroxene grains are rare, but a few remnants of orthopyroxenes are still existent in each thin section. Their ruptured texture leaves the origin of these pyroxenes impossible to be determined from a thin section and they are thus chosen for the microprobe analysis. Pyroxenes yield susceptibility values ranging from 6 000 to 40 000 $x10^{-5}$ κ. Pyroxenes show a strong foliation, especially in the direction of amphibolite and pyritic veins cutting them. Sample from DH 7 at the depth of 186.60 meters (Fig. 9) has 52 % tremolite, 17 % talc, 13 % sulfides, 12 %

chlorite, 6 % pyroxene, biotite and magnetite as accessory mineral. The texture of minerals suggests that prior to alteration 2/3 of mineralization was pyroxene and 1/3 olivine.

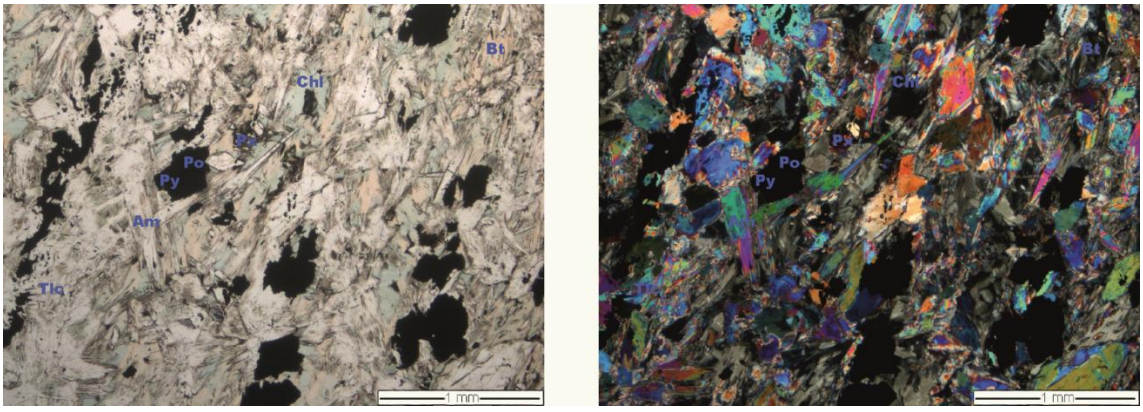

Figure 9. Pyroxenite from DH 7 at the depth of 184.60 m. Photograph on the left is taken in straight light and the one on the right with crossed polarizers. Mineral abbreviations are as follows: Chl = chlorite, Bt = biotite, Tlc = talc, Am = amphibole, Py = pyrite, Po = pyrrhotite and Px = pyroxene.

4.2.5. Peridotite

One or two layers of homogeneous and even-grained peridotite are situated between the pyroxenite layers and are distinguishable from their dark greenish grey color. They have high amounts of olivine, yet some half of the thin sections are amphibole. This olivine that is likely metamorphic by origin is discussed further in the mineralogy section. Peridotite has susceptibility values ranging between 20 000–50 000 x10^{-5} κ. Sample in DH 7 from the depth of 189.20 m (Fig. 10) has 45 % olivine, 28 % amphibole, 23 % sulfides and chlorite, talc and also rutile as an accessory mineral.

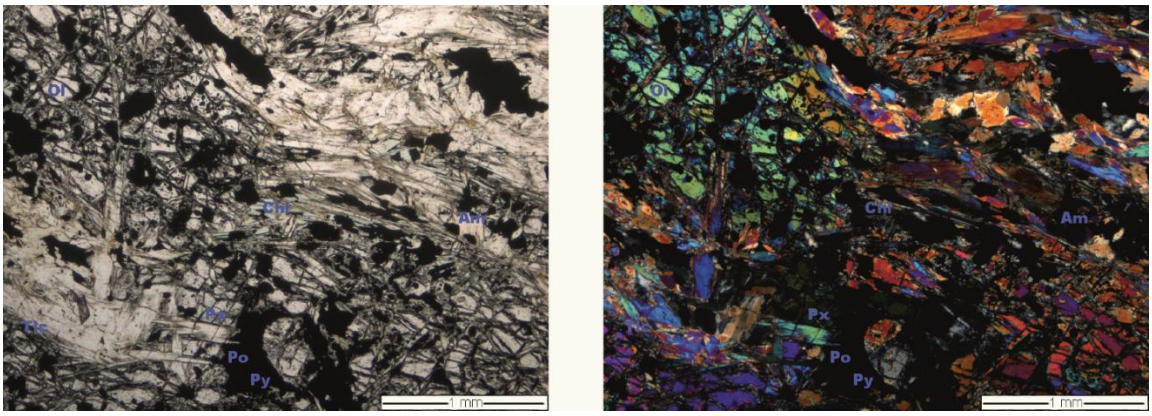

Figure 10. Peridotite from DH 7 at the depth of 189.20 m. Photograph on the left is taken in straight light and the one on the right with crossed polarizers. Mineral abbreviations are as follows: Chl = chlorite, Bt = biotite, Tlc = talc, Am = amphibole, Py = pyrite, Po = pyrrhotite and Px = pyroxene.

4.2.6. Chlorite-talc-tremolite schists

Chlorite and talc -schists are found all-around the intrusion. They are probably remnants of pyroxene- or olivine-bearing rocks that have been strongly metamorphosed. They are dark or light greenish grey to light brownish grey, heterogeneous and contain ranging amounts of sulfides. Tremolite is the most common amphibole within the drill cores and thus some instances of these rocks have been named tremolite-talc rock or tremolite-chlorite schists for classification. These rocks yield a wide range of susceptibility at 20–1,500 $x10^{-5}$ κ.

Chlorite-talc schist from DH 7 at depth of 83.05 m has 45 % plagioclase, 35 % amphibole and 10 % K-feldspar (Fig. 11). Accessory minerals are biotite, chlorite, sulfides, zircon and carbonate. Sample at the depth of 85.2 meters has 50 % talc, 40 % chlorite, 7 % pyroxene and sulfides and titanite as accessory minerals. DH 12 sample at depth of 68.80 m has 40 % talc, 23 % chlorite, 22 % plagioclase, 10 % quartz and 5 % plagioclase. Amphibole points to precedent pyroxenes. Grain size varies between 0.2–0.5 mm for the main minerals and 0.2–1.0 mm for the sulfides.

Chlorite-tremolite schist (Fig. 12) in DH 7 at the depth of 198.60 m has 45 % tremolite, 45 % chlorite, 5 % sulfides and talc and pyroxenes as accessory minerals. Sulfides are orientated mostly along the direction of foliation. Grain size is 0.2–0.5, except for pyroxene remnants (0.2–0.3 mm).

Talc-tremolite schist sample from DH 9 at the depth of 88.40 and 91.20 meters has 55–60 % talc, 35–36 % tremolite, 8 % rutile (Fig. 13) and quartz as an accessory mineral. The habitus of the tremolite indicates a possibility of them having been pyroxene cumulates. Grain size varies between 0.2–1.2 mm. Previous sample has in addition titanite as accessory mineral and is strongly foliated. Grain size is fine at 0.1–0.6 mm.

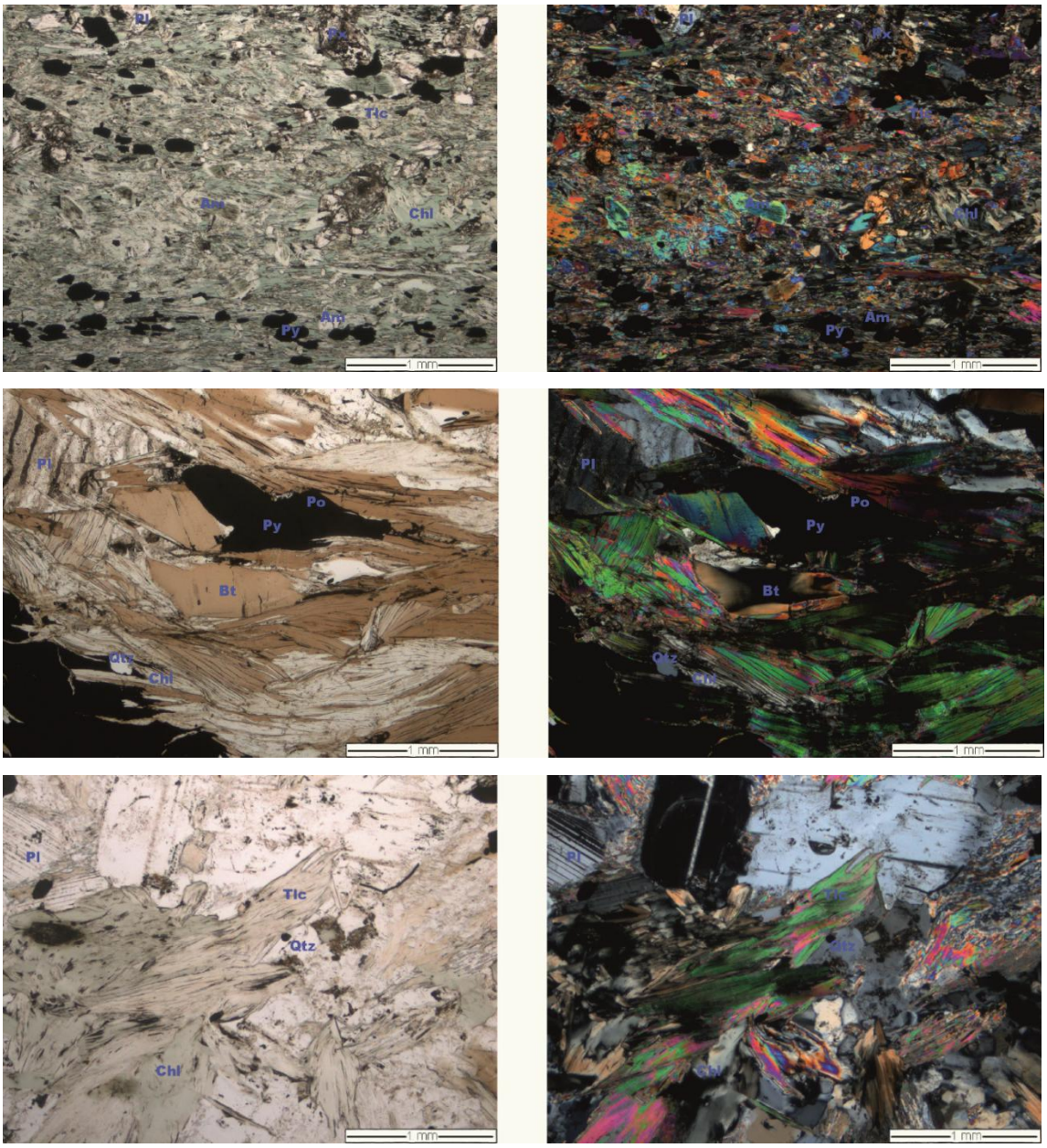

Figure 11. Talc-chlorite schists from DH 7 at the depth of 83.05 m (upper), from DH 9 at the depth of 88.40 m (middle) and from DH 12 at the depth of 68.60 m (lower). Photographs on the left are taken in straight light and the ones on the right with crossed polarizers. Mineral abbreviations are as follows: Chl = chlorite, Bt = biotite, Tlc = talc, Am = amphibole, Py = pyrite, Po = pyrrhotite and Px = pyroxene.

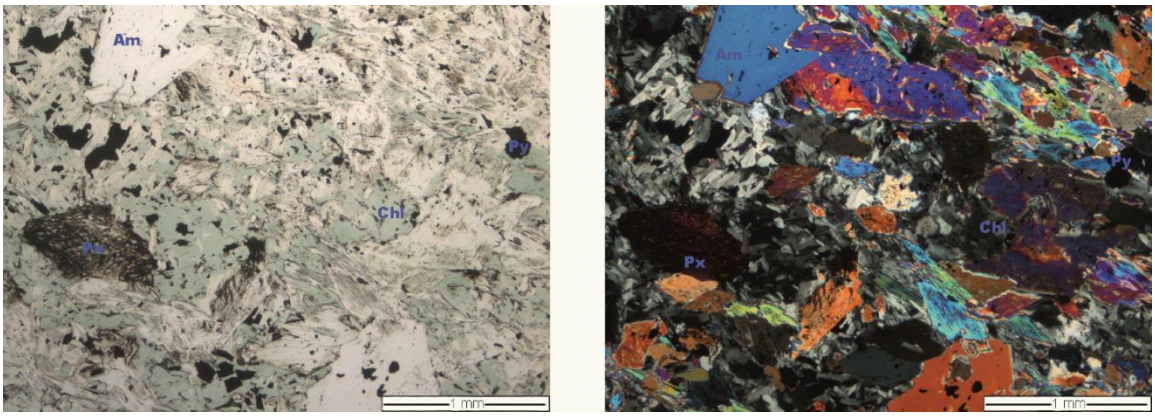

Figure 12. Chlorite-tremolite schist from DH 7 at drill core depth of 198.60 m. Photograph on the left is taken in straight light and the one on the right with crossed polarizers. Mineral abbreviations are as follows: Am = amphibole, Chl = chlorite and Px = pyroxene.

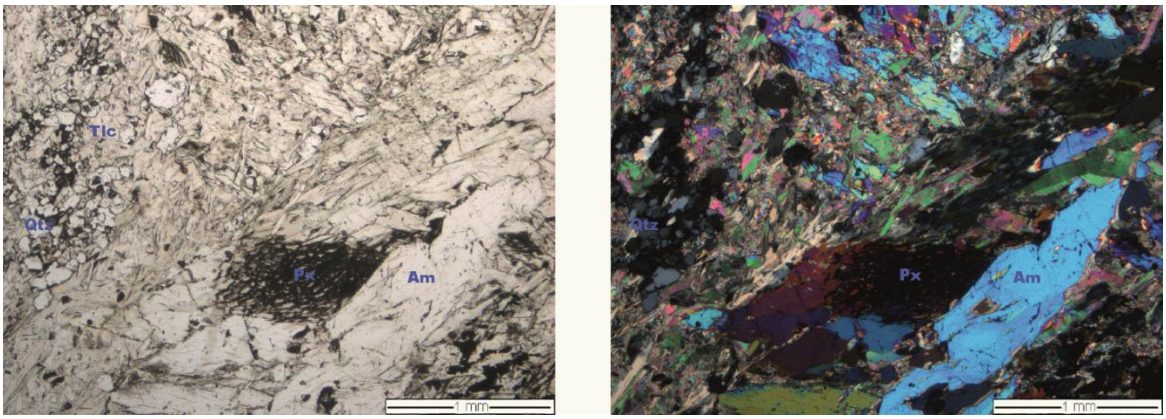

Figure 13. Talc-tremolite schist from DH 9 at drill core depth of 91.20 m. Photograph on the left is taken in straight light and the one on the right with crossed polarizers. Mineral abbreviations are as follows: Am = amphibole, Px = pyroxene, Qtz = quartz and Tlc = talc.

4.3. Rocks surrounding the intrusion

4.3.1. Granitic gneiss

Granitic gneiss is met only in DH 7 and it occurs as the contact rock between the tonalitic country rock and the intrusion. This gneiss varies from light brownish grey to light grey and is often cut by 10–50 cm thick granitic pegmatite veins. Most of these veins are texturally homogeneous with susceptibility ranging from 5–10 $x10^{-5}$ κ.

4.3.2. Biotite paragneiss

Biotite paragneiss is the country rock at the end of DH 10. It is strongly foliated and lightly greyish of brownish in color. Chunks of biotite mineralization are visible in the

drill core, although the even-grained parts resemble granitic gneiss in composition. Susceptibility of the biotite paragneiss is 15–45 x10^{-5} κ.

4.3.3. Diabase

Diabase is seen the southern drill core as one instance in DH 8 and two in DH 10. It is a dark grey, even-grained and shows some metamorphic alteration and foliation. The minerals are 40 % plagioclase, 55 % amphiboles and 5 % biotite (Fig. 14). Plagioclase and amphiboles have a texture suggesting pressurized solution during metamorphism.

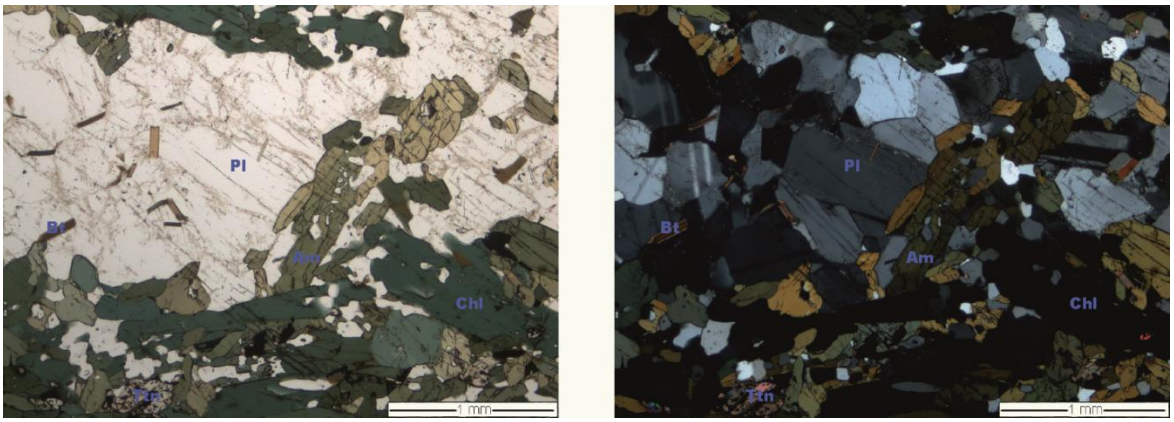

Figure 14. Diorite DH 10 at the depth of 56.80 m. Photographs on the right are taken in straight light and the ones on the left with crossed polarizers. Mineral abbreviations are as follows: Am = amphibole, Chl = chlorite and Px = pyroxene.

4.3.4. Diorite

Diorite is the northern contact rock for the intrusion at DH 11 where it makes nearly half of the drill core. Its relationship with the diabase is unknown and their relationship is further discussed in chapter 5.4. Diorite along the northernmost intrusion boundaries is dark grey or black and has an even-grained homogenous texture. It shows mostly no metamorphic alteration or foliation and cuts the intrusion sharply.

4.3.5. Tonalite

Tonalite lies on top of the intrusion. Tonalite has a light whitish grey color and evenly grained heterogeneous texture. Non-sulfidic layer yields susceptibility values of 20–40 x10^{-5} κ and the more sulfide-rich layer yields susceptibility from 150–200 x10^{-5} κ. The tonalite has 55 % plagioclase, 20 % quartz, 12 % chlorite and 8 % biotite (Fig. 15). Deformation on quartz and plagioclase grains is notable, although they have a coarse

heterogeneous grain size between 0.2–1.0 mm, biotite and chlorite are slightly coarser (0.6–1.2 mm).

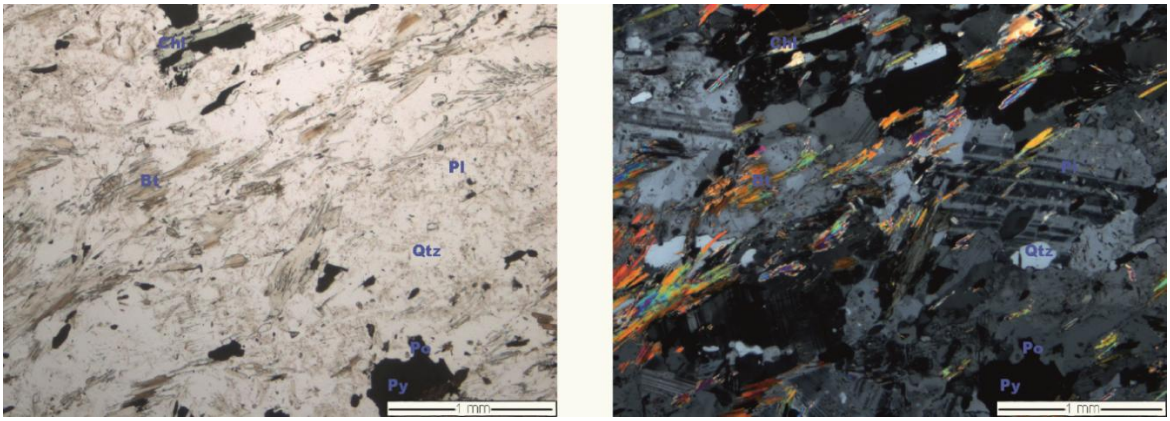

Figure 15. Tonalite sample in DH 9 at the depth of 82.50 m. Photograph on the left is taken without polarizers in straight light and one on the right with crossed polarizers. Given minerals are marked with purple. Mineral abbreviations are as follows: Am = amphibole, Chl = chlorite and Px = pyroxene.

4.3.6. Biotite schist

Biotite schist is a black, homogenous and even-grained rock with a susceptibility of 40 $x10^{-5}$ κ. It is visible in DH 7 between two gneisses and another in DH 9 at the depth of 100.25 meters (Fig. 16). The latter has 60 % biotite, 23 % plagioclase, 8 % quartz, 7 % sulfides and chlorite, rutile and zircon as accessory minerals. The sulfides are foliated along biotite. Quartz is present as small fish-shaped chunks. Sample from DH 9 from the depth of 100.25 m has 24 % biotite, 26 % sulfides 16 % chloride, 14 % talc, 12 % plagioclase, 7 % pyroxene and quartz, rutile, apatite and zircon as accessory minerals.

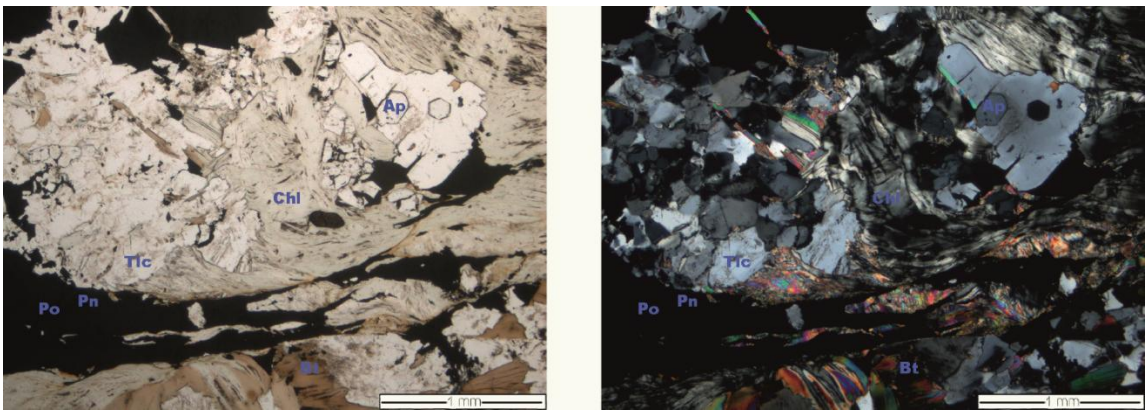

Figure 16. Biotite schists from DH 12 at drill core depth of 68.90 m and drill core 9 at drill core depth of 100.25 m (pic). Photograph on the left is taken in straight light and the one on the right with crossed polarizers. Mineral abbreviations are as follows: Am = amphibole, Chl = chlorite and Px = pyroxene.

4.3.7. Mica schist

Mica schist from DH 10 at the depths of 86.6 m and 104.3 m (Fig. 17) have 45–60 % amphibole, 14–28 % quartz, 13–18 % plagioclase. The latter has 8 % sulfides and rutile and carbonate as accessory minerals and the previous apatite, zircon, biotite and carbonate. Mica schists are quite even-grained and their texture is homogenous.

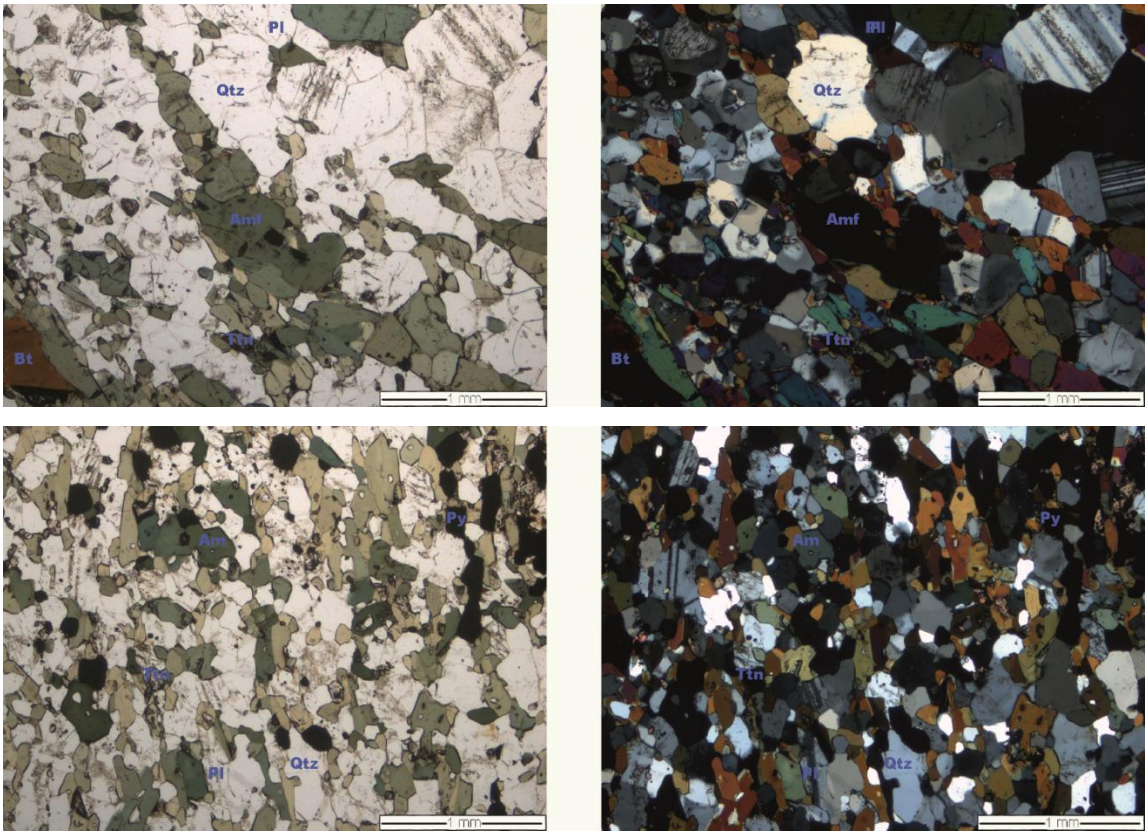

Figure 17. Mica schists from DH 10 at the depths of 86.60 m (upper) and 104.30 m (lower). Photographs on the left are taken in straight light and the ones on the right with crossed polarizers. Mineral abbreviations are as follows: Am = amphibole, Chl = chlorite and Px = pyroxene.

4.3.8. Amphibolite

Amphibolite appears mostly in DH 10, but is also found in DH 8 (Fig. 18). It is dark greenish grey or light greenish grey in color, even-grained and fine- to medium-grained. Susceptibility values are 20–80 x10^{-5} κ. Sample from DH 8 at the depth of 119.25 m has 68 % amphibole and 29 % plagioclase. Twinning of the plagioclase grains is badly ruptured likely due to the amount of metamorphism. Accessory minerals are titanite, sulfides and zircon.

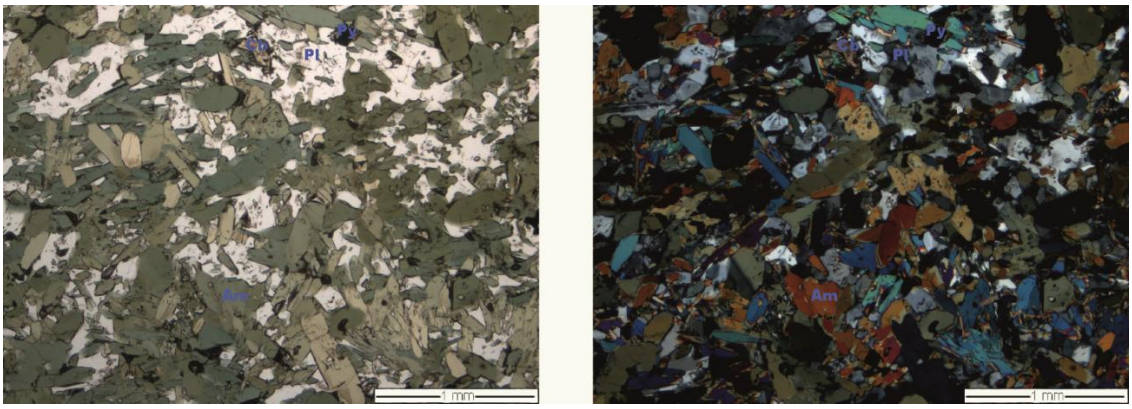

Figure 18. Amphibolite from DH 8 at the depth of 119.25 m. Photograph on the left is taken in straight light and the one on the right with crossed polarizers. Mineral abbreviations are as follows: Am = amphibole, Chl = chlorite and Px = pyroxene.

4.4. Dikes

4.4.1. Amphibolite

Amphibolite dikes consist of homogenous amphiboles and occur as 2–5 cm thick dike swarms. These swarms occur mostly in gabbroic rocks and can have a total length of several meters. The dark green or greenish gray dikes are again quite homogenous and medium- to coarse-grained.

4.4.2. Granites and granitic pegmatites

Granitic and pegmatitic dikes are distinguished from each other by their textures and mineralogy, yet continuity between different drill holes is from time to time less obvious. Pegmatitic dikes have the same main mineral composition as granitic dikes, yet they have a very coarse grain size and one of the dikes also has a sulfide vein cutting it. Granitic dikes consist of quartz and differing amounts of both feldspars and have a medium-grained and heterogenic texture and pinkish or light grey colorization.

5. DRILL CORE AND ROCK-TYPE GEOCHEMISTRY

The samples were chosen for the geochemical analysis by their lithological locations in the intrusion and its vicinity as in addition to the aim of covering each rock type within the intrusion. In this chapter, the data is presented as drill core logs to visualize the change of the major- and selected trace-elements within each drill core, as well as typical geochemical composition and variation within each rock-type.

5.1. Drill core geochemistry

Chemical layering in DH 7 (Fig. 19) shows two major anomalies at 78.50 and 184.60–195.30 meters where Mg# ((MgO/40.304)/(MgO/40.304)+(FeOtot/71.846)*100), Cr, Ni and Zn show high values. The maximums likely indicate intrusion boundaries and the more stable amounts the middle of the intrusion. The amount of these elements is quite constant throughout most of DH 7, but show more inconsistency and scattering on the proposed boundaries. Also CaO seems to constantly rise towards the bottom from roughly 4 wt. -% to 20 wt. -% towards the end of the drill core.

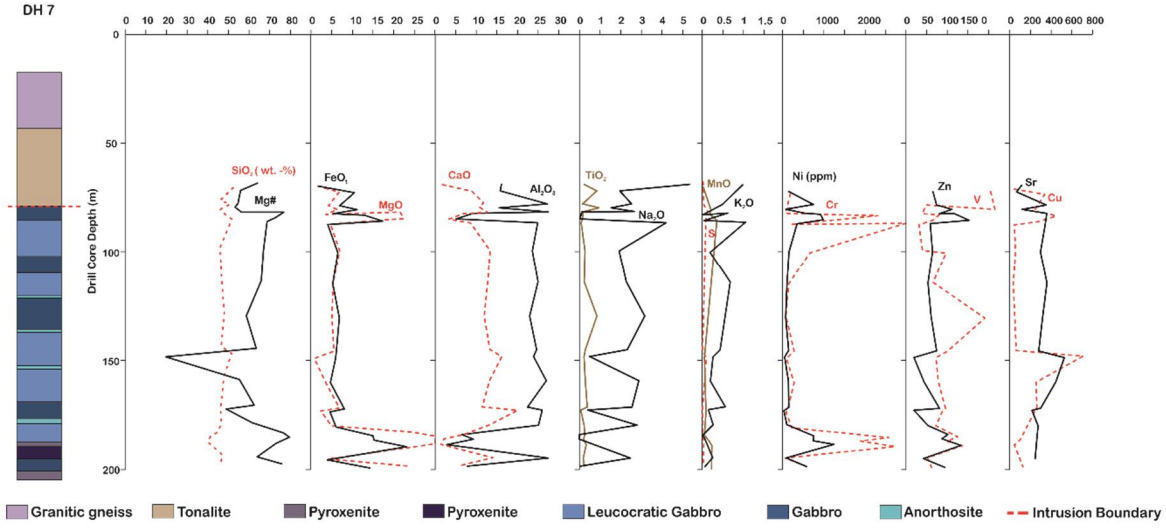

Figure 19. Chemical variation in drill core 7 based on whole-rock XRF-analyses. Lithology is given on the left and variation of selected elements and Mg# ((MgO/40.304)/(MgO/40.304)+ (FeO_{tot}/71.846)*100) in correlation with drill core depth on the right. Simplified lithology is given on the left for reference and in depth lithology in Figure 3.

In DH 8 trace- and major elements (Fig. 20) show sudden changes between the depths of 80–130 m. This indicates that the diorite cuts the intrusion. After this the element composition reverts to same as before it, and is thus likely to mark continuity of the intrusion and suggests that the diorite is a younger dike.

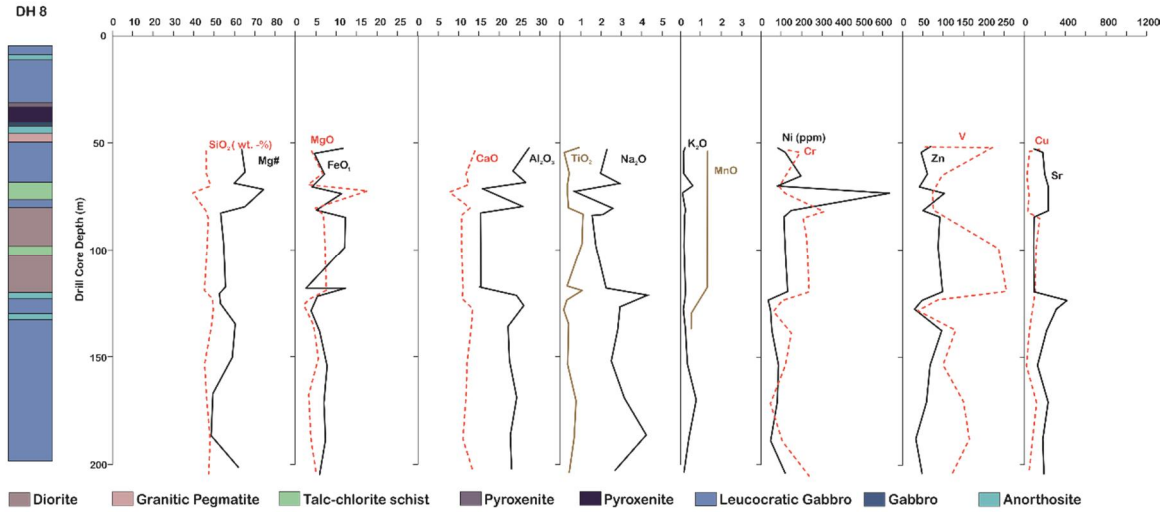

Figure 20. Chemical variation in drill core 8 based on drill core logs and whole-rock XRF-analyses. Lithology is given on the left and variation of selected elements and Mg# ((MgO/40.304)/(MgO/40.304)+(FeO_{tot}/71.846)*100) in correlation with drill core depth on the right. Simplified lithology is given on the left for reference and in depth lithology in Figure 3.

Geochemical layering (Fig. 21) on DH 10 shows an anomaly at 54.30 m where the diorite dike turns into a leucocratic gabbro. This fits with the “diorite-anomaly” in DH 8 as well as the compositions of the gabbros following it. After 113.70 m the composition changes as the gabbroic layers are followed by biotite paragneiss. This layer also shows sudden rise in potassium and manganese as on the top of DH 7. This is thus likely the bottom or a footwall contact with the biotite paragneiss and the intrusion around the depth of 115.00–147.50 m.

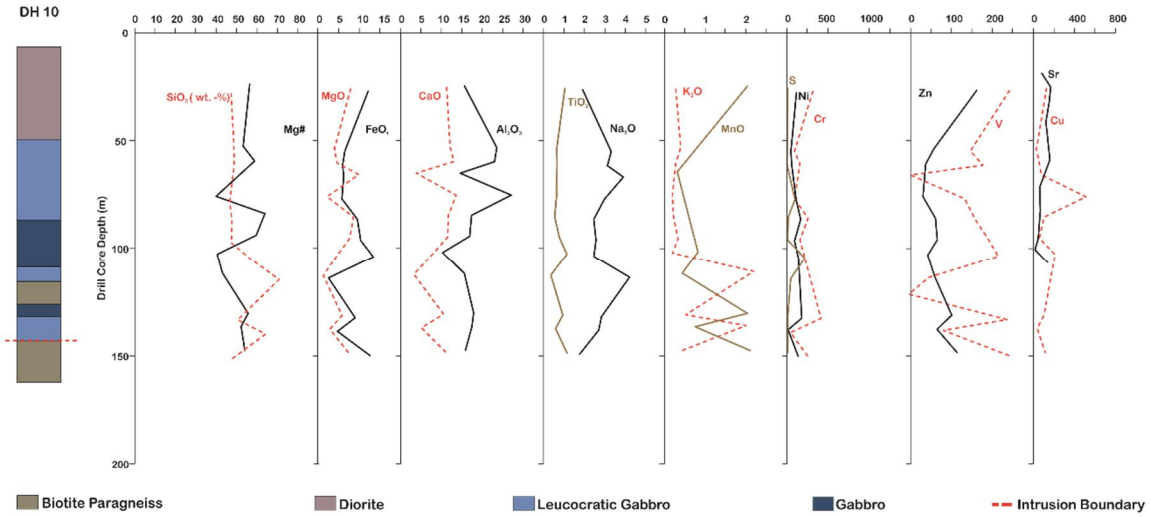

Figure 21. Chemical variation in drill core 10 based on drill core logs and whole-rock XRF-analyses. Lithology is given on the left and variation of selected elements and Mg# ((MgO/40.304)/(MgO/40.304)+(FeO_{tot}/71.846)*100) in correlation with drill core depth on the right. Simplified lithology is given on the left for reference and in depth lithology in Figure 3.

Major and trace-elements in DH 9 (Fig. 22) show similarity to DH 7 as the gabbroic layer and its edges at 18.30 m and 91.20 m. Barium and chromium are both low until the end of the pyroxenite layer. The shallower contact is likely the footwall contact of the intrusion.

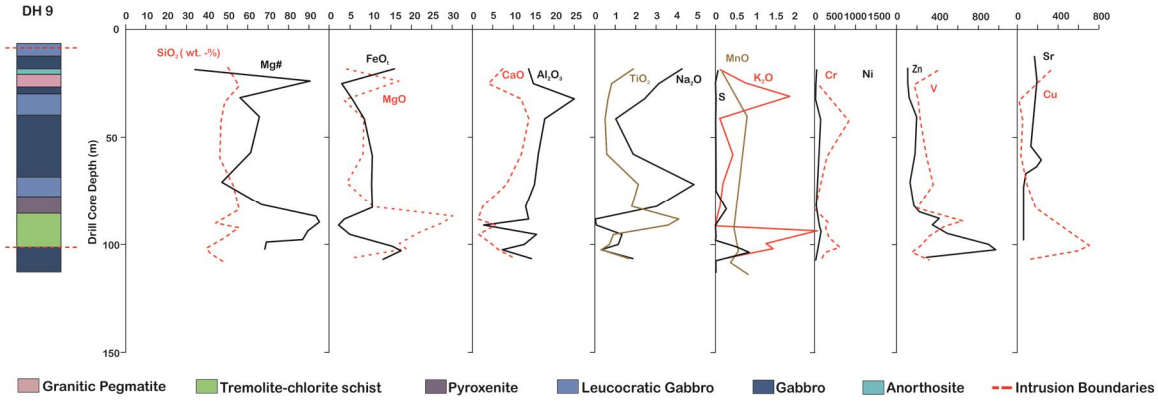

Figure 22. Chemical variation in drill core 9 based on drill core logs and whole-rock XRF-analyses. Lithology is given on the left and variation of selected elements and Mg# ((MgO/40.304)/(MgO/40.304)+(FeO_{tot}/71.846)*100) in correlation with drill core depth on the right. Simplified lithology is given on the left for reference and in depth lithology in Figure 3.

Chemical layering in DH 12 (Fig. 23) shows some variation in the major elements compared to DH 9, yet an anomaly similar to DH 9 is distinguishable. Mg# is mainly around 55.0 for the middle drill core, although it peaks strongly at 82.90 m rock type

changes from talc-chlorite schist into an amphibolite. Again, this likely marks the bottom of the intrusion.

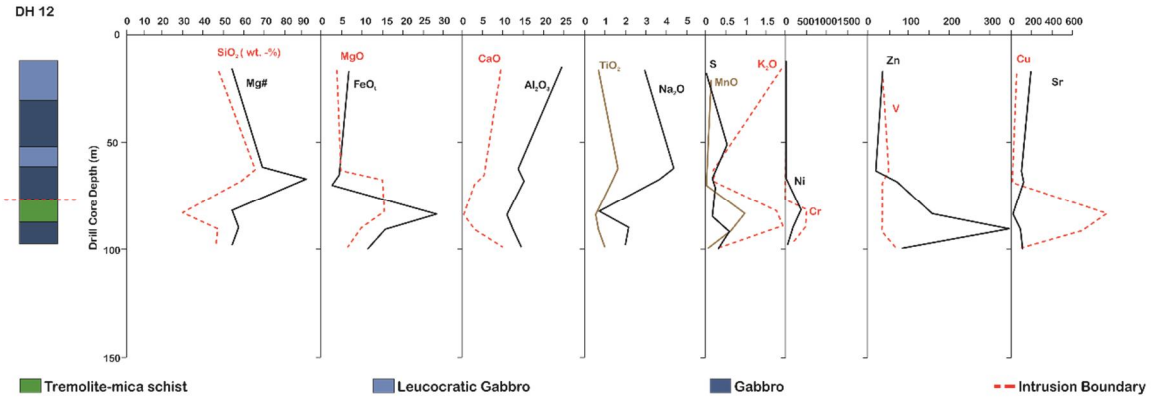

Figure 23. Chemical variation in drill core 12 based on drill core logs and whole-rock XRF-analyses. Lithology is given on the left and variation of selected elements and Mg# ((MgO/40.304)/(MgO/40.304)+(FeO_{tot}/71.846)*100) in correlation with drill core depth on the right. Simplified lithology is given on the left for reference and in depth lithology in Figure 3.

In DH 11 major and trace-elements (Fig. 24) show only little change during the diorite layer until 61.95 meters. The tremolite-mica and -chlorite schists shown make a stable level at 65–80 m on the Mg# and major elements. This anomaly is likely a thin elongation of the intrusion and marks its northernmost border. The bottom of DH 11 also shows the highest amount of sulfides compared to the other drill holes.

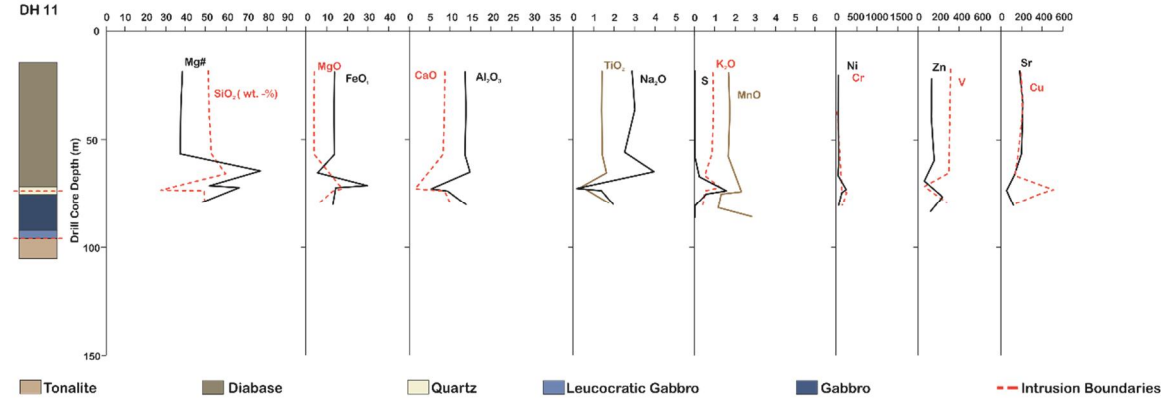

Figure 24. Chemical variation in drill core 11 based on drill core logs and whole-rock XRF-analyses. Lithology is given on the left and variation of selected elements and Mg# ((MgO/40.304)/(MgO/40.304)+(FeO_{tot}/71.846)*100) in correlation with drill core depth on the right. Simplified lithology is given on the left for reference and in depth lithology in Figure 3.

5.2. The mafic intrusion

5.2.1. Leucocratic gabbro

Leucocratic gabbros (Table 1) are derived from other gabbros by their Al_2O_3 content being more than 20 wt. -%. The composition of these rocks ranges between 44.70–50.00 wt. -% SiO_2, 0.10–0.87 wt. -% TiO_2, 21.70–27.50 wt. -% Al_2O_3, 4.19–8.32 wt. -% FeO_{tot}, 0.06–0.12 wt. -% MnO, 2.93–6.74 wt. -% MgO, 8.24–13.77 wt. -% CaO, 1.95–4.27 wt. -% Na_2O, 0.14–1.05 wt. -% K_2O and 0–0.15 wt. -% P_2O_5. Magnesium-number ((MgO/40.304)/(MgO/40.304)+(FeOtot/71.846)*100) ranges from 48.28 to 69.8. Sulfur ranges from none to 0.92 wt. -%.

5.2.2. Gabbro

Analyzed gabbros (Table 2) along the drill core samples show overall alike chemical composition, with the DH 7 72.50–72.75 m sample being more silica-rich than other samples. Gabbros have SiO_2 values of 46.80–51.00 wt. -%, 0.41–0.85 wt. -% TiO_2, 15.10–16.60 wt. -% Al_2O_3, 9.45–10.80 wt. -% FeO_{tot}, 0.14–0.15 wt. -% MnO, 6.76–8.02 wt. -% MgO, 8.49–11.38 wt. -% CaO, 1.99–2.57 wt. -% Na_2O, 0.19–0.29 wt. -% K_2O and 0.04–0.11 wt. -% P_2O_5. Mg-numbers range from 56.8–64.0. Sulfur is abundant in many samples and ranges from 0.12–0.33 wt. -%.

5.2.3. Anorthosite

Anorthositic rocks (Table 3) are analyzed from two spots in DH 7 and one spots in both DH's 8 and 10. Slightly more altered sample at the depth of 148.95 meters has 50.90 wt. -% SiO_2, 0.24 wt. -% TiO_2, 23.70 wt. -% Al_2O_3, 6.31 wt. -% FeO_{tot}, 0.04 wt. -% MnO, 0.73 wt. -% MgO, 15.89 wt. -% CaO, 0.73 wt. -% Na_2O, 0.22 wt. -% K_2O and 0.015 wt. -% P_2O_5. The non-altered sample at the depth of 173.40 meters has of 45.70 wt. -% SiO_2, 0.074 wt. -% TiO_2, 26.00 wt. -% Al_2O_3, 4.90 wt. -% FeO_{tot}, 0.08 wt. -% MnO, 2.26 wt. -% MgO, 19.81 wt. -% CaO, 0.47 wt. -% Na_2O, 0.11 wt. -% K_2O and 0.016 wt. -% P_2O_5. Anorthosite at stratigraphically lower depth has a higher magnesium-number at 49.2 compared to the stratigraphically higher level anorthosite at 19.5. The sample from DH 8 has 49.10 wt. -% SiO_2, 0.18 wt. -% TiO_2, 26.30 wt. -% Al_2O_3, 3.96 wt. -% FeO_{tot}, 0.06 wt. -% MnO, 2.15 wt. -% MgO, 13.43 wt. -% CaO, 2.91 wt. -% Na_2O, 0.13 wt. -% K_2O and 0.02 wt. -% P_2O_5. Sample from DH 10 has

49.50 wt. -% SiO_2, 0.61 wt. -% TiO_2, 26.60 wt. -% Al_2O_3, 5.90 wt. -% FeO_{tot}, 0.04 wt. -% MnO, 1.89 wt. -% MgO, 13.39 wt. -% CaO, 3.01 wt. -% Na_2O, 0.17 wt. -% K_2O and 0.08 wt. -% P_2O_5.

Table 1. Whole-rock composition for leucocratic gabbros within the intrusion. Mg# is based on (MgO/40.304)/(MgO/40.304)+(FeO_{tot}*0.85/71.846)*100.

	Leucocratic gabbro						
	DH 7	DH 7	DH 7	DH 7	DH 7	DH7	DH 7
	78.30-78.70	81.90-82.40	86.95-87.35	99.85-100.30	114.40-114.75	130.05-130.45	145.35-145.80
SiO_2 (wt. %)	45.10	46.20	50.00	44.30	45.40	46.60	45.20
TiO_2	0.17	0.16	0.10	0.28	0.25	0.87	0.30
Al_2O_3	27.00	27.40	24.20	22.90	24.50	22.40	24.10
Cr_2O_3	0.02	0.02	0.03	0.10	0.02	0.02	0.04
FeO_{tot}	7.17	5.63	4.23	6.73	5.60	7.14	6.39
MnO	0.08	0.10	0.06	0.11	0.08	0.10	0.10
MgO	4.23	3.59	4.65	6.74	5.29	4.92	5.45
CaO	11.59	12.46	8.24	13.22	12.82	11.51	12.85
Na_2O	2.59	2.77	4.22	1.96	2.34	3.21	2.37
K_2O	0.47	0.60	1.05	0.16	0.66	0.23	0.40
P_2O_5	<0.01375	<0.01375	<0.01375	0.02	0.04	0.04	0.02
SUM	98.41	98.93	96.77	96.52	96.99	97.03	97.23
Mg#	55.30	57.20	69.75	67.74	66.47	59.12	64.15
As (ppm)	<20	<20	<20	<20	<20	<20	<20
Ba	61	113	192	<30	59	<30	35
Bi	<30	<30	<30	<30	<30	<30	<30
Ce	<30	<30	31	<30	<30	<30	<30
Cl	153	187	189	172	135	172	167
Cr	115	127	196	668	156	126	290
Cu	750	387	43	59	33	<20	61
Ga	22	27	<20	<20	<20	<20	25
La	<30	<30	<30	<30	<30	<30	<30
Mo	<10	<10	<10	<10	<10	<10	<10
Nb	<7	<7	<7	<7	<7	<7	<7
Ni	749	546	353	158	112	81	153
Pb	<20	<20	30	<20	<20	<20	<20
Rb	37	49	79	22	54	17	35
S	9210	2921	309	324	147	<60	606
Sb	<100	<100	<100	<100	<100	<100	<100
Sc	<20	<20	<20	21	<20	21	<20
Sn	23	<20	24	21	<20	<20	<20
Sr	358	362	349	303	365	322	285
Th	21	11	14	23	19	13	15
U	<10	<10	<10	<10	<10	<10	<10
V	48	39	31	97	64	193	101
Y	7	<7	8	<7	<7	<7	12
Zn	75	82	60	65	54	61	74
Zr	31	25	30	25	32	47	30
C (wt. %)	<0.05	<0.05	0.08	<0.05	<0.05	<0.05	<0.05
S (wt. %)	-	-	-	-	-	-	-

Table 1 continued…

	Leucocratic gabbro								
	DH 7	DH 7	DH 7	DH 7	DH 8	DH 8	DH 8	DH 8	DH 8
	159.60-160.00	171.70-172.05	179.90-180.30	194.80-195.30	53.90-54.40	64.65-65.00	70.00-70.50	81.25-81.60	123.15-123.65
SiO_2 (wt. %)	45.90	44.70	45.20	46.30	45.40	45.10	47.90	45.70	48.90
TiO_2	0.30	0.39	0.24	0.20	0.21	0.44	0.36	0.40	0.34
Al_2O_3	26.20	21.70	24.50	27.10	27.50	23.40	26.70	25.90	24.40
Cr_2O_3	0.04	0.02	0.03	0.02	0.03	0.02	0.01	0.05	0.01
FeO_{tot}	4.86	8.32	6.31	4.19	4.66	7.14	4.25	5.30	5.55
MnO	0.06	0.12	0.11	0.07	0.07	0.12	0.07	0.09	0.08
MgO	3.36	6.74	4.87	3.88	3.97	6.54	3.04	4.83	2.93
CaO	12.66	10.94	12.71	13.65	13.77	11.93	12.51	12.57	10.88
Na_2O	2.90	2.57	2.84	2.54	2.28	1.95	2.89	2.56	4.27
K_2O	0.16	0.53	0.22	0.21	0.14	0.16	0.60	0.24	0.21
P_2O_5	0.03	<0.01375	<0.01375	0.02	0.02	0.04	0.03	0.02	0.03
SUM	96.47	96.04	97.03	98.18	98.06	96.83	98.35	97.66	97.61
Mg#	59.19	62.94	61.82	65.99	64.11	65.78	60.02	65.65	52.53
As (ppm)	<20	<20	<20	<20	<20	<20	<20	<20	<20
Ba	46	160	<30	<30	<30	<30	130	46	47
Bi	<30	<30	<30	<30	<30	<30	<30	<30	<30
Ce	<30	<30	<30	<30	<30	<30	<30	<30	<30
Cl	172	213	143	140	177	195	178	166	280
Cr	285	138	233	132	194	117	86	308	100
Cu	251	<20	<20	<20	47	30	<20	36	<20
Ga	24	<20	21	22	<20	<20	28	24	26
La	<30	<30	<30	<30	<30	<30	<30	<30	<30
Mo	<10	<10	<10	<10	<10	<10	<10	<10	<10
Nb	<7	<7	<7	<7	<7	<7	<7	<7	<7
Ni	150	157	108	96	113	193	77	141	28
Pb	<20	<20	<20	<20	<20	<20	<20	<20	<20
Rb	16	47	17	23	18	21	53	33	14
S	1716	229	<60	<60	101	269	132	230	78
Sb	<100	<100	<100	<100	<100	<100	<100	<100	<100
Sc	<20	<20	<20	<20	<20	<20	<20	<20	<20
Sn	<20	<20	<20	25	<20	<20	<20	24	20
Sr	451	305	278	250	178	202	240	240	422
Th	21	12	14	18	12	10	15	12	24
U	<10	<10	<10	<10	<10	<10	<10	<10	<10
V	77	96	73	50	57	98	84	74	89
Y	7	<7	9	<7	<7	11	13	<7	11
Zn	44	82	54	43	47	61	42	51	49
Zr	33	34	27	22	22	30	45	29	37
C (wt. %)	<0.05	<0.05	<0.05	<0.05	<0.05	0.08	<0.05	0.06	<0.05
S (wt. %)	-	-	-	-	-	-	-	-	-

Table 1 continued…

	Leucocratic gabbro						
	DH 8	DH 8	DH 8	DH 8	DH 10	DH 10	DH 12
	153.50-153.95	170.70-171.10	188.15-188.55	203.90-204.30	54.30-54.80	60.90-61.40	16.85-17.35
SiO_2 (wt. %)	45.00	45.90	47.50	46.80	47.90	48.10	47.00
TiO_2	0.37	0.78	0.68	0.45	0.63	0.64	0.63
Al_2O_3	22.50	24.30	23.00	23.20	23.50	22.90	24.50
Cr_2O_3	0.02	0.01	0.02	0.03	0.01	0.02	0.01
FeO_{tot}	7.90	7.04	7.41	5.97	6.70	6.13	6.88
MnO	0.12	0.07	0.07	0.10	0.09	0.06	0.07
MgO	5.48	3.22	3.30	4.59	3.70	4.28	3.82
CaO	12.11	11.61	11.02	13.45	12.09	12.99	9.71
Na_2O	2.47	3.12	4.18	2.64	3.37	3.18	3.00
K_2O	0.33	0.76	0.40	0.16	0.37	0.26	1.91
P_2O_5	0.03	0.15	0.02	0.07	0.03	0.01	0.07
SUM	96.32	96.95	97.59	97.45	98.40	98.57	97.59
Mg#	59.26	48.97	48.28	61.74	53.65	59.43	53.79
As (ppm)	<20	<20	<20	<20	<20	<20	<20
Ba	45	231	91	<30	77	52	112
Bi	<30	<30	<30	<30	<30	<30	<30
Ce	<30	35	<30	<30	<30	<30	<30
Cl	194	171	272	148	217	158	220
Cr	114	41	104	233	66	132	35
Cu	26	110	<20	46	27	52	59
Ga	25	23	30	28	20	<20	29
La	<30	<30	<30	<30	<30	<30	<30
Mo	<10	<10	<10	<10	<10	<10	<10
Nb	<7	<7	<7	<7	<7	<7	<7
Ni	78	72	37	110	44	48	46
Pb	<20	<20	<20	<20	<20	<20	<20
Rb	36	46	31	13	20	14	115
S	239	2367	176	860	489	302	2318
Sb	<100	<100	<100	<100	<100	<100	<100
Sc	<20	22	21	<20	<20	21	<20
Sn	<20	<20	<20	<20	<20	<20	22
Sr	125	237	184	194	244	182	190
Th	24	<10	16	16	11	<10	<10
U	<10	<10	<10	<10	<10	<10	<10
V	100	152	167	125	148	177	139
Y	7	14	8	10	7	18	15
Zn	68	59	33	49	54	36	37
Zr	13	43	46	30	49	39	39
C (wt. %)	0.06	<0.05	<0.05	<0.05	<0.05	<0.05	<0.05
S (wt. %)	-	-	-	-	-	-	-

Table 2. Whole-rock composition for gabbros within the intrusion. Mg# is based on (MgO/40.304)/(MgO/40.304)+(FeO_{tot}*0.85/71.846)*100.

	Gabbro			Gabbropegmatite
	DH 7	DH 10	DH 10	DH 8
	72.50-72.75	86.10-86.60	96.00-96.50	137.55-138.00
SiO_2 (wt. %)	50.20	46.90	46.80	47.70
TiO_2	0.85	0.51	0.74	0.41
Al_2O_3	15.10	17.10	16.60	22.30
Cr_2O_3	0.03	0.03	0.02	0.02
FeO_{tot}	10.80	9.45	10.17	5.98
MnO	0.14	0.15	0.14	0.09
MgO	6.76	8.02	7.11	4.42
CaO	8.49	11.38	11.18	13.13
Na_2O	1.99	2.48	2.57	2.78
K_2O	0.20	0.19	0.29	0.24
P_2O_5	0.11	0.04	0.05	0.05
SUM	94.67	96.24	95.68	97.12
Mg#	56.77	64.03	59.46	60.77
As (ppm)	<20	<20	<20	<20
Ba	53	34	50	<30
Bi	<30	<30	<30	<30
Ce	<30	<30	<30	<30
Cl	286	238	392	123
Cr	194	219	134	142
Cu	333	98	52	49
Ga	27	<20	20	<20
La	<30	<30	<30	<30
Mo	<10	<10	<10	<10
Nb	<7	<7	<7	<7
Ni	150	151	78	46
Pb	<20	<20	<20	<20
Rb	11	<10	14	17
S	3287	1452	1262	270
Sb	<100	<100	<100	<100
Sc	23	26	32	30
Sn	<20	<20	<20	<20
Sr	69	111	118	224
Th	21	<10	<10	19
U	<10	<10	<10	<10
V	207	158	191	132
Y	15	<7	16	7
Zn	66	59	63	96
Zr	80	29	38	36
C (wt. %)	<0.05	<0.05	<0.05	<0.05
S (wt. %)	-	-	-	-

5.2.4. Pyroxenite

Two pyroxenites (Table 3) are analyzed from DH 7 and they yield similar results: 44.50–44.60 wt. -% SiO_2, 0.24–0.27 wt. -% TiO_2, 6.14–7.46 wt. -% Al_2O_3, 14.67–15.12 wt. -% FeO_{tot}, 0.131–0.225 wt. -% MnO, 23.10–24.50 wt. -% MgO, 5.69–6.95 wt. -% CaO, 0.06–0.09 wt. -% Na_2O, 0.01 wt. -% K_2O and 0–0.03 wt. -% P_2O_5. Pyroxenites from DH 7 have magnesium-numbers of 77.3. and 76.8 respectively.

5.2.5. Peridotite

Two homogenous peridotite samples (Table 3) were analyzed from DH 7 at the depth of 186.70 m, with composition of: 40.30 wt. -% SiO_2, 0.22 wt. -% TiO_2, 8.88 wt. -% Al_2O_3, 0.19 wt. -% Cr_2O_3, 17.20 wt. -% FeO_{tot}, 0.17 wt. -% MnO, 29.60 wt. -% MgO, 2.08 wt. -% CaO, 0.00 wt. -% Na_2O, 0.02 wt. -% P_2O_5. Second sample has somewhat more ferrous content at 39.10 wt. -% SiO_2, 0.35 wt. -% TiO_2, 2.41 wt. -% Al_2O_3, 25.80, 0.19 wt. -% Cr_2O_3wt. -% , 25.80 FeO_{tot}, 0.081 wt. -% MnO, 30.00 wt. -% MgO, 1.32 wt. -% CaO, 0.00 wt. -% Na_2O, 0.00 wt. -% K_2O and 0.014 wt. -% P_2O_5The samples have Mg-numbers of 80.0 and 73.1.

5.2.6. Chlorite and talc-bearing schists

Three tremolite-chlorite schists (Table 4) are analyzed from DH 7 and two from DH9 (25.65m and 82.90 m). Samples in DH 7 have values ranging from 43.20–48.30 wt. -% SiO_2, 0.15–0.95 wt. -% TiO_2, 4.64–14.70 wt. -% Al_2O_3, 11.34–17.46 wt. -% FeO_{tot}, 0.18–0.36 wt. -% MnO, 6.35–22.30 wt. -% MgO, 3.16–10.59 wt.- % CaO, 0.08–1.55 wt. -% Na_2O, 0.01–0.23 wt. -% K_2O and 0.00–0.12 wt. -% P_2O_5. Sample in DH 9 has 54.30 wt. -% SiO_2, 0.78 wt. -% TiO_2, 14.20 wt. -% Al_2O_3, 3.00 wt. -% FeO_{tot}, 0.03 wt. -% MnO, 16.10 wt. -% MgO, 3.67 wt.- % CaO, 3.01 wt. -% Na_2O, 0.75 wt. -% K_2O, and 0.23 wt. -% P_2O_5. The Mg# for samples in DH 7 ranges from 54.01–77.68 and for DH 9 it is 91.85.

Two talc-chlorite schists are analyzed from DH 9 and one from DH 11 (Table 4). There is a somewhat notable variance within DH 9 as the samples have: 43.60–54.70 wt. -% SiO_2, 3.54–3.93 wt. -% TiO_2, 2.52–13.20 wt. -% Al_2O_3, 0.04–0.05 Cr_2O_3, 2.36–3.58 wt. -% FeO_{tot}, 0.10–0.11 wt. -% MnO, 28.00–30.30 wt. -% MgO, 1.25–5.57 wt. -% CaO, 0.05–0.11 Na_2O, 0.93–2.46 wt. -% P_2O_5. These samples have Mg#'s of 94.7 for the

stratigraphically higher sample and 96.1 for the lower. The sample in DH 11 has 54.70 wt. -% SiO_2, 1.58 wt. -% TiO_2, 14.60 wt. -% Al_2O_3, 6.30 wt. -% FeO_{tot}, 0.02 wt. -% MnO, 9.34 wt. -% MgO, 3.91 wt. -% NaO, 0.44 wt. -% K_2O, 0.28 wt. -% P_2O_5, and Mg# of 75.7.

Table 3. Whole-rock composition for pyroxenites, anorthosites and peridotites within the intrusion. Mg# is based on (MgO/40.304)/(MgO/40.304)+(FeO_{tot}*0.85/71.846)*100.

	Anorthosite	Anorthosite	Anorthosite	Anorthosite	Pyroxenite	Pyroxenite	Peridotite	Peridotite
	DH 7	DH 7	DH 8	DH 10	DH 7	DH 7	DH 7	DH 7
	148.45-148.95	173.00-173.40	127.90-128.50	76.60-76.95	184.00-184.60	198.50-199.00	186.30-186.70	188.90-189.20
SiO_2 (wt. %)	50.90	45.70	49.10	45.90	44.50	44.60	40.30	39.10
TiO_2	0.24	0.07	0.18	0.61	0.27	0.24	0.22	0.35
Al_2O_3	23.70	26.00	26.30	26.60	6.14	7.46	8.88	2.41
Cr_2O_3	0.01	0.01	0.01	0.01	0.37	0.09	0.27	0.40
FeOtot	6.31	4.90	3.96	5.90	15.12	14.67	15.48	23.22
MnO	0.04	0.08	0.06	0.04	0.13	0.23	0.17	0.23
MgO	0.73	2.26	2.15	1.89	24.50	23.10	29.60	30.00
CaO	15.89	19.81	13.43	13.39	6.95	5.69	2.08	1.32
Na_2O	0.56	0.47	2.91	3.01	0.06	0.09	0.05	<0.0337
K_2O	0.22	0.11	0.13	0.17	0.01	0.01	0.01	<30614
P_2O_5	0.02	0.02	0.02	0.08	<0.01375	0.03	0.02	0.01
SUM	98.62	99.44	98.24	97.61	98.04	96.20	97.07	97.04
Mg#	19.53	49.15	53.25	40.17	77.27	76.76	80.04	73.05
As (ppm)	<20	<20	<20	<20	<20	<20	<20	<20
Ba	<30	<30	<30	50	<30	<30	<30	<30
Bi	<30	<30	<30	<30	<30	<30	<30	<30
Ce	<30	<30	<30	<30	<30	<30	<30	<30
Cl	93	81	140	172	65	85	192	447
Cr	102	94	57	75	2557	641	1875	2704
Cu	705	<20	<20	505	<20	112	<20	30
Ga	28	36	28	27	<20	<20	<20	<20
La	<30	<30	<30	<30	<30	<30	<30	<30
Mo	<10	<10	<10	<10	<10	<10	<10	<10
Nb	<7	<7	<7	<7	<7	<7	<7	<7
Ni	57	39	38	99	764	600	744	1217
Pb	<20	<20	<20	<20	<20	<20	<20	<20
Rb	24	18	18	<10	13	16	16	<10
S	8860	108	221	10850	108	1487	154	826
Sb	<100	<100	<100	<100	<100	<100	<100	<100
Sc	<20	<20	<20	<20	<20	<20	20	<20
Sn	33	<20	<20	23	21	35	<20	36
Sr	533	220	318	272	<10	<10	<10	<10
Th	15	16	14	<10	21	17	15	18
U	<10	<10	<10	<10	<10	<10	<10	<10
V	73	89	39	133	126	61	99	137
Y	<7	<7	<7	16	8	<7	<7	<7
Zn	20	21	30	28	102	94	88	134
Zr	39	14	24	69	<10	17	11	19
C (wt. %)	0.05	<0.05	<0.05	<0.05	<0.05	<0.05	0.08	0.07
S (wt. %)	-	-	-	-	-	-	-	-

Table 4. Whole-rock composition for tremolite-chlorite, chlorite-talc and tremolite-talc schists. Mg# is based on (MgO/40.304)/(MgO/40.304)+(FeO_{tot}*0.85/71.846)*100.

	Tremolite-chlorite	Tremolite-chlorite	Tremolite-chlorite-talc	Tremolite-talc schist	Chlorite-biotite-	Chlorite-talc schist
	DH 7	DH 9	DH 9	DH 12	DH 11	DH 8
	85.20-85.60	25.15-25.65	82.40-82.90	68.00-69.00	72.50-73.00	72.95-73.35
SiO_2 (wt. %)	47.50	53.40	55.00	57.80	27.10	39.30
TiO_2	0.15	0.78	1.76	1.33	0.19	0.33
Al_2O_3	4.64	14.20	12.70	15.20	4.90	15.50
Cr_2O_3	0.44	0.02	0.00	<0.002	0.02	0.02
FeO_{tot}	17.46	3.00	10.80	3.00	29.87	11.43
MnO	0.36	0.03	0.09	0.03	0.07	0.17
MgO	22.30	16.10	10.80	14.80	14.70	16.40
CaO	3.16	3.67	2.46	3.12	0.92	7.80
Na_2O	0.08	3.01	3.00	3.72	0.12	0.68
K_2O	0.01	0.75	0.11	0.19	1.22	0.09
P_2O_5	<0.01375	0.23	0.25	0.15	0.22	0.03
SUM	96.10	95.19	96.97	99.33	79.34	91.74
Mg#	72.82	91.85	67.72	91.20	50.79	75.06
As (ppm)	<20	<20	<20	<20	<20	<20
Ba	<30	70	53	48	69	<30
Bi	<30	<30	<30	<30	<30	<30
Ce	<30	57	52	51	<30	<30
Cl	67	223	102	87	81	175
Cr	3029	142	20	<20	136	122
Cu	273	<20	184	27	501	<20
Ga	<20	<20	23	<20	30	21
La	<30	<30	<30	<30	<30	<30
Mo	<10	<10	<10	<10	<10	<10
Nb	<7	<7	9	<7	<7	<7
Ni	988	67	68	53	237	636
Pb	<20	27	<20	25	<20	<20
Rb	16	52	20	11	101	19
S	3284	128	29430	1384	151400	<60
Sb	<100	<100	<100	<100	<100	<100
Sc	<20	32	32	<20	<20	<20
Sn	27	<20	<20	25	34	<20
Sr	<10	172	70	119	<10	<10
Th	25	22	21	14	13	15
U	<10	<10	<10	<10	18	<10
V	64	121	148	140	62	75
Y	<7	31	49	36	<7	<7
Zn	153	30	57	75	221	103
Zr	<10	137	252	252	39	21
C (wt. %)	<0.05	0.07	0.05	<0.05	<0.05	<0.05
S (wt. %)	-	-	-	-	22.5	-

Table 4 continued…

	Talc-chlorite	Talc-chlorite	Talc-chlorite-	Tremolite-biotite	Tremolite-chlorite	Tremolite-chlorite
	DH 9	DH 9	DH 11	DH 12	DH 7	DH 7
	88.40-88.90	91.20-91.70	66.30-66.60	90.30-91.30	80.20-80.50	82.70-83.05
SiO_2 (wt. %)	43.60	54.70	57.90	46.10	48.30	43.20
TiO_2	3.93	3.54	1.58	0.67	0.95	0.18
Al_2O_3	13.20	2.53	14.60	12.60	14.70	8.42
Cr_2O_3	0.05	0.04	<0.002	0.08	0.02	0.33
FeO_{tot}	3.58	2.36	6.30	15.75	11.34	12.96
MnO	0.10	0.11	0.02	0.07	0.21	0.18
MgO	30.30	28.00	9.34	9.76	6.35	21.50
CaO	1.25	5.57	3.72	2.99	10.59	6.42
Na_2O	0.05	0.11	3.91	2.20	1.55	0.16
K_2O	0.00	0.00	0.44	1.93	0.23	0.03
P_2O_5	0.93	2.46	0.28	0.10	0.12	<0.01375
SUM	96.99	99.43	98.09	92.24	94.35	93.37
Mg#	94.66	96.14	75.67	56.52	54.01	77.68
As (ppm)	<20	<20	<20	<20	<20	<20
Ba	107	104	90	262	31	<30
Bi	<30	<30	<30	<30	<30	<30
Ce	59	74	36	32	<30	<30
Cl	103	185	121	186	332	97
Cr	328	278	<20	515	146	2292
Cu	<20	<20	128	686	226	439
Ga	29	<20	<20	<20	27	<20
La	<30	<30	<30	<30	<30	<30
Mo	<10	<10	<10	<10	<10	<10
Nb	42	60	<7	<7	<7	<7
Ni	126	159	40	204	84	920
Pb	<20	<20	24	<20	<20	<20
Rb	17	<10	37	121	17	10
S	<60	130	21660	63710	1169	5495
Sb	<100	<100	<100	<100	<100	<100
Sc	54	41	36	22	27	<20
Sn	<20	25	20	<20	<20	26
Sr	<10	<10	123	87	116	<10
Th	34	69	<10	11	15	12
U	<10	<10	<10	<10	<10	<10
V	589	415	295	136	217	80
Y	190	288	26	15	28	<7
Zn	183	150	68	360	112	118
Zr	317	178	144	107	86	<10
C (wt. %)	0.06	<0.05	<0.05	0.06	<0.05	0.05
S (wt. %)	-	-	-	7.91	-	-

5.3. Rocks surrounding the intrusion

5.3.1. Biotite paragneiss

Biotite paragneiss (Table 5) was analyzed from DH 10 from the depth of 138.55 meters. It consists of 63.00 wt. -% SiO_2, 0.56 wt. -% TiO_2, 17.40 wt. -% Al_2O_3, 2.09–5.37 wt. -% FeO_{tot}, 0.06 wt. -% MnO, 2.52 wt. -% MgO, 4.97 wt. -% CaO, 2.74 wt. -% Na_2O, 2.00 wt. -% K_2O, 0.19 wt. -% P_2O_5 and 1.46 wt. -% S.

5.3.2. Tonalite

Tonalite sample (Table 5) was analyzed from DH 10 at the depth of 114.10 m. Tonalite has values for 69.50 wt. -% SiO_2, 0.34 wt. -% TiO_2, 15.80 wt. -% Al_2O_3, 2.78 wt. -% FeO_{tot}, 0.03 wt. -% MnO, 1.01 wt. -% MgO, 3.20 wt. -% CaO, 4.25 wt. -% Na_2O, 2.19 wt. -% K_2O and 0.15 wt. -% P_2O_5. The sample has 4.50 wt. -% S and its Mg# is 43.2.

5.3.3. Biotite schist

Three biotite schists (Table 6) are analyzed from DH 9 and one from DH 12. These samples have ranging amounts of 29.59–47.80 wt. -% SiO_2, 0.31–0.87 wt. -% TiO_2, 6.76–15.30 wt. -% Al_2O_3, 4.97–28.25 wt. -% FeO_{tot}, 0.05–0.21 wt. -% MnO, 15.40–22.40 wt. -% MgO, 0.48–5.95 wt. -% CaO, 0.33–1.32 wt. -% Na_2O, 1.26–2.54 wt. -% K_2O and 0.07–0.30 wt. -% P_2O_5. Mg # ranges between 53.34 and 90.44. Sulfur is high in DH 12 and two samples in DH9 at 5.36–9.89 wt. -%.

5.3.4. Amphibolite

Ten amphibolite samples (Table 6) are analyzed from DH's 8–12. These samples have 29.59–45.30–56.00 wt. -% SiO_2, 0.46–1.86 wt. -% TiO_2, 9.60–16.90 wt. -% Al_2O_3, 8.84–15.75 wt. -% FeO_{tot}, 0.06–0.30 wt. -% MnO, 4.09–12.80 wt. -% MgO, 7.27–13.01 wt. -% CaO, 0.35–0.47 wt. -% Na_2O, 0.11–0.47 wt. -% K_2O, 0.03–0.62 wt. -% P_2O_5. Mg # ranges between 35.3 and 66.7. Sulfur ranges between 0.04–5.73 wt. -% and is highest in DH's 10 and 11.

5.3.5 Mica schist

Two mica schists (Table 6) are analyzed from DH 7 at depths of 32.20 and 69.75 m. The latter has 48.00 wt. -% SiO_2, 0.64 wt. -% TiO_2, 24.80 wt. -% Al_2O_3, 5.58 wt. -%

FeO_{tot}, 0.06 wt. -% MnO, 3.57 wt. -% MgO, 11.59 wt. -% CaO, 2.44 wt. -% Na_2O, 1.86 wt. -% K_2O, 0.05 wt. -% K_2O. The sample at the stratigraphically higher level at 32.20 m has 71.80 wt. -% SiO_2, 0.24 wt. -% TiO_2, 15.80 wt. -% Al_2O_3, 1.87 wt. -% FeO_{tot}, 0.01 wt. -% MnO, 1.68 wt. -% MgO, 1.78 wt. -% CaO, 5.45 wt. -% Na_2O, 0.98 wt. -% K_2O, 0.06 wt. -% K_2O.

Table 5. Whole-rock composition for tonalite, dikes, biotite paragneiss, diabase and diorite outside of the intrusion. Mg# is based on (MgO/40.304)/(MgO/40.304)+(FeO_{tot}*0.85/71.846)*100.

	Tonalite	Biotite paragneiss	Diabase	Diabase	Diabase	Diabase	Diabase
	DH 10	DH 10	DH 8	DH 8	DH 8	DH 10	DH 10
	113.70-114.10	138.55-139.15	84.30-84.65	98.70-99.10	119.25-119.60	26.60-27.00	149.80-150.25
SiO_2 (wt. %)	69.50	63.00	46.50	46.10	44.90	46.60	46.60
TiO_2	0.34	0.56	1.08	1.05	1.08	0.98	1.10
Al_2O_3	15.80	17.40	15.70	15.60	15.60	15.30	15.70
Cr_2O_3	<0.002	0.00	0.03	0.03	0.03	0.04	0.03
FeO_{tot}	2.78	4.83	12.24	12.15	12.06	11.79	12.42
MnO	0.03	0.06	0.19	0.18	0.20	0.19	0.20
MgO	1.01	2.52	6.66	7.00	7.28	7.45	6.92
CaO	3.20	4.97	10.75	10.79	11.12	11.13	10.74
Na_2O	4.25	2.74	1.55	1.72	2.21	1.94	1.82
K_2O	2.19	2.00	0.20	0.18	0.24	0.26	0.32
P_2O_5	0.15	0.19	0.11	0.11	0.12	0.10	0.11
SUM	99.25	98.28	95.01	94.90	94.84	95.77	95.96
Mg#	43.24	52.24	53.30	54.72	55.87	57.00	53.89
As (ppm)	<20	58	<20	<20	<20	<20	<20
Ba	750	612	<30	<30	37	<30	50
Bi	<30	<30	<30	<30	<30	<30	<30
Ce	54	65	<30	<30	<30	<30	<30
Cl	163	247	339	347	355	373	287
Cr	<20	27	212	223	239	248	218
Cu	<20	29	128	106	98	119	139
Ga	23	<20	27	<20	<20	<20	23
La	<30	34	<30	<30	<30	<30	<30
Mo	<10	<10	<10	<10	<10	<10	<10
Nb	<7	<7	<7	<7	<7	<7	<7
Ni	<20	<20	103	112	121	107	121
Pb	26	22	<20	<20	<20	<20	<20
Rb	85	96	17	16	14	22	15
S	4503	1458	1407	955	898	1082	1530
Sb	<100	<100	<100	<100	<100	<100	<100
Sc	<20	<20	39	33	45	42	32
Sn	<20	20	<20	23	26	25	21
Sr	303	462	98	96	98	103	114
Th	10	15	17	25	17	10	15
U	<10	<10	<10	<10	<10	<10	<10
V	48	81	254	239	259	242	243
Y	13	19	17	16	22	15	19
Zn	56	62	92	88	98	159	110
Zr	116	141	67	63	77	60	70
C (wt. %)	<0.05	<0.05	0.06	<0.05	<0.05	<0.05	<0.05
S (wt. %)	-	-	-	-	-	-	-

Table 5 continued…

	Diorite	Diorite	Diorite	Diorite	Diorite
	DH 9	DH 11	DH 11	DH 11	DH 12
	72.00-72.30	18.60-19.05	36.15-36.55	56.50-56.90	63.35-63.85
SiO_2 (wt. %)	52.20	49.80	50.00	51.00	64.20
TiO_2	2.09	1.39	1.37	1.41	1.58
Al_2O_3	15.00	13.80	14.00	13.80	13.80
Cr_2O_3	<0.002	<0.002	0.00	<0.002	<0.002
FeO_{tot}	10.53	14.22	13.95	14.22	4.58
MnO	0.07	0.20	0.19	0.19	0.03
MgO	4.61	4.07	3.81	3.96	4.79
CaO	8.13	8.42	8.31	8.03	5.42
Na_2O	4.82	2.80	2.93	2.48	4.41
K_2O	0.19	0.82	0.88	0.81	0.18
P_2O_5	0.33	0.25	0.25	0.29	0.26
SUM	97.97	95.76	95.68	96.19	99.25
Mg#	47.87	37.51	36.42	36.87	68.68
As (ppm)	<20	<20	<20	<20	<20
Ba	75	245	310	410	114
Bi	<30	<30	<30	<30	<30
Ce	54	34	56	44	51
Cl	263	352	469	649	163
Cr	<20	<20	24	<20	<20
Cu	103	194	211	164	<20
Ga	25	25	25	<20	25
La	<30	<30	<30	<30	<30
Mo	<10	<10	<10	<10	<10
Nb	<7	<7	<7	<7	10
Ni	<20	44	42	49	<20
Pb	<20	<20	<20	<20	28
Rb	14	34	38	39	14
S	3451	1028	912	881	2495
Sb	<100	<100	<100	<100	<100
Sc	30	25	33	30	<20
Sn	<20	26	<20	<20	<20
Sr	65	177	207	194	98
Th	25	<10	15	15	16
U	25	<10	<10	<10	<10
V	305	306	300	286	201
Y	52	33	29	32	57
Zn	41	132	128	150	21
Zr	192	134	126	136	262
C (wt. %)	<0.05	<0.05	<0.05	<0.05	<0.05
S (wt. %)	-	-	-	-	-

Table 6. Whole-rock composition for amphibolites and mica- and biotite schists within the intrusion. Mg# is based on (MgO/40.304)/(MgO/40.304)+(FeO_{tot}*0.85/71.846)*100.

	Amphibolite DH 8 52.10-52.50	Amphibolite DH 9 18.30-18.80	Amphibolite DH 9 41.50-41.90	Amphibolite DH 9 57.90-58.40	Amphibolite DH 9 106.80-107.15	Amphibolite DH 10 103.70-104.30	Amphibolite DH 10 132.25-132.80
SiO_2 (wt. %)	48.20	50.10	46.30	45.70	47.20	56.00	49.70
TiO_2	0.94	1.86	0.46	0.56	1.59	1.11	0.90
Al_2O_3	14.50	13.60	16.90	15.40	13.80	10.50	17.60
Cr_2O_3	0.02	<0.002	0.12	0.05	0.02	<0.002	0.05
FeOtot	11.79	15.75	8.84	10.71	13.41	13.32	8.94
MnO	0.19	0.06	0.15	0.15	0.19	0.07	0.19
MgO	6.04	4.09	8.45	8.49	5.98	4.36	5.37
CaO	10.07	7.27	13.01	11.28	9.83	7.83	10.23
Na_2O	2.10	4.26	1.00	1.83	1.82	2.51	2.84
K_2O	0.22	0.12	0.11	0.44	0.30	0.17	0.49
P_2O_5	0.12	0.62	0.03	0.04	0.31	0.81	0.08
SUM	94.18	97.73	95.37	94.64	94.46	96.67	96.38
Mg#	51.80	35.26	66.73	62.45	48.33	40.71	55.76
As (ppm)	<20	<20	<20	<20	<20	<20	130
Ba	<30	70	<30	<30	106	64	85
Bi	<30	<30	<30	<30	<30	<30	<30
Ce	<30	74	<30	<30	<30	142	<30
Cl	345	287	153	241	222	246	196
Cr	132	<20	826	311	147	<20	339
Cu	145	327	60	42	102	207	71
Ga	<20	<20	<20	<20	<20	28	23
La	<30	<30	<30	<30	<30	<30	<30
Mo	<10	<10	<10	<10	<10	<10	<10
Nb	<7	<7	<7	<7	<7	<7	<7
Ni	76	84	162	140	77	123	159
Pb	<20	<20	<20	<20	<20	<20	<20
Rb	15	12	14	25	14	<10	31
S	1321	8287	402	990	3010	21270	1326
Sb	<100	<100	<100	<100	<100	<100	<100
Sc	34	29	43	33	23	<20	38
Sn	23	<20	<20	21	<20	23	22
Sr	89	79	125	162	142	90	198
Th	24	17	23	14	14	16	<10
U	<10	12	<10	<10	<10	<10	<10
V	223	347	181	238	263	214	239
Y	14	57	15	21	30	115	23
Zn	71	30	73	64	120	40	98
Zr	84	160	17	28	132	326	59
C (wt. %)	<0.05	<0.05	<0.05	<0.05	<0.05	<0.05	<0.05
S (wt. %)	-	-	-	-	-	-	-

Table 6 continued…

	Amphibolite DH 11 73.50-74.00	Amphibolite DH 11 79.90-80.40	Amphibolite DH 12 98.80-99.40	Mica schist DH 7 69.35-69.75	Mica schist DH 9 32.20-32.70
SiO_2 (wt. %)	47.60	48.00	45.30	71.80	48.00
TiO_2	0.53	1.63	0.92	0.24	0.64
Al_2O_3	9.60	14.10	14.10	15.80	24.80
Cr_2O_3	0.04	0.02	0.03	<0.002	<0.002
FeOtot	14.31	13.59	11.52	1.87	5.58
MnO	0.30	0.20	0.18	0.01	0.06
MgO	12.80	5.71	6.28	1.68	3.57
CaO	8.32	10.09	9.70	1.78	11.59
Na_2O	1.34	1.93	2.03	5.45	2.44
K_2O	0.47	0.35	0.37	0.98	1.86
P_2O_5	0.08	0.29	0.07	0.06	0.05
SUM	95.38	95.91	90.50	99.67	98.58
Mg#	65.23	46.85	53.35	65.31	57.30
As (ppm)	<20	24	1627	<20	<20
Ba	60	109	57	297	155
Bi	<30	<30	<30	<30	<30
Ce	<30	33	<30	41	<30
Cl	89	265	266	158.00	131
Cr	243	159	173	<20	<20
Cu	393	113	105	34	24
Ga	25	27	24	<20	24
La	<30	<30	<30	<30	<30
Mo	<10	<10	<10	<10	<10
Nb	<7	<7	<7	<7	<7
Ni	124	70	73	<20	41
Pb	<20	<20	<20	22	<20
Rb	40	18	19	39	119
S	57320	3126	6900	266	2000
Sb	<100	<100	<100	<100	<100
Sc	<20	33	39	<20	<20
Sn	<20	<20	<20	<20	<20
Sr	47	117	108	108	156
Th	10	13	18	16	12
U	<10	<10	<10	<10	<10
V	96	266	273	<30	159
Y	13	32	14	17	13
Zn	232	123	87	<20	37
Zr	88	129	48	118	34
C (wt. %)	<0.05	<0.05	0.05	<0.05	<0.05
S (wt. %)	4.8	-	-	-	-

Table 6 continued…

	Biotite-chlorite schist DH 9 100.20-100.70	Biotite-talc schist DH 9 102.70-103.30	Biotite-talc-chlorite schist DH 9 95.55-96.00	Biotite-talc-tremolite schist DH 12 82.90-83.40
SiO_2 (wt. %)	39.30	41.10	47.80	29.50
TiO_2	0.67	0.31	0.87	0.53
Al_2O_3	11.80	6.76	15.30	10.80
Cr_2O_3	0.09	0.04	0.05	0.08
FeOtot	15.66	17.64	4.97	28.25
MnO	0.16	0.21	0.07	0.05
MgO	17.30	18.60	22.40	15.40
CaO	4.45	5.95	1.48	0.48
Na_2O	1.11	0.33	1.32	0.76
K_2O	1.26	1.40	2.54	1.78
P_2O_5	0.09	0.21	0.30	0.07
SUM	91.88	92.53	97.10	87.70
Mg#	69.85	68.86	90.44	53.34
As (ppm)	<20	<20	<20	<20
Ba	118	131	232	157
Bi	<30	<30	<30	<30
Ce	<30	<30	<30	<30
Cl	124	125	149	122
Cr	611	254	347	537
Cu	704	584	<20	929
Ga	30	<20	36	<20
La	<30	<30	<30	<30
Mo	<10	<10	<10	<10
Nb	<7	<7	<7	<7
Ni	134	93	165	389
Pb	<20	<20	<20	<20
Rb	78	79	169	130
S	53630	86300	397	98930
Sb	<100	<100	<100	<100
Sc	20	<20	25	<20
Sn	20	30	<20	27
Sr	19	<10	50	14
Th	19	18	18	<10
U	<10	16	<10	<10
V	183	98	262	141
Y	16	<7	36	<7
Zn	423	458	223	163
Zr	60	32	52	42
C (wt. %)	0.08	0.07	<0.05	0
S (wt. %)	-	-	-	15

5.4. Dikes

5.4.1. Diabase

Three samples of diabase (Table 5) were analyzed from DH 8 and two from DH 10. These analyzes yield results similar to each other, yet the SiO_2 content seems to decrease the deeper the samples are from DH 8, which has 44.90–46.50 wt. -% SiO_2, 1.05–1.08 wt. -% TiO_2, 15.60–15.70 wt. -% Al_2O_3, 12.06–12.24 wt. -% FeO_{tot}, 0.18–

0.20 wt. -% MnO, 6.66–7.28 wt. -% MgO, 10.75–11.12 wt. -% CaO, 1.55–2.21 wt. -% Na_2O, 0.18–0.24 wt. -% K_2O, 0.11–0.12 wt. -% P_2O_5 and 0.09–0.14 wt. -% S. Samples from DH 10 have 46.60 wt. -% SiO_2, 0.98–1.10 wt. -% TiO_2, 15.30–15.70. wt. -% Al_2O_3, 11.79–12.42 wt. -% FeO_{tot}, 0.19–0.20 wt. -% MnO, 6.92–7.45 wt. -% MgO, 10.74–11.13 wt. -% CaO, 1.82–1.94 wt. -% Na_2O, 0.26–0.32 wt. -% K_2O, 0.10–0.11 wt. -% P_2O_5. Analyzed diabase samples have magnesium-numbers of 53.30–57.00.

5.4.2. Diorite

Three diorite (Table 5) samples were analyzed from DH 11 and from DH 9 and DH 12 each. Samples from DH 9 and DH 11 show similar compositions of 49.80–52.20 wt. -% SiO_2, 1.37–2.09 wt. -% TiO_2 13.80–15.00 wt. -% Al_2O_3, 10.53–14.22 wt. -% FeOtot, 0.07–0.20 wt. -% MnO, 3.81–4.61 wt. -% MgO, 8.13–8.42 wt. -% CaO, 2.48–4.82 wt. -% Na_2O, 0.19–0.88 wt. -% K_2O, 0.25–0.33 wt. -% P_2O_5 and 0.08–0.35 wt. -% S. Diorites in DH's 9 and 11have Mg# of 47.9–54.7. The sample from DH 12 has 64.20 wt. -% SiO_2, 1.58 wt. -% TiO_2 13.80 wt. -% Al_2O_3, 4.58 wt. -% FeOtot, 0.03 wt. -% MnO, 4.79 wt. -% MgO, 5.42 wt. -% CaO, 4.41 wt. -% Na_2O, 0.18 wt. -% K_2O, 0.26 wt. -% P_2O_5 and 0.25 wt. -% S.

5.5. Ni, Cu, Au and Platinum-group elements

Platinum-group elements, nickel, copper and gold (PGE, Table 7)) were analyzed from 22 samples from DH 7, 16 from DH 8, nine from DH 10, 13 from DH 9, seven from DH 11, and six from DH 12. DH 7 shows signs of amounts of none to 12 ppb of given PGE's except at the depth of 99.85 it has 28 palladium and 21 ppb platinum and 171.70 meters 22 ppb gold, 29 ppb palladium, 41 ppb platinum and 3–8 ppb of other PGE's. DH 8 shows very small contents. The DH 10 at the depth of 96.00 and 103.70 meters has 854 and 122 ppb gold respectively. The amount of gold is high also in DH 9, which has gold ranging from <5–63 ppb, except at the depths of 100.20 and 102.70 has 146 and 233 ppb gold. DH 11 has 178 ppm gold at 73.00 m. DH 12 is the most enriched on palladium, platinum, rhodium and rubidium in the sample at the depth of 83.40 meters shows 70 ppb Au, 6 ppb Pd, 7 ppb Pt. Otherwise DH 12 mostly resembles DH 11. Nickel is most abundant in DHs 7, where it varies between 39–1217 ppm. In other drill cores the amounts are less than 200 ppm, except in a talc-tremolite schists in DH 8 and

DH 12 that have 636 and 389 ppm respectively. Copper varies mostly from <20 to 387 ppm, except DH 7 has 750 ppm at 78.50 m and DH's 9 and 12 both have >500 ppm copper layers at around depth of 90 m.

Table 7. Analyzed nickel, copper and platinum-group elements from selected drill core samples within and outside of the intrusion. n.a. = not analyzed.

Drill hole	Depth	Rock type	Ni (ppm)	Ir (ppb)	Os (ppb)	Ru (ppb)	Rh (ppb)	Pt (ppb)	Pd (ppb)	Au (ppb)	Cu (ppm)
DH 7	69.35-69.75	Mica schist	<20	n.a.	n.a.	n.a.	n.a.	<5	<5	<5	34
	72.50-72.75	Gabbro	150	<1	<1	3	2	12	10	10	333
	78.30-78.70	Leucocratic gabbro	749	n.a.	n.a.	n.a.	n.a.	10	23	7	750
	80.20-80.50	Tremolite-chlorite schist	84	n.a.	n.a.	n.a.	n.a.	8	7	7	226
	81.90-82.40	Leucocratic gabbro	546	n.a.	n.a.	n.a.	n.a.	13	18	9	387
	82.70-83.05	Tremolite-chlorite schist	920	1	1	3	<1	5	5	6	439
	85.20-85.60	Tremolite-chlorite schist	988	n.a.	n.a.	n.a.	n.a.	<5	<5	<5	273
	86.95-87.35	Leucocratic gabbro	353	n.a.	n.a.	n.a.	n.a.	21	28	<5	43
	99.85-100.30	Gabbro	158	n.a.	n.a.	n.a.	n.a.	<5	<5	<5	59
	114.40-114.75	Leucocratic gabbro	112	n.a.	n.a.	n.a.	n.a.	<5	<5	<5	33
	130.05-130.45	Gabbro	81	n.a.	n.a.	n.a.	n.a.	<5	<5	<5	<20
	145.35-145.80	Gabbro	153	n.a.	n.a.	n.a.	n.a.	<5	<5	<5	61
	148.45-148.95	Anorthosite	57	n.a.	n.a.	n.a.	n.a.	<5	<5	<5	705
	159.60-160.00	Leucocratic gabbro	150	3	4	8	4	41	29	22	251
	171.70-172.05	Gabbro	157	n.a.	n.a.	n.a.	n.a.	<5	<5	<5	<20
	173.00-173.40	Anorthosite	39	n.a.	n.a.	n.a.	n.a.	<5	<5	<5	<20
	179.90-180.30	Gabbro	108	n.a.	n.a.	n.a.	n.a.	29	<5	<5	<20
	184.00-184.60	Pyroxenite	764	n.a.	n.a.	n.a.	n.a.	<5	<5	<5	<20
	186.30-186.70	Peridotite	744	n.a.	n.a.	n.a.	n.a.	<5	<5	<5	<20
	188.90-189.20	Peridotite	1217	n.a.	n.a.	n.a.	n.a.	<5	<5	<5	30
	194.80-195.30	Leucocratic gabbro	96	n.a.	n.a.	n.a.	n.a.	<5	<5	<5	<20
	198.50-199.00	Pyroxenite	600	n.a.	n.a.	n.a.	n.a.	<5	<5	<5	112
DH 8	52.10-52.50	Amphibolite	76	n.a.	n.a.	n.a.	n.a.	7	7	<5	145
	53.90-54.40	Leucocratic gabbro	113	n.a.	n.a.	n.a.	n.a.	<5	<5	<5	47
	64.65-65.00	Gabbro	193	n.a.	n.a.	n.a.	n.a.	<5	<5	<5	30
	70.00-70.50	Leucocratic gabbro	77	n.a.	n.a.	n.a.	n.a.	<5	<5	<5	<20
	72.95-73.35	Chlorite-talc schist	636	<1	<1	<1	<1	2	1	<2	<20
	81.25-81.60	Gabbro	141	n.a.	n.a.	n.a.	n.a.	<5	<5	<5	36
	84.30-84.65	Diabase	103	n.a.	n.a.	n.a.	n.a.	<5	<5	<5	128
	98.70-99.10	Diabase	112	n.a.	n.a.	n.a.	n.a.	<5	<5	<5	106
	119.25-119.60	Diabase	121	n.a.	n.a.	n.a.	n.a.	<5	<5	<5	98
	123.15-123.65	Leucocratic gabbro	28	n.a.	n.a.	n.a.	n.a.	<5	<5	<5	<20
	127.90-128.50	Anorthosite	38	n.a.	n.a.	n.a.	n.a.	<5	<5	<5	<20
	137.55-138.00	Gabbropegmatite	46	n.a.	n.a.	n.a.	n.a.	<5	<5	<5	49
	153.50-153.95	Gabbro	78	n.a.	n.a.	n.a.	n.a.	<5	<5	<5	26
	170.70-171.10	Leucocratic gabbro	72	n.a.	n.a.	n.a.	n.a.	<5	<5	7	110
	188.15-188.55	Leucocratic gabbro	37	<1	<1	<1	<1	1	1	2	<20
	203.90-204.30	Gabbro	110	n.a.	n.a.	n.a.	n.a.	<5	<5	5	46
DH 10	26.60-27.00	Diabase	107	n.a.	n.a.	n.a.	n.a.	<5	<5	<5	119
	54.30-54.80	Leucocratic gabbro	44	n.a.	n.a.	n.a.	n.a.	<5	<5	<5	27
	60.90-61.40	Leucocratic gabbro	48	n.a.	n.a.	n.a.	n.a.	<5	<5	6	52
	76.60-76.95	Anorthosite	99	<1	<1	<1	<1	2	2	13	505
	86.10-86.60	Gabbro	151	n.a.	n.a.	n.a.	n.a.	<5	<5	<5	98
	96.00-96.50	Gabbro	78	n.a.	n.a.	n.a.	n.a.	<5	<5	854	52
	103.70-104.30	Amphibolite	123	n.a.	n.a.	n.a.	n.a.	<5	<5	122	207
	132.25-132.80	Amphibolite	159	n.a.	n.a.	n.a.	n.a.	<5	<5	<5	71
	149.80-150.25	Diabase	121	n.a.	n.a.	n.a.	n.a.	<5	<5	<5	139
DH 9	18.30-18.80	Amphibolite	84	n.a.	n.a.	n.a.	n.a.	<5	<5	44	327
	25.15-25.65	Tremolite-chlorite schist	67	n.a.	n.a.	n.a.	n.a.	<5	<5	<5	<20
	32.20-32.70	Mica schist	41	n.a.	n.a.	n.a.	n.a.	<5	<5	63	24
	41.50-41.90	Amphibolite	162	n.a.	n.a.	n.a.	n.a.	<5	<5	13	60
	57.90-58.40	Amphibolite	140	n.a.	n.a.	n.a.	n.a.	<5	<5	29	42
	72.00-72.30	Diorite	<20	n.a.	n.a.	n.a.	n.a.	<5	<5	52	103
	82.40-82.90	Tremolite-chlorite-talc schist	68	n.a.	n.a.	n.a.	n.a.	<5	<5	40	184
	88.40-88.90	Talc-chlorite schist	126	n.a.	n.a.	n.a.	n.a.	<5	<5	<5	<20
	91.20-91.70	Talc-chlorite schist	159	n.a.	n.a.	n.a.	n.a.	<5	<5	<5	<20
	95.55-96.00	Biotite-talc-chlorite schist	165	n.a.	n.a.	n.a.	n.a.	9	12	<5	<20
	100.20-100.70	Biotite-chlorite schist	134	n.a.	n.a.	n.a.	n.a.	<5	5	146	704
	102.70-103.30	Biotite-talc schist	93	n.a.	n.a.	n.a.	n.a.	6	<5	233	584
	106.80-107.15	Amphibolite	77	n.a.	n.a.	n.a.	n.a.	<5	<5	16	102
DH 11	18.60-19.05	Leucocratic gabbro	44	n.a.	n.a.	n.a.	n.a.	6	<5	7	194
	36.15-36.55	Leucocratic gabbro	42	n.a.	n.a.	n.a.	n.a.	6	<5	13	211
	56.50-56.90	Leucocratic gabbro	49	n.a.	n.a.	n.a.	n.a.	<5	<5	18	164
	66.30-66.60	Talc-chlorite-tremolite schist	40	n.a.	n.a.	n.a.	n.a.	<5	<5	22	128
	72.50-73.00	Chlorite-biotite-tremolite-talc schis	237	n.a.	n.a.	n.a.	n.a.	<5	7	178	501
	73.50-74.00	Amphibolite	124	n.a.	n.a.	n.a.	n.a.	<5	<5	34	393
	79.90-80.40	Amphibolite	70	n.a.	n.a.	n.a.	n.a.	<5	<5	83	113
DH 12	16.85-17.35	Leucocratic gabbro	46	n.a.	n.a.	n.a.	n.a.	<5	<5	35	59
	63.35-63.85	Diorite	<20	n.a.	n.a.	n.a.	n.a.	<5	<5	<5	<20
	68.00-69.00	Tremolite-talc schist	53	n.a.	n.a.	n.a.	n.a.	<5	<5	<5	27
	82.90-83.40	Biotite-talc-tremolite schist	389	n.a.	n.a.	n.a.	n.a.	7	6	70	929
	90.30-91.30	Tremolite-biotite schist	204	n.a.	n.a.	n.a.	n.a.	<5	<5	48	686
	98.80-99.40	Amphibolite	73	n.a.	n.a.	n.a.	n.a.	<5	<5	12	105

5.6. Trace- and rare-earth elements (REE)

When normalized against chondritic composition, the trace-elements (Table 8, Appendix 12.4) in gabbroic rocks show a depleting trend with a positive Sr anomaly in the leucocratic gabbros (Fig. 25) and a negative in the others. The previously ultramafic rocks show a negative Sr anomaly and mostly a depleting trend. Overall country rocks and diorites seem to have higher values from chondrite composition whereas the intrusion rocks yield relatively closer values. The tremolite and talc-based schists also have more chondritic values than gabbros, which could fit the assumption of them being the first crystallize in the intrusion. The pyroxenite sample analyzed shows huge anomalies at U, Th and K and likely has been enriched in the heavier elements. REE's (Fig. 26, Appendix 12.4) show Eu anomalies in gabbros, which is also notable in the pyroxenite sample. DH 10 has a notable negative Nb anomaly in all its rock types. In DH's 7 and 8 tremolite-talc schists have negative Sr anomalies in contrast to the positive anomalies in leucocratic gabbros, indicating that the plagioclase crystallization took place and they floated upwards during the formation of the mafic layers.

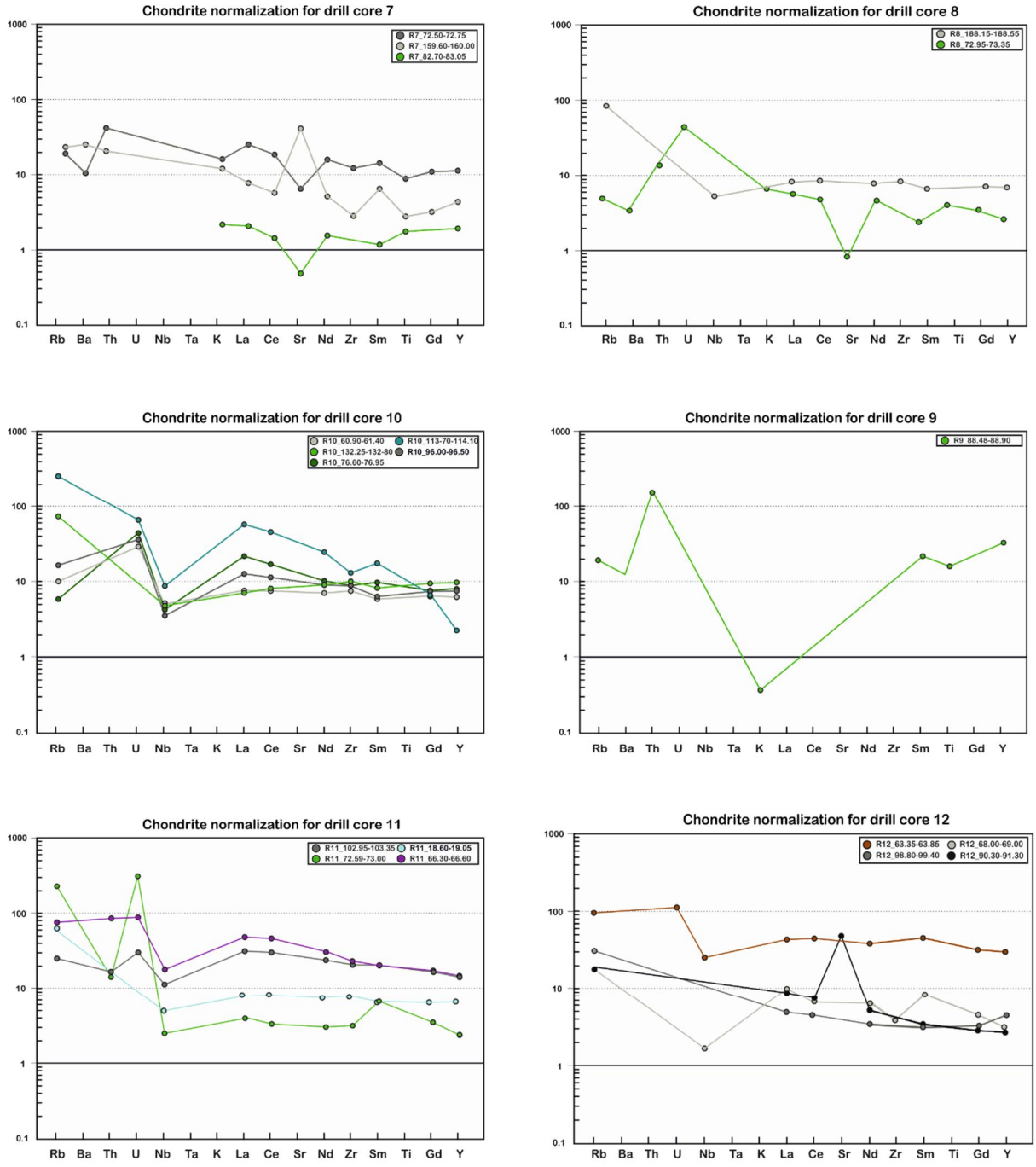

Figure 25. Chondrite –normalized plots for all samples. Darker grey colorization marks gabbro, lightly grey leucocratic gabbro, green either amphibolite or schists, turquoise biotite schist, light purple diorite and orange marks biotite paragneiss. Chondrite values after Sun et al. (1980).

Biotite paragneiss has a heavy REE depleting trend. All the samples analyzed have HREE-enriched trends.

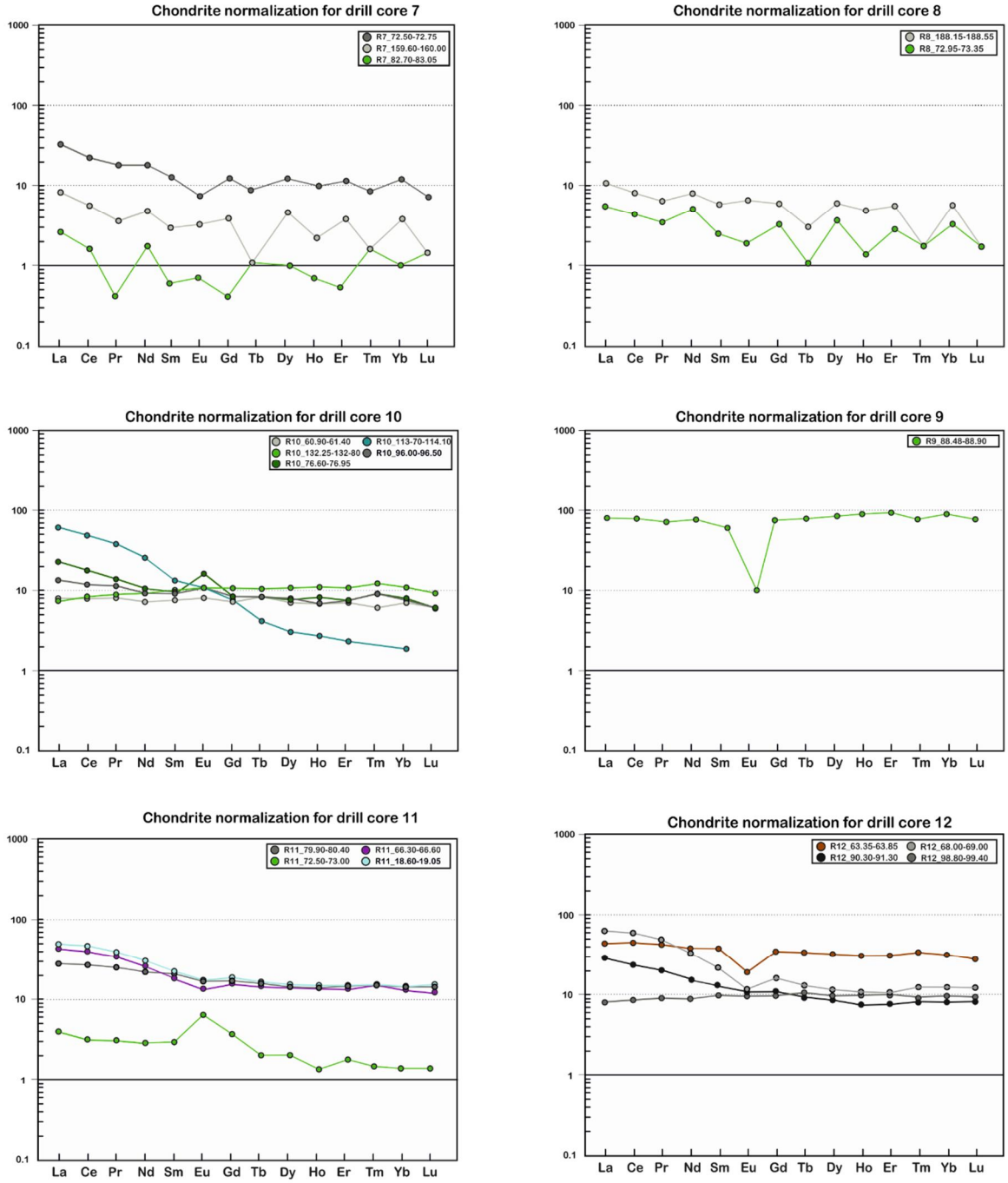

Figure 26. Chondrite –normalized REE compositions for all samples. Darker grey colorization marks gabbro, lightly grey leucocratic gabbro, green either amphibolite or schists, turquoise biotite schist, light purple diorite and orange marks biotite paragneiss. Chondritic composition after Boynton (1984).

6. MINERALOGY AND MINERAL CHEMISTRY

In this work mineral observations are based on thin section samples and CIPW – normative compositions. Minerals for EDS –microprobe analyzes were selected from thin sections and based on the bulk rock composition of the samples. CIPW-normative mineral compositions (Appendix 12.3) are mainly used to support and give backbone for assumptions of the precedent mineralogy. It is also worth noting that normative compositions work best on averages, and extremes such as anorthositic rocks might have a higher degree of misinterpretations. Overall metamorphosis within the intrusion shows varying levels of mineral alteration and is thus resulting in altered mafic minerals – It is likely that most of pyroxenes have altered into amphiboles, most of olivine into talc and serpentinite, biotite into chlorite and roughly ½ of anorthositic plagioclase into clinozoisite.

CIPW-normalized mineral compositions between each drill core show compositional changes of crystallizing minerals (Fig. 27) and a changes between rock type compositions. Olivine and pyroxenes are the most abundant in tremolite-based rocks. In pyroxenites and peridotite olivine and pyroxene both make 30–60 % of total minerals. Both types of gabbros contain some plagioclase phenocrysts and olivine (10–20 % of total minerals) along with more abundant pyroxenes which makes about 1/3 of the total rock minerals. Some pyroxene mineralization is also observed in anorthositic layers and pyroxenes also make 3–70 % of minerals in DH 7 at drill core length of 73–100 m.

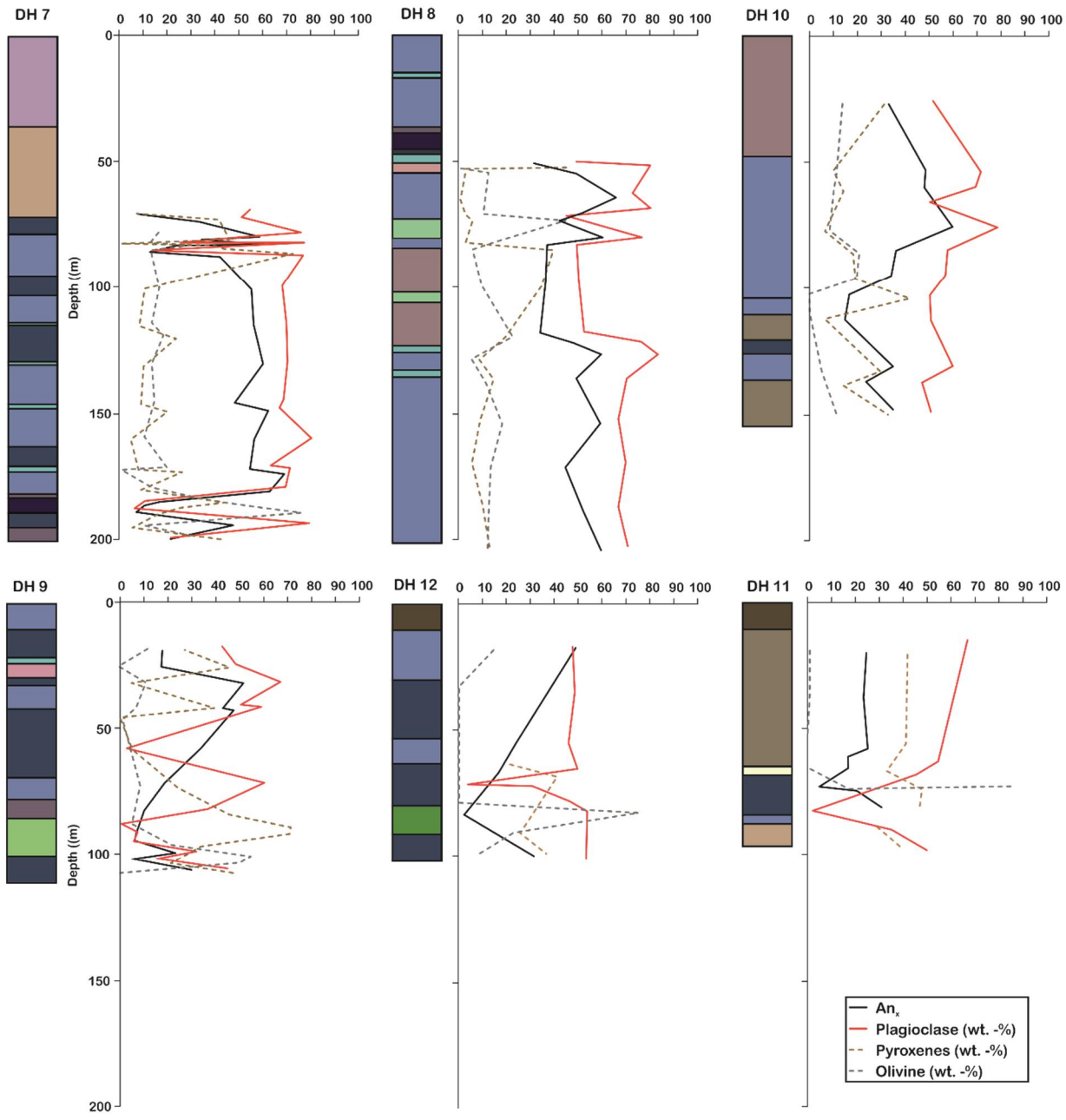

Figure 27. Calculated CIPW-normative mineralizations for each whole-rock chemical dataset of the Kuohatti mafic layered intrusion in response to drill core depth. Legend for simplified drill core rock types are given in Figures 4 and 5.

CIPW-normalized compositions of the leucocratic gabbros have notably high plagioclase-contents (Table 9). According to the normalized values, the leucocratic gabbros are composed of 66.2–80.2 vol. -% plagioclase, some pyroxenes and up to 17.7 vol. -% olivine.

Table 8. Selected CIPW-normalized mineral composition of leucocratic gabbros. For tables of all samples, see appendix 12.3.

	Leucocratic gabbro							
	DH 7	DH 7	DH 7	DH 7	DH 8	DH 8	DH 10	DH 12
	78.30-78.70	86.95-87.35	130.05-130.45	194.80-195.30	53.90-54.40	188.15-188.55	60.90-61.40	16.85-17.35
Quartz	0.00	0.00	0.00	0.00	0.00	0.00	0.00	0.00
Plagioclase	74.75	75.89	69.36	79.53	80.23	66.82	69.04	66.22
Orthoclase	2.78	6.44	1.42	1.24	0.83	2.42	1.54	11.58
Nepheline	3.22	1.77	3.30	2.97	2.79	7.20	3.49	4.69
Corundum	1.19	1.18	0.00	0.00	0.00	0.00	0.00	0.01
Diopside	0.00	0.00	9.21	4.75	3.21	10.06	14.19	0.00
Hypersthene	0.00	0.00	0.00	0.00	0.00	0.00	0.00	0.00
Wollastonite	0.00	0.00	0.00	0.00	0.00	0.00	0.00	0.00
Olivine	17.74	14.55	14.93	11.09	12.46	12.12	10.48	16.09
Rutile	0.00	0.00	0.00	0.00	0.00	0.00	0.00	0.00
Ilmenite	0.32	0.19	1.71	0.38	0.42	1.33	1.23	1.23
Hematite	0.00	0.00	0.00	0.00	0.00	0.00	0.00	0.00
Apatite	0.00	0.00	0.09	0.05	0.05	0.05	0.02	0.16
An	58.44	42.27	47.44	63.09	65.66	43.89	48.15	48.91

This normalization indicates a composition more closely to an olivine gabbro in comparison to the lack of remnants of olivine in the thin sections. The gabbros (Table 10) on the other hand show a different mineralization as the major pyroxene in samples from DH' 8 and 10 is clinopyroxene, which is in line with them being more mafic than the leucocratic gabbros. The sample from DH 7 differs from the previous, as the major pyroxene is hypersthene.

Table 9. CIPW-normalized mineral composition of gabbros.

	Gabbro		Gabbropegmatite	
	DH 7	DH 10	DH 10	DH 8
	72.50-72.75	86.10-86.60	96.00-96.50	137.55-138.00
Quartz	3.67	0.00	0.00	0.00
Plagioclase	51.21	58.02	57.03	70.69
Orthoclase	1.30	1.18	1.83	1.42
Nepheline	0.00	0.07	0.05	1.43
Diopside	8.58	18.19	19.24	14.55
Hypersthene	33.26	0.00	0.00	0.00
Olivine	0.00	21.45	20.26	10.98
Ilmenite	1.71	1.01	1.46	0.82
Apatite	0.25	0.09	0.14	0.12
An	33.44	36.32	34.35	49.13

The samples show huge change though, as the main minerals swap between plagioclase-hypersthene-diopside and plagioclase-diopside-olivine or even plagioclase-hypersthene

in one sample. This is neither observable as different gabbroic layers, which makes it more probable to be a normative error. The gabbros also have more than twice the amount of magnetite, ilmenite and apatite compared to the leucocratic gabbros.

The pyroxenes and peridotites show normative compositions close to their assumed rocks-types (Table 11). According to CIPW-normative compositions, anorthosites should have $An_{59.4}$–$An_{68.9}$ and compose mainly of plagioclase and 6.94–25.1 vol. -% diopside. This indicates that the metamorphic alteration is visible also in CIPW-normative compositions, which leads to them resulting in inaccurate compositions. In this case, the high amount of clinozoisite is likely misinterpreted as diopside.

Table 10. CIPW-normalized mineral composition of pyroxenites, anorthosites and peridotites

	Anorthosite	Anorthosite	Anorthosite	Anorthosite	Pyroxenite	Pyroxenite	Peridotite	Peridotite
	DH 7	DH 7	DH 8	DH 10	DH 7	DH 7	DH 7	DH 7
	148.45-148.95	173.00-173.40	127.90-128.50	76.60-76.95	184.00-184.60	198.50-199.00	186.30-186.70	188.90-189.20
Quartz	10.42	0.00	0.00	0.00	0.00	0.00	0.00	0.00
Plagioclase	67.18	72.08	84.42	78.01	17.34	21.50	10.96	6.73
Orthoclase	1.36	0.65	0.77	1.06	0.06	0.06	0.06	0.00
Nepheline	0.00	0.44	0.00	4.36	0.00	0.00	0.00	0.00
Corundum	0.00	0.00	0.00	0.00	0.00	0.00	5.22	0.02
Diopside	15.20	25.07	6.94	6.40	14.46	6.82	0.00	0.00
Hypersthene	5.35	0.00	2.52	0.00	25.15	35.68	26.07	16.12
Olivine	0.00	1.58	4.95	8.79	42.29	35.40	57.21	76.41
Ilmenite	0.46	0.13	0.34	1.20	0.51	0.47	0.44	0.68
Apatite	0.05	0.05	0.05	0.19	0.19	0.07	0.05	0.02
An	62.36	68.92	59.37	60.00	16.86	20.74	10.54	6.73

Tremolite-talc based schists have high variations of plagioclase content (Table 12), and only one sample exceeds 50 vol. -% Schists with less plagioclase have either more quartz or higher amounts of olivine than their counterparts. Amount of pyroxene varies between 8.4–71.1 %. Ilmenite and magnetite make 1.9–6.6 % of total minerals in rock.

Table 11. CIPW-normalized mineral composition of tremolite-talc schists.

	Talc-chlorite schist	Talc-chlorite schist	Talc-chlorite-tremolite schist	Tremolite-biotite schist	Tremolite-chlorite schist	Tremolite-chlorite schist	Tremolite-chlorite schist	Tremolite-chlorite schist	Tremolite-chlorite-talc schist	Tremolite-talc schist	Chlorite-biotite-tremolite-talc	Chlorite-talc schist
	DH 9	DH 9	DH 11	DH 12	DH 7	DH 7	DH 7	DH 9	DH 9	DH 12	DH 11	DH 8
	88.40-88.90	91.20-91.70	66.30-66.60	90.30-91.30	80.20-80.50	82.70-83.05	85.20-85.60	25.15-25.65	82.40-82.90	68.00-69.00	72.50-73.00	72.95-73.35
Quartz	0.00	8.48	8.43	0.00	1.93	0.00	0.00	0.00	8.99	5.59	0.00	0.00
Plagioclase	0.55	7.37	50.67	35.64	48.32	25.32	13.52	44.32	37.05	46.33	3.99	48.23
Orthoclase	0.06	0.06	2.66	12.35	1.42	0.18	0.06	4.67	0.65	1.12	0.00	0.59
Nepheline	0.00	0.00	0.00	0.00	0.00	0.00	0.00	0.00	0.00	0.00	0.73	0.00
Leucite	0.00	0.00	0.00	0.00	0.00	0.00	0.00	0.00	0.00	0.00	2.41	0.00
Kalsilite	0.00	0.00	0.00	0.00	0.00	0.00	0.00	0.00	0.00	0.00	3.42	0.00
Corundum	13.48	0.00	1.63	1.82	0.00	0.00	0.00	2.42	3.90	3.58	2.79	0.19
Diopside	0.00	1.84	0.00	0.00	17.08	8.42	2.87	0.00	0.00	0.00	0.00	0.00
Hypersthene	71.00	69.31	32.88	25.52	29.06	30.84	63.62	46.10	45.37	40.50	0.00	5.65
Olivine	4.98	0.00	0.00	23.05	0.00	34.89	19.63	0.37	0.00	0.00	85.57	44.58
Ilmenite	7.69	5.24	3.06	1.39	1.92	0.36	0.30	1.56	3.46	2.54	0.46	0.68
Apatite	2.22	5.75	0.67	0.23	0.28	0.00	0.00	0.56	0.60	0.35	0.63	0.07

Plagioclase and its An-component do not show such a clear divide between rock types (Fig. 29), but correlate more along the depth and location within each drill core. This is the most visible in DH's 7, 9 and 10. The amount of plagioclase mostly varies between 40–65 % in gabbroic rocks, yet occasional plummet of 20 % in plagioclase composition is visible where the rock type changes from leucocratic gabbro into a gabbro and in DH 7 between 73–100 m. Anorthositic layers constantly have $An_{>60}$ and at least 80 % plagioclase.

6.1. Olivine

Olivine is found only in two thin section from DH 7 at the depths of 184.60 and 189.60 m. Olivine grains were analyzed from one peridotite thin sections in DH 7 at the depth of 189.20 m. In total 6 gains are analyzed with 1–3 points each (see Appendix 12.5.1). Olivine grains are quite healthy and thus a method of measuring the composition from rim to the core is used and likely to present variation in some grain compositions. Olivine composition (Table 13) result as 38.0–39.2 wt. -% SiO_2, 0.0–0.4 wt. -% TiO_2, 0.0 wt. -% Al_2O_3, 17.0–18.5 wt. -% FeO, 0.2–0.4 MnO, 41.2–42.5 wt. -% MgO, 0.0–0.1 wt. -% CaO, 0.0–0.2 wt. -% Ba and 0.0–0.3 wt. -% NiO. Olivine end-members show little variation in end-member composition $(Mg_{1.6},Fe_{0.4})SiO_4$ and the analyzed samples are Forsterite at $Fo_{81.7–80.1}$.

6.2. Pyroxene

Pyroxenes are seen as very small remnants in pyroxenites and peridotite. They have a grain size of 0.1–0.2 mm and are in a poor condition. Three metapyroxene thin sections were chosen for pyroxene analyses from DH 7 at the depths of 83.05 and 184.60 m and from DH 9 at the depth of 100.25 m. From each thin section 6–8 grains from 3–4 different spots are analyzed and then determined whether they are amphibole or pyroxene. The pyroxene grains on the rocks are in quite a ruptured shape and only their central parts are analyzed for the best possible accuracy and to avoid the contamination from grain boundaries. One pyroxene sample yielded results of an amphibole. Pyroxene samples (Table 13, Fig. 28) yield 55.5–62.6 wt. -% SiO_2, 0.0–0.3 wt. -% TiO_2, 0.0–0.5 wt. -% Al_2O_3, FeO amounts of 2.4–17.3 wt. -%, 0.2–0.8 MnO, 22.7–30.3 wt. -% MgO, 0.1–0.9 wt. -% CaO, 0.0–0.1 wt. -% Na_2O and K_2O. 0.0–0.3 Cr_2O_3, 0.0–0.3 wt. -% NiO and 0.0–0.1 Sr. In addition 0.1 wt. -% Barium is analyzed for grains in sample 184.60, but is left out from other pyroxene analyses as it showed possible interference with FeO. Pyroxene end-members (Fig. 28) vary between $(Mg_{13}, Fe_{0.5})Si_2O_6$ and $(Mg_{1.3}, Fe_{0.5})Si_2O_6$ and are orthopyroxene.

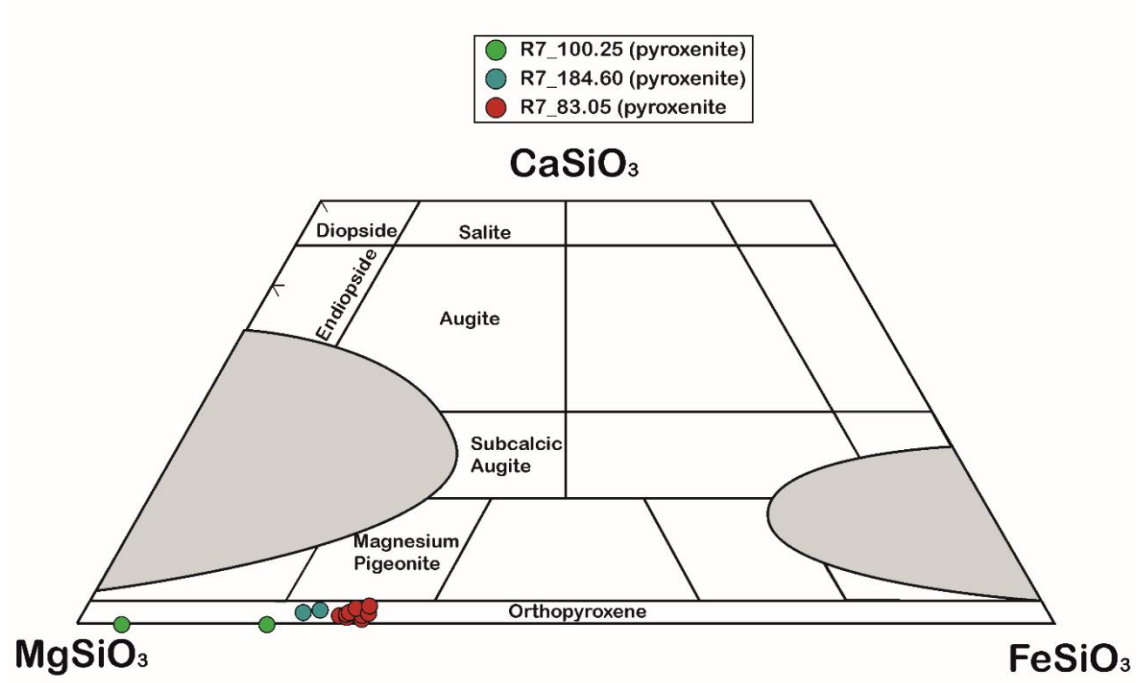

Figure 28. End-member composition for the analyzed pyroxenites after the classification of Deer et al. (1963b)

Table 12. Chemical composition of selected mineral samples analyzed with electron microprobe, their balanced mineral compositions and end-member compositions for pyroxenes, olivine and plagioclase. n.a. = not analyzed. Anx = Ca/(Na+Ca+K)*100, Enx = Mg/(Mg+Fe)*100 and Fox = Mg/(Mg+Fe)*100.

	Olivine		Pyroxene				Plagioclase					Amphibole				
	R7		R7	R9	R7		R7	R7	R7	R8	R12	R7	R9	R7	R7	R7
	189.20		184.60	100.25	83.05		173.00	82.15	194.80	54.05	68.80	184.60	100.25	83.05	198.60	189.20
SiO_2 (wt. -%)	41.43		56.44	62.56	56.25		44.77	51.44	49.03	47.35	57.86	57.43	57.37	56.56	56.37	57.00
TiO_2	0.09		0.05	0.00	0.09		0.03	0.02	0.02	0.03	0.03	0.03	0.12	0.09	0.13	0.11
Al_2O_3	0.00		0.02	0.47	0.13		34.40	29.98	31.74	32.69	25.96	0.45	1.08	1.22	0.81	0.68
FeO	16.97		13.78	2.42	16.25		0.05	0.02	0.03	0.02	0.04	3.87	2.65	6.31	7.86	4.76
MnO	0.33		0.68	0.15	0.58		0.01	0.02	0.01	0.01	0.02	0.16	0.34	0.28	0.32	0.20
MgO	39.55		25.26	30.32	23.23		0.01	0.00	0.00	0.00	0.01	22.92	22.63	21.13	20.82	23.53
CaO	0.10		0.75	0.05	0.50		18.64	13.39	15.89	16.85	8.34	12.15	12.75	11.70	10.51	10.13
Na_2O	0.00		0.01	0.07	0.02		0.96	4.00	2.90	2.13	6.80	0.06	0.23	0.15	0.11	0.10
K_2O	0.00		0.02	0.04	0.01		0.02	0.02	0.01	0.03	0.19	0.01	0.04	0.03	0.01	0.04
Ba	0.06		0.06	0.00	0.00		0.03	0.01	0.04	0.07	0.05	0.10	0.00	0.00	0.00	0.00
Cr_2O_3	n.a.		0.08	0.02	0.09		0.04	0.01	0.01	0.00	0.01	0.05	0.06	0.07	0.07	0.11
Ni	0.09		0.03	0.01	0.13		n.a.	n.a.	n.a.	n.a.	n.a.	0.08	0.03	0.07	0.06	0.07
Sr	0.00		0.05	0.00	0.01		0.02	0.03	0.01	0.02	0.05	0.01	0.00	0.00	0.00	0.00
Tot	98.63		97.23	96.11	97.29		98.97	98.93	99.69	99.21	99.35	97.31	97.30	97.61	97.09	96.74
Si	1.1		2.1	2.2	2.1		2.1	2.4	2.3	2.2	2.6	7.9	7.9	7.9	7.9	7.9
Ti	0.0		0.0	0.0	0.0		0.0	0.0	0.0	0.0	0.0	0.0	0.0	0.0	0.0	0.0
Al	0.0		0.0	0.0	0.0		1.8	1.6	1.7	1.7	1.3	0.1	0.2	0.2	0.1	0.1
Fe	0.4		0.4	0.1	0.5		0.0	0.0	0.0	0.0	0.0	0.4	0.3	0.7	0.9	0.6
Mn	0.0		0.0	0.0	0.0		0.0	0.0	0.0	0.0	0.0	0.0	0.0	0.0	0.0	0.0
Mg	1.5		1.4	1.6	1.3		0.0	0.0	0.0	0.0	0.0	4.7	4.6	4.4	4.4	4.9
Ca	0.0		0.0	0.0	0.0		1.0	0.7	0.8	0.9	0.4	1.8	1.9	1.7	1.6	1.5
Na	0.0		0.0	0.0	0.0		0.1	0.4	0.3	0.2	0.6	0.0	0.1	0.0	0.0	0.0
K	0.0		0.0	0.0	0.0		0.0	0.0	0.0	0.0	0.0	0.0	0.0	0.0	0.0	0.0
Ba	0.0		0.0	n.a.	0.0		0.0	0.0	0.0	0.0	0.0	0.0	0.0	0.0	0.0	0.0
Cr	n.a.		0.0	0.0	0.0		0.0	0.0	0.0	0.0	0.0	0.0	0.0	0.0	0.0	0.0
Ni	0.0		0.0	0.0	0.0		n.a.	n.a.	n.a.	n.a.	n.a.	0.0	0.0	0.0	0.0	0.0
Sr	0.0		0.0	0.0	0.0		0.0	0.0	0.0	0.0	0.0	0.0	0.0	0.0	0.0	0.0
O	4.0		6.0	6.0	6.0		8.0	8.0	8.0	8.0	8.0	23.0	23.0	23.0	23.0	23.0
Tot_{cat}	2.9		3.9	3.8	3.9		5.0	5.0	5.0	5.0	5.0	0.0	0.0	0.0	0.0	0.0
Fo_X	80.6	En_X	75.3	95.6	71.0	An_X	91.4	64.8	75.2	81.3	40.1					
		Fs_X	23.0	4.3	27.9											
		Wo_X	1.6	0.1	1.1											

6.3. Plagioclase

Plagioclase is present throughout the intrusion and its composition and amount varies greatly between rock-types. Plagioclase grains were analyzed from five thin sections: two leucocratic gabbros from DH 7 at the depth of 82.15 and 194.80 m, one leucocratic gabbro from DH 8 at the depth of 54.05 m, one anorthosite from DH 7 from the depth of 173.00 m and one tremolite-talc schist from DH 12 at the depth of 68.80 m. Plagioclase shows significant compositional variation (Table 13, Fig. 39) between drill cores (Fig. 4 and Fig. 5) and has 44.1–59.3 wt. -% SiO_2, 0.0–0.1 wt. -% TiO_2, 24.6–34.8 wt. -% Al_2O_3, 0.0–0.2 wt. -% FeO, 6.6–18.6 wt. -% CaO, 0.6–0.71 wt. -% Na_2O, 0.0–0.9 wt. -% K_2O, 0.0–0.2 wt. -% Ba and 0.0–0.1 wt. -% Sr. End-member formulae for plagioclase shows great variation between: $(Na_{0.6},Ca_{0.3})Al(Si_{2.7},Al_{0.3})O_{8.0}$ – $(Ca_{1.0},Na_{0.1})Al(Al_{0.8},Si_{2.2})O_{8.0}$ and $An_{33.5–94.0}$.

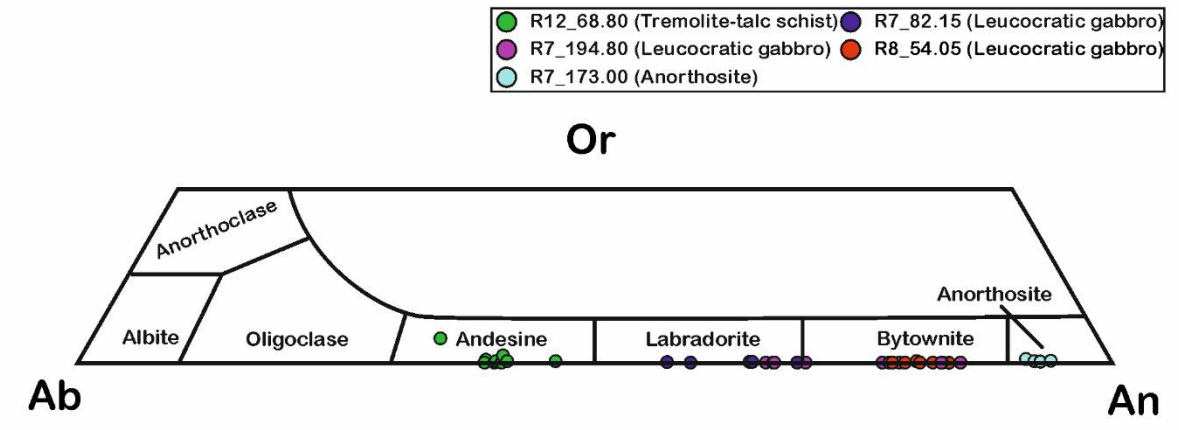

Figure 29. End-member composition for the analyzed plagioclases for Na_2O and CaO after Deer et al. (1963a)

6.4. Amphibole

Amphibole was analyzed from five thin sections: three pyroxenites in DH7 at the depths of 83.04 m and 184.60 m and DH 9 at the depth of 100.25 m, one talc-biotite schist from DH 9 at the depth of 100.25 m, and one peridotite from DH 7 at the depth of 189.20 m. Compositional elements vary between 54.6–57.8 wt. -% SiO_2, 0.0–0.6 wt. -% TiO_2, 0.1–2.1 wt. -% Al_2O_3, 2.1–10.6 wt. -% FeO, 0.0–0.6 MnO, 20.2–24.8 wt. -%

MgO, 7.6–13.5 wt. -% CaO, 0.0–0.4 wt. -% Na_2O 0.0–0.1 wt. -% K_2O, 0.0.–0.3 Ba (in the analyzed samples), 0.0–0.3 Cr_2O_3, 0.0–0.2 wt. -% NiO and 0.0 Sr. End-members for amphibole (Fig. 30) vary between $(Ca_{1.9})(Mg_{4.3},Fe_{0.7},Al_{0.2})Si_8O_{23}(OH)$, $(Ca_{1.1})(Mg_{5.1},Fe_{0.8})Si_8O_{23}(OH)$ and $(Ca_{1.9})(Mg_{4.7},Fe_{0.2},Al_{0.1})Si_8O_{23}(OH)$.

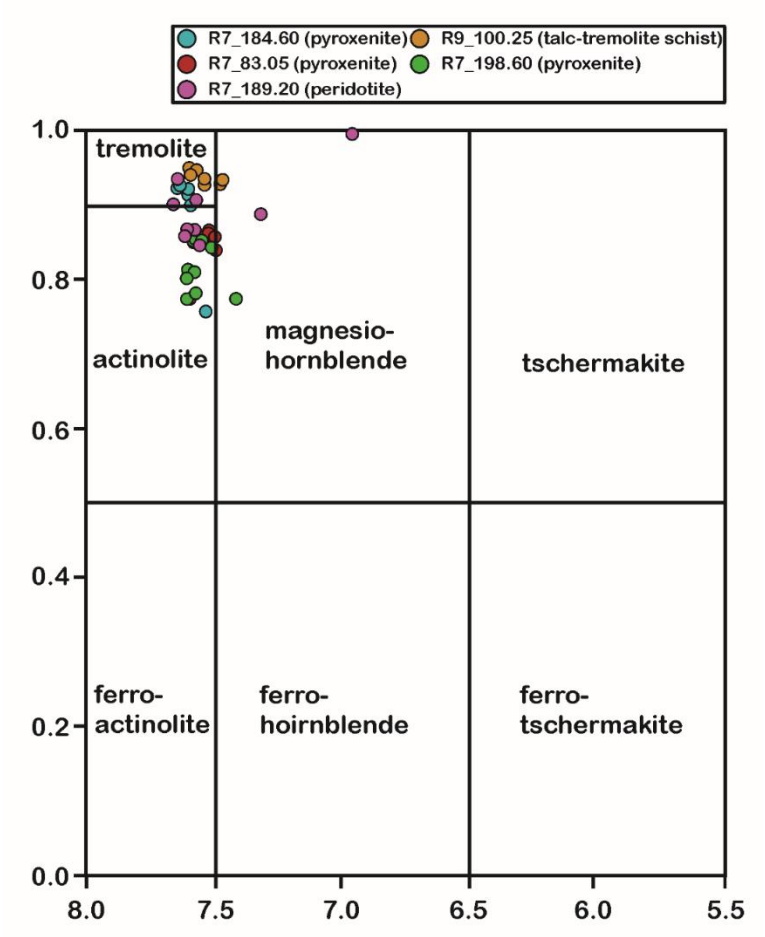

Figure 30. Amphiboles analyzed from the Kuohatti mafic intrusion shown in the classification diagram of Leake (1978).

6.5. Magnetite

Magnetite is found at the end of DH 7 and the beginning of DH 8, in gabbros within proximity of peridotite and pyroxenite layers. It has a grain size of 0.2–2.0 mm, which is likely affected by metamorphosis to some degree.

7. ISOTOPE GEOCHEMISTRY

7.1 U-Pb ages from Zircon

In total 26 zircon grains (Fig. 31) were analyzed from a talc-chlorite schist in DH 9 at the depth of 88.90–91.20 m (A2427) and 26 zircon grains (Fig. 33) from a leucocratic gabbro in DH 10 at the depth of 102.80–105.30 (A2444).

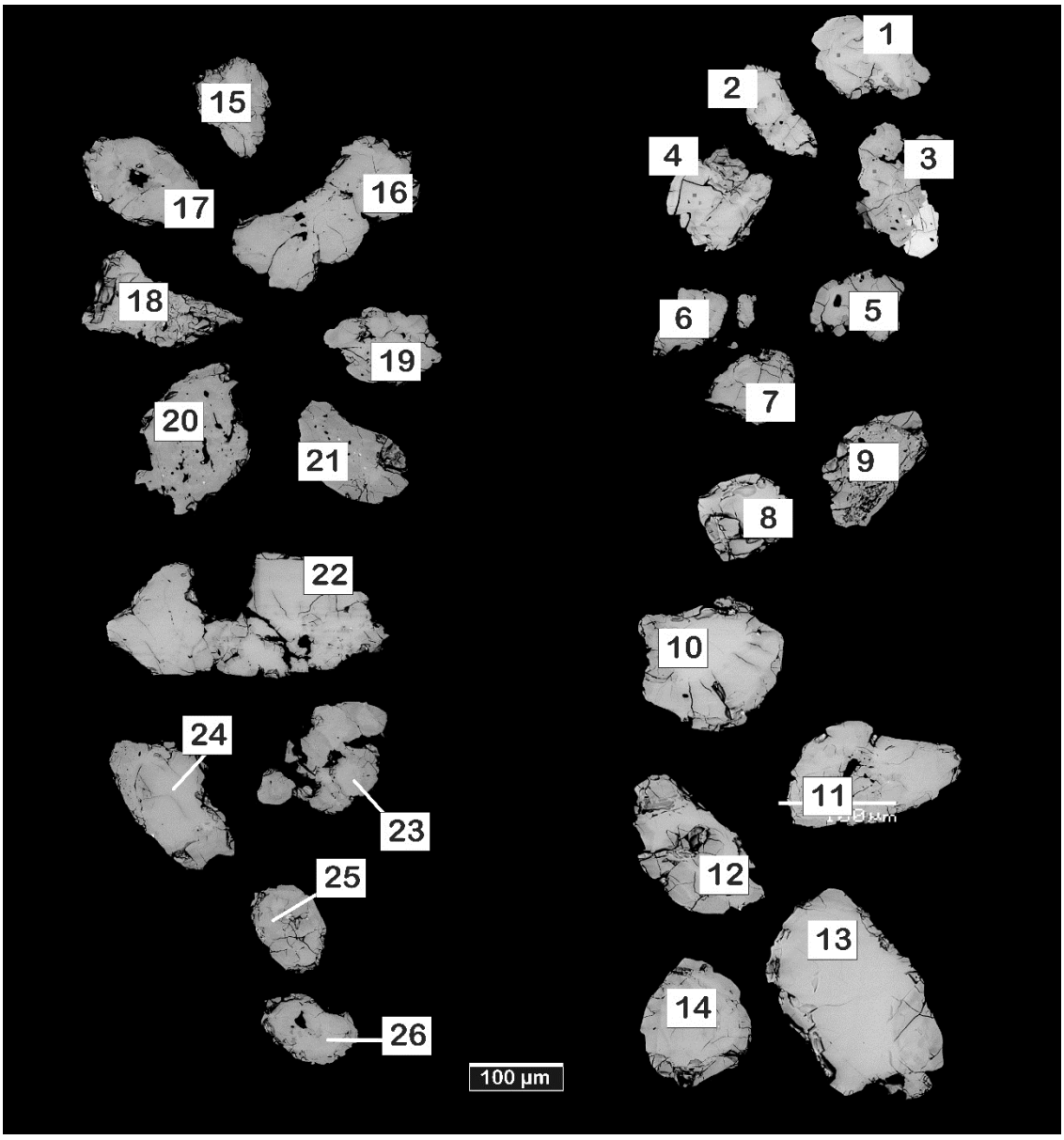

Figure 31. Analyzed zircon grains for sample A2427 (talc-chlorite schist). Numbers marked are sample labels and also represent the spot of analysis.

7.1.1 Talc-chlorite schist (A2427)

A2427 represents the Archean greenschist and is analyzed for the age of the intrusion's likely wall rock. It has 178 ppm Zr and some ruptured grains of zircon visible in thin sections. The grains (Fig. 31) show faint irregular zoning. The analyzed zircons have 18–88 ppm U and 52–428 ppm Pb (Table 14). Common lead proportion ($^{206}Pb_c$) in the grains range between 0.02–2.88 %. ^{207}Pb and ^{206}Pb ratios ($^{207}Pb/^{206}Pb$) range from 0.1804–0.2089 and 1σ values between 0.0008–0.0014, ^{207}Pb and ^{235}U ($^{207}Pb/^{235}U$) ratios range from 7.8283–16.8516 and their 1σ values between 0.1673–0.2446 and ^{206}Pb and ^{238}U ($^{206}Pb/^{238}U$) vary between 0.2845–0.6044 and 1σ 0.0040–0.0084. Rho value vary between 0.89–0.95, concordance between 56–107 %. $^{207}Pb/^{206}Pb$ ages are 2683–2893 Ma with an 1σ error of 8–11 Ma (Fig. 32). Two groups are set at 2.84 Ga and 2.70 Ga.

Table 14. U/Pb data for zircon samples from A2427 (talc-chlorite schist), calculated after Stacey and Kramers (1975).

A2427 Zircon	U (ppm)	Pb (ppm)	$^{206}Pb_c$(%)	$^{207}Pb/^{206}Pb$	1SE	$^{207}Pb/^{235}U$	1SE	$^{206}Pb/^{238}U$	1SE	Rho	Concordance (%)	$^{207}Pb/^{206}Pb$ age (Ma)	1s	$^{207}Pb/^{235}U$ age	1s	$^{206}Pb/^{238}U$ age	1s
A2427-1	31	141	0.02	0.2086	0.0011	14.9302	0.2159	0.5192	0.0072	0.929	93	2894	9	2811	14	2696	31
A2427-2	26	127	0.02	0.2048	0.0012	13.2901	0.1951	0.4706	0.0066	0.912	87	2865	10	2700	14	2486	29
A2427-3	28	97	0.02	0.2035	0.0012	13.0674	0.1913	0.4658	0.0065	0.915	86	2854	10	2685	14	2465	29
A2427-4	19	297	0.03	0.2063	0.0013	15.2174	0.2262	0.5350	0.0075	0.902	96	2877	10	2829	14	2762	32
A2427-5	24	167	2.88	0.1833	0.0012	12.5560	0.1846	0.4967	0.0071	0.894	93	2683	11	2647	14	2600	31
A2427-6	18	112	1.91	0.1845	0.0013	13.3113	0.1997	0.5233	0.0075	0.877	98	2694	12	2702	14	2713	32
A2427-7	71	101	1.23	0.1887	0.0009	12.4043	0.1753	0.4767	0.0067	0.947	90	2731	8	2636	13	2513	29
A2427-8	27	130	0.02	0.2022	0.0011	16.8516	0.2446	0.6044	0.0084	0.925	107	2844	9	2926	14	3048	34
A2427-9	86	145	1.10	0.1867	0.0008	12.7289	0.1792	0.4945	0.0069	0.952	94	2713	7	2660	13	2590	30
A2427-10	30	428	0.02	0.2069	0.0011	15.4823	0.2241	0.5427	0.0076	0.928	97	2882	9	2845	14	2795	32
A2427-11	36	106	1.59	0.1864	0.0011	12.4052	0.1795	0.4827	0.0068	0.920	91	2710	9	2636	14	2539	29
A2427-12	31	127	0.02	0.2073	0.0012	13.8952	0.2024	0.4861	0.0068	0.922	89	2885	9	2743	14	2554	29
A2427-13	33	139	0.02	0.2046	0.0011	14.3216	0.2077	0.5077	0.0071	0.925	92	2863	9	2771	14	2647	30
A2427-14	30	102	0.02	0.2044	0.0011	15.2893	0.2223	0.5424	0.0076	0.923	98	2862	9	2833	14	2794	32
A2427-15	25	269	0.02	0.2032	0.0013	14.0967	0.2080	0.5030	0.0070	0.909	92	2852	10	2756	14	2627	30
A2427-16	25	93	0.02	0.2058	0.0012	14.9224	0.2193	0.5258	0.0074	0.913	95	2873	10	2810	14	2724	31
A2427-17	30	135	1.22	0.1959	0.0012	14.5770	0.2122	0.5397	0.0076	0.916	98	2792	10	2788	14	2782	32
A2427-18	20	337	0.03	0.2085	0.0013	15.8179	0.2349	0.5504	0.0077	0.903	98	2894	10	2866	14	2827	32
A2427-19	31	125	2.42	0.1910	0.0012	12.8712	0.1877	0.4888	0.0069	0.907	90	2751	10	2670	14	2566	30
A2427-20	32	79	0.02	0.2015	0.0012	13.8747	0.2024	0.4993	0.0070	0.920	92	2839	9	2741	14	2611	30
A2427-21	36	52	0.02	0.1899	0.0011	12.3290	0.1798	0.4708	0.0066	0.920	91	2742	9	2630	14	2487	29
A2427-22	28	140	0.02	0.2051	0.0012	15.1889	0.2227	0.5370	0.0075	0.916	97	2868	10	2827	14	2771	31
A2427-23	38	72	0.02	0.1958	0.0011	12.8488	0.1871	0.4758	0.0066	0.922	90	2792	9	2669	14	2509	29
A2427-24	30	137	0.02	0.2031	0.0012	15.1362	0.2214	0.5405	0.0075	0.918	98	2851	9	2824	14	2786	31
A2427-25	24	94	0.03	0.1948	0.0014	11.0769	0.1673	0.4124	0.0058	0.886	80	2783	11	2530	14	2226	26
A2427-26	49	153	2.03	0.1995	0.0013	7.8232	0.1148	0.2845	0.0040	0.900	56	2822	11	2211	13	1614	20

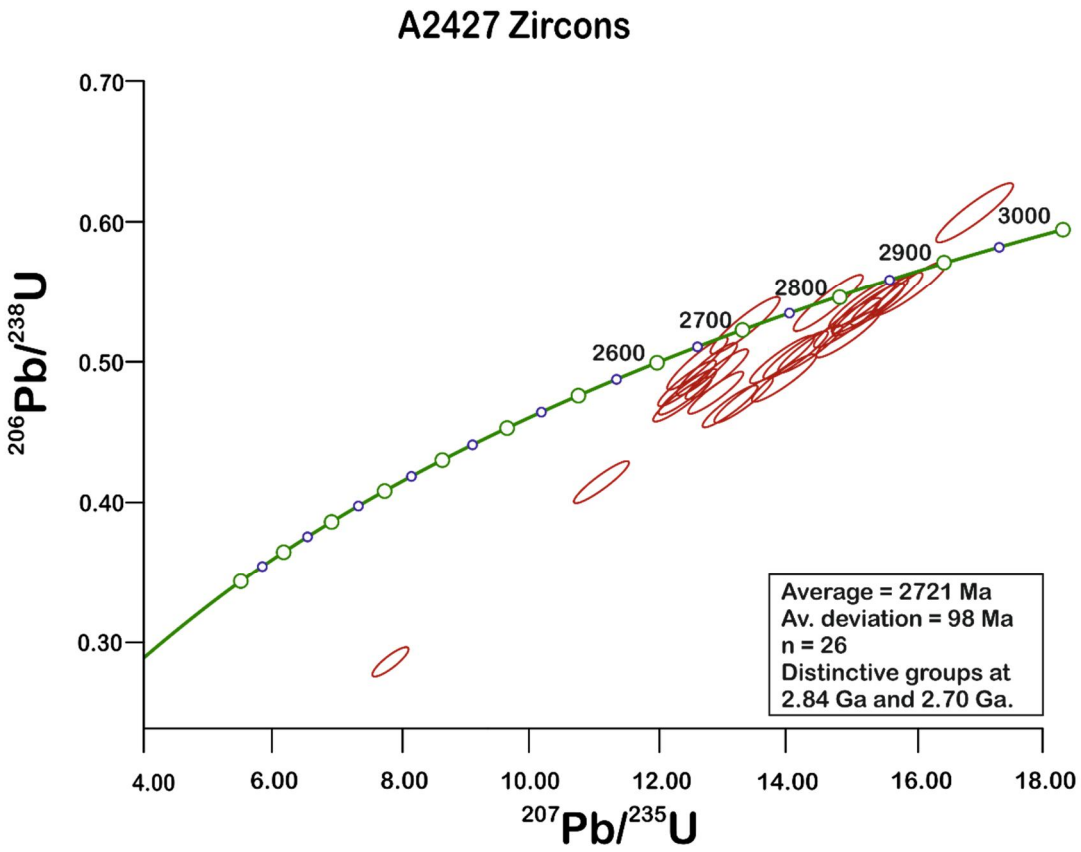

Figure 32. Concordia diagram for zircons analyses for sample A2427 (talc-chlorite schist).

7.1.2 Leucocratic gabbro (A2444)

Sample A2444 is a leucocratic gabbro located on the western boundary of the intrusion. The sample location is a few meters away from the contact to the wall rocks. The whole rock sample has 326 ppm Zr and small and ruptured zircon grains are visible in the thin section sample. The analyzed zircons (Fig. 33) have 12–476 ppm U and 7–300 ppm Pb (Table 15) and show less zoning than in A2427, and contain more inclusions than A2427. $^{206}Pb_c$ in the grains range between 0.00–2.39 %. $^{207}Pb/^{206}Pb$ range from 0.1675–0.2036 and 1σ values between 0.0004–0.0010, $^{207}Pb/^{235}U$ ratio ranges from 12.5366–16.7956 and 1σ values between 0.1836–0.2505 and $^{206}Pb/^{238}U$ range between 0.4492–0.6094 and 1σ 0.0074–0.0089. Rho value vary between 0.95–0.99, concordance between 84–112 %. $^{207}Pb/^{206}Pb$ ages result 2533–2855 Ma with an 1σ error of 4–8 Ma (Fig. 34). Two groups are set at 2.88 Ga and 2.72 Ga.

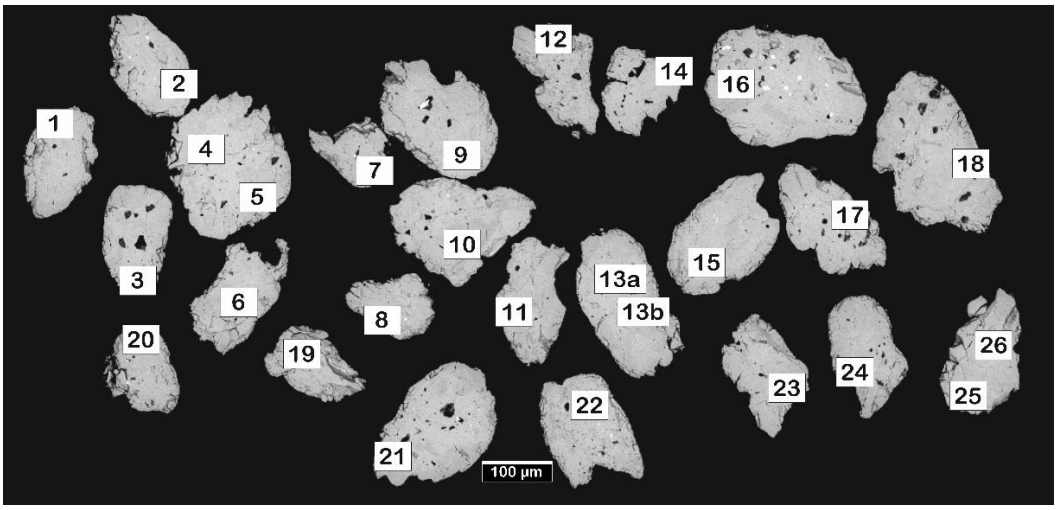

Figure 33. Analyzed zircon grains for sample A2444 (leucogabbro). Numbers marked are sample labels and also represent the spot of analysis.

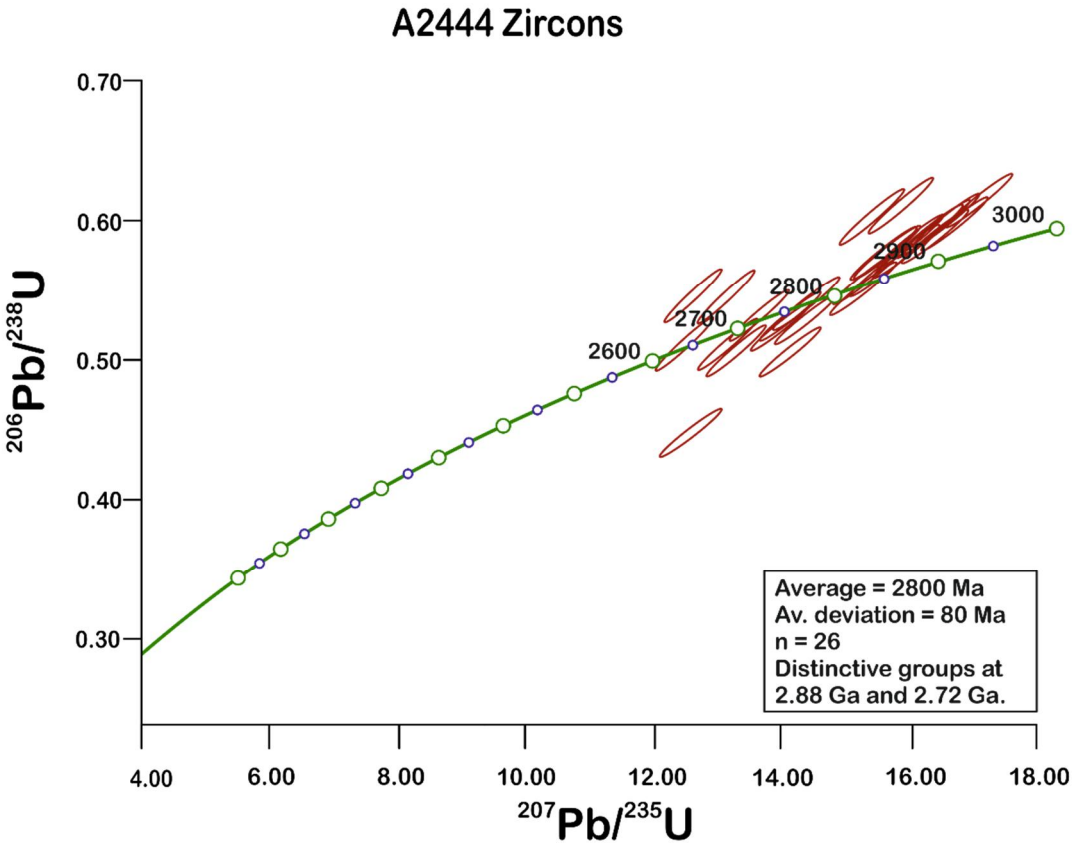

Figure 34. Concordia diagram for zircons analyses of sample A2444 (leucogabbro).

Table 15. U/Pb data for zircon samples from A2444 (leucogabbro), calculated after Stacey and Kramers (1975).

A2444	U (ppm)	Pb (ppm)	$^{206}Pb_c$(%)	$^{207}Pb/^{206}Pb$	1SE	$^{207}Pb/^{235}U$	1SE	$^{206}Pb/^{238}U$	1SE	Rho	Concor-dance (%)	$^{207}Pb/^{206}Pb$ age (Ma)	1s	$^{207}Pb/^{235}U$ age (Ma)	1s	$^{206}Pb/^{238}U$ age (Ma)	1s
A2444-1	52	45	1.00	0.2024	0.0006	14.1177	0.2092	0.5058	0.0074	0.98	92	2846	5	2758	14	2639	31
A2444-2	84	58	0.00	0.1926	0.0006	14.1141	0.2088	0.5316	0.0077	0.98	99	2764	5	2757	14	2748	33
A2444-3	324	300	2.39	0.2036	0.0006	16.7956	0.2480	0.5984	0.0087	0.98	103	2855	5	2923	14	3023	35
A2444-4	203	215	0.11	0.2014	0.0005	15.2744	0.2247	0.5502	0.0080	0.98	99	2837	4	2833	14	2826	33
A2444-5	131	104	0.21	0.1990	0.0005	16.0843	0.2369	0.5861	0.0085	0.98	105	2818	4	2882	14	2974	35
A2444-6	76	69	0.34	0.2028	0.0006	16.4758	0.2437	0.5893	0.0086	0.98	104	2849	5	2905	14	2987	35
A2444-7	41	32	0.95	0.2007	0.0006	15.6426	0.2318	0.5652	0.0082	0.98	101	2832	5	2855	14	2888	34
A2444-8	419	274	0.33	0.1746	0.0004	13.1097	0.1928	0.5446	0.0079	0.99	107	2602	4	2688	14	2803	33
A2444-9	437	363	0.13	0.1891	0.0005	15.8666	0.2333	0.6086	0.0088	0.99	112	2734	4	2869	14	3064	35
A2444-10	12	7	0.03	0.2024	0.0010	12.5366	0.1910	0.4492	0.0066	0.95	84	2846	8	2645	14	2392	29
A2444-11	476	346	0.60	0.1865	0.0005	13.1438	0.1943	0.5111	0.0074	0.98	97	2712	5	2690	14	2661	32
A2444-12	98	73	0.83	0.1972	0.0006	14.3859	0.2125	0.5290	0.0077	0.98	97	2803	5	2775	14	2737	32
A2444-13a	234	247	0.89	0.1931	0.0005	14.3673	0.2116	0.5396	0.0078	0.98	99	2769	4	2774	14	2782	33
A2444-13b	126	116	0.21	0.2004	0.0005	16.3948	0.2416	0.5935	0.0086	0.98	106	2829	4	2900	14	3003	35
A2444-14	332	219	0.20	0.1862	0.0005	13.6355	0.2007	0.5312	0.0077	0.98	101	2708	4	2725	14	2747	32
A2444-15	170	171	0.00	0.2006	0.0005	15.9865	0.2357	0.5780	0.0084	0.98	104	2831	4	2876	14	2940	34
A2444-16	135	156	0.00	0.2023	0.0005	16.9987	0.2505	0.6094	0.0089	0.98	108	2845	4	2935	14	3068	35
A2444-17	434	292	0.23	0.1675	0.0005	12.5968	0.1857	0.5454	0.0079	0.98	110	2533	5	2650	14	2806	33
A2444-18	352	208	0.15	0.1768	0.0005	12.4696	0.1836	0.5114	0.0074	0.98	101	2623	4	2640	14	2663	32
A2444-19	169	113	0.00	0.1992	0.0005	15.3517	0.2262	0.5589	0.0081	0.98	102	2820	4	2837	14	2862	34
A2444-20	202	241	1.12	0.1931	0.0006	14.1751	0.2102	0.5323	0.0078	0.98	98	2769	5	2761	14	2751	33
A2444-21	292	187	0.29	0.1901	0.0005	13.2810	0.1961	0.5068	0.0074	0.98	96	2743	5	2700	14	2643	31
A2444-22	72	60	0.56	0.2008	0.0007	16.5105	0.2458	0.5962	0.0087	0.97	106	2833	6	2907	14	3015	35
A2444-23	70	52	0.34	0.1938	0.0006	14.0150	0.2083	0.5244	0.0076	0.97	97	2775	5	2751	14	2718	32
A2444-24	166	127	0.38	0.1969	0.0005	15.6819	0.2312	0.5776	0.0084	0.98	104	2801	4	2858	14	2939	34
A2444-25	212	162	0.75	0.1860	0.0005	15.4156	0.2271	0.6011	0.0087	0.98	111	2707	4	2841	14	3034	35
A2444-26	93	80	0.80	0.1967	0.0007	15.6479	0.2325	0.5769	0.0084	0.97	104	2799	5	2856	14	2936	34

7.2 U-Pb Ages from Monazite

7.2.1 Talc-chlorite schist (A2427)

A2427 yielded multiple monazite grains (Fig. 35) during the preparation and the picked monazite grains are thus analyzed in addition to the previous zircons. The analyzed monazite grains have 71–460 ppm U and 210–1714 ppm Pb (Table 16). $^{206}Pb_c$ in the grains range between 0.00–3.15 %. $^{207}Pb/^{206}Pb$ range from 0.1143–0.1857 and 1σ values between 0.0006–0.008, $^{207}Pb/^{235}U$ ratios range from 5.5228–13.3600 and their 1σ values between 0.1186–0.2829 and $^{206}Pb/^{238}U$ vary between 0.3319–0.5217 and 1σ 0.0072–0.0113. Rho value vary between 0.97–0.99, concordance between 72–103 %. $^{207}Pb/^{206}Pb$ ages result of ages between 1869–2705 Ma and indicate three different age groups at 1869±10 Ma, 2512±7 Ma and 2603±7 Ma (Fig. 36). Three groups are set at 2.68 Ga, 2.40 Ga and 1.92 Ga.

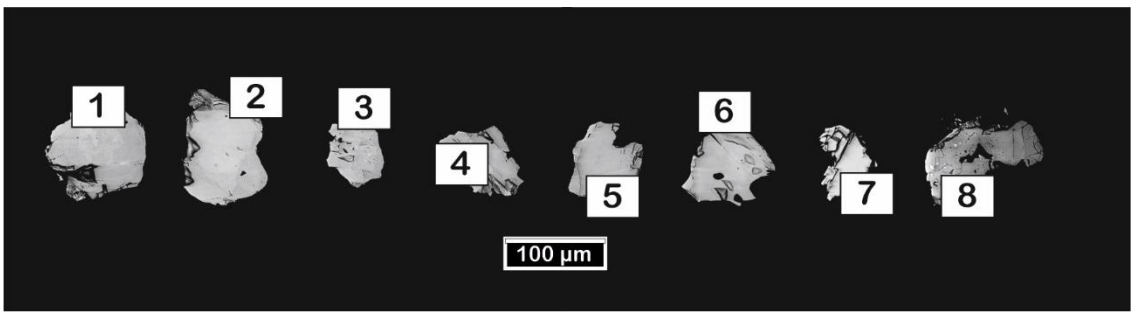

Figure 35. Analyzed monazite grains for sample A2427 (talc-chlorite schist). Numbers marked are sample labels and also represent the spot of analysis.

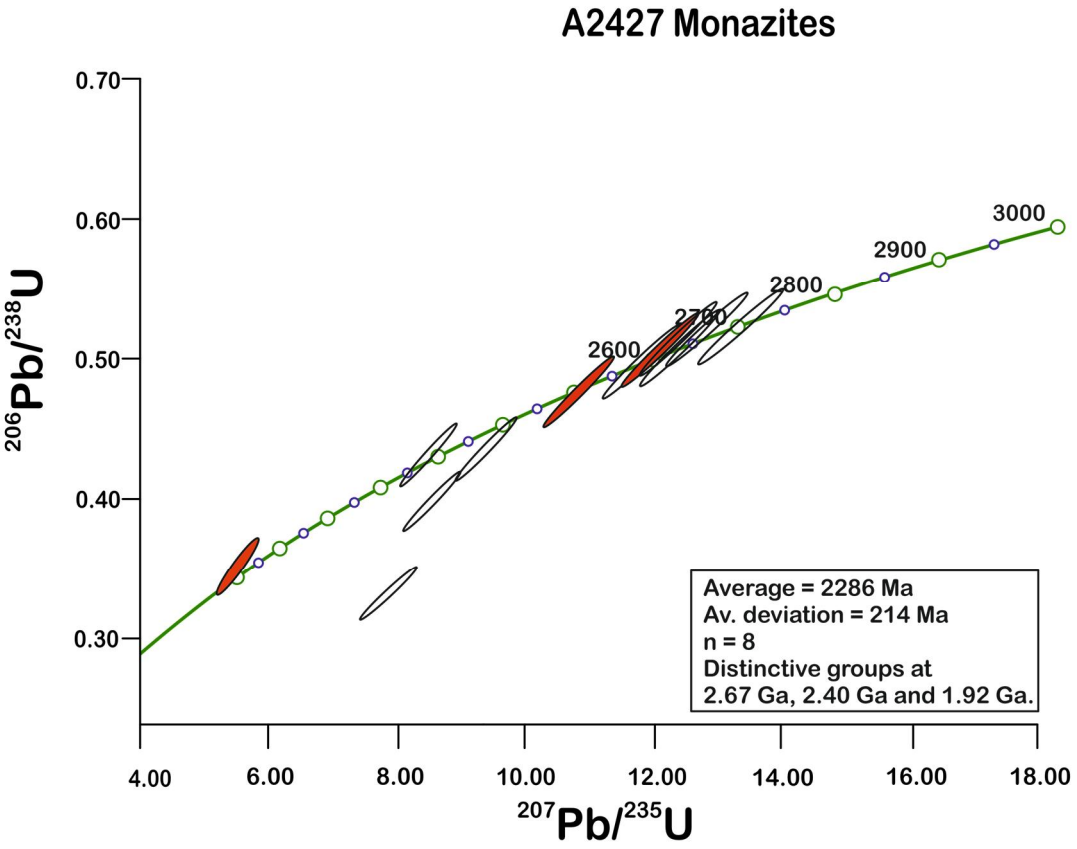

Figure 36. Concordia diagram for monazite analyses of sample A2427 (talc-chlorite schist). Areas marked with red represent ages that comply with deformative events on the area.

Table 16. U/Pb data for monazite samples from A2427 (talc-chlorite schist), calculated with methods of Stacey and Kramers (1975).

A2427 Monazite	U (ppm)	Pb (ppm)	$^{206}Pb_c$(%)	$^{207}Pb/^{206}Pb$	1SE	$^{207}Pb/^{235}U$	1SE	$^{206}Pb/^{238}U$	1SE	Rho	Concor-dance (%)	$^{207}Pb/^{206}Pb$ age (Ma)	1s	$^{207}Pb/^{235}$ U age (Ma)	1s	$^{206}Pb/^{238}$ U age (Ma)	1s
A2427Mz-1	110	425	0.01	0.1857	0.0007	13.3600	0.2829	0.5217	0.0113	0.98	100	2705	6	2705	20	2706	48
A2427Mz-1b	157	503	0.01	0.1567	0.0006	9.3810	0.1988	0.4343	0.0094	0.98	96	2420	7	2376	19	2325	42
A2427Mz-2	460	1714	0.00	0.1738	0.0006	12.1083	0.2552	0.5053	0.0110	0.99	102	2594	5	2613	20	2637	47
A2427Mz-2b	81	210	0.19	0.1143	0.0006	5.5228	0.1186	0.3505	0.0076	0.97	103	1869	10	1904	18	1937	36
A2427Mz-2c	114	401	0.01	0.1654	0.0007	10.8438	0.2300	0.4755	0.0103	0.98	100	2512	7	2510	20	2508	45
A2427Mz-3	215	526	0.00	0.1721	0.0006	7.8740	0.1666	0.3319	0.0072	0.98	72	2578	6	2217	19	1848	35
A2427Mz-4	140	524	0.00	0.1779	0.0007	12.4328	0.2630	0.5067	0.0110	0.98	100	2634	6	2638	20	2643	47
A2427Mz-5	201	736	0.00	0.1726	0.0006	11.8215	0.2497	0.4968	0.0108	0.99	101	2583	6	2590	20	2600	46
A2427Mz-6	71	269	0.01	0.1746	0.0008	12.3539	0.2628	0.5131	0.0111	0.98	103	2603	7	2632	20	2670	47
A2427Mz-7	185	588	0.97	0.1432	0.0006	8.5022	0.1804	0.4307	0.0093	0.98	99	2266	7	2286	19	2309	42
A2427Mz-8	128	491	2.17	0.1791	0.0008	12.8305	0.2725	0.5196	0.0113	0.98	98	2644	7	2667	20	2698	48
A2427Mz-8b	220	650	3.15	0.1561	0.0007	8.5478	0.1815	0.3973	0.0086	0.98	83	2413	7	2291	19	2156	40

7.3 Sm-Nd ages from whole-rock composition

Sm-Nd isotope compositions are analyzed from samples A2426 (diabase) and A2427 (gabbro). A2426 is a diabase from DH11 at the depth of 54.60–56.50 m. It has 4.92

ppm Sm, 20.58 ppm Nd and $^{147}Sm/^{144}Nd$ 0.1444 and $^{143}Nd/^{144}Nd$ of 0.511676 which result in an age of 2 393 Ma with and ε_{Nd} of -2.7 and an error range of 71 Ma (Table 17). Sample A2427 is a talc-chlorite schist from DH 9 at the depth of 88.90–91.20 m. It has 14.44 ppm Sm and 36.36 ppm Nd. $^{147}Sm/^{144}Nd$ 0.2401 and $^{143}Nd/^{144}Nd$ 0.513185 which result in an age of 2 393 Ma, ε_{Nd} of -2.8 and an error range of 71 Ma. For T(0) the A2426 has -18.80 and the A2427 10.63.

Table 17. Sm-Nd isotope data for samples A2426 (diabase) and A2427 (talc-chlorite schist.).

Sample	Sm (ppm)	Nd (ppm)	$^{147}Sm/^{144}Nd$	$^{143}Nd/^{144}Nd$	T (Ma)	eps(T)
A2426	4.92	20.58	0.1444	0.511676	2400	-2.7
A2427	14.44	36.36	0.2401	0.513185	2440	-3.0

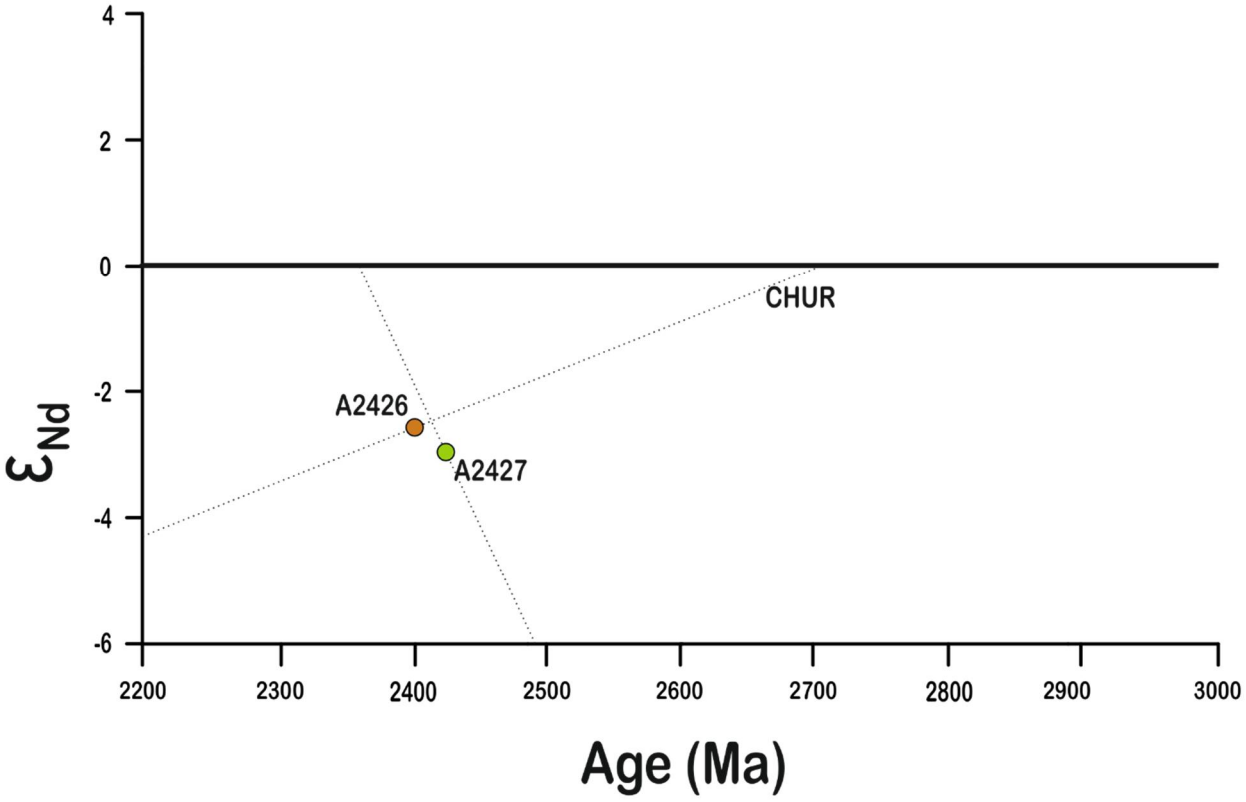

8. DISCUSSION

8.1 Layering

Is seems that Archean mafic-ultramafic layered intrusions have typically gone through high mineralogical and textural alteration, especially in their most mafic parts (Polat et al 2012.), due to greenschist-granulite facies metamorphosis as well as possible hydrothermal alteration or partial melting (Windley et al 1981, Korsch and Gulson 1985 Lambert et al. 1989 and Hoatson and Sun 2002). In comparison, the Proterozoic intrusions have usually gone through more lower to amphibolite facies metamorphic alteration throughout the whole intrusion, rocks have altered into metaperidotite or -pyroxenite and partial melting is less common (Mutanen and Huhma 2001 and Hanski et al. 2010), the most altered example being the Portimo intrusion (Alapieti et al 1990). The alteration also poses a possibility of errors for the Sm-Nd analysis in chapter 7, since the system could have been opened (Hanski et al. 2010) multiple times due to the metamorphic events in the Karelian (Kontinen et al. 2007, Lauri et al. 2011 and Lahtinen et al. 2015). Although the intrusion is strongly metamorphosed (Fig. 43) it is still possible to note textures and structural layers common in layered intrusions (Wager and Brown 1968, Naslund and McBirney 1996, Hall 1996, Namur et al. 2015). The plagioclase phenocrysts mainly visible in the field outcrops (Fig. 3C) and chemical composition of leucocratic gabbros make most of the textural layering within the intrusion (Wager and Brown 1968, Zhou et al 2005), whereas actual modal or grainsize based layering are nigh visible. Cryptic layering is well visible in mineral- and rock compositions and is used as a base along with rock types when modeling the intrusion in figure 39.

The intrusion can be divided into 3–4 different layers, the floor and the roof of the intrusion, with floor beginning after the tonalite-gneiss contact in the east and the roof in contact with the biotite paragneiss. The whole shape of the intrusion is a droplet like sheet with its ‘tail’ pointing towards north at DH 12 where the intrusion ends as a thin tail and the head or center lying between drill cores 7 and 8. The anorthositic and leucogabbroic layers

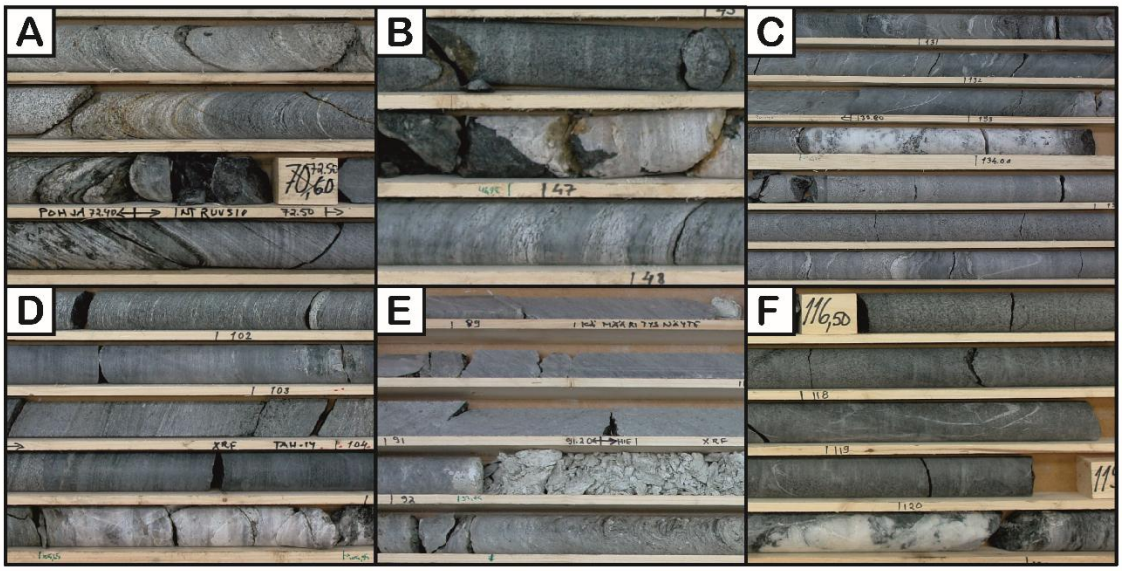

Figure 38. A) Contact between the intrusions bottom layer and tonalitic bedrock, B) contact between the intrusion and diorite in DH 10 and C) contact between the intrusion's roof and biotite paragneiss at the end of DH 10. Figures D (A2444)–E (A2427) show samples chosen for the U-Pb isotope analysis and figure F shows the sample chosen for Sm-Nd analysis (A2426).

visible in drill cores 7 and 8 also seem to continue and surface as outcrops some 100 meters south from the drill holes as depicted by Tapio Halkoaho (Mikkola et al. 2013), and thus give some insight of the intrusions current, well rotated positioning (Fig. 39). Anorthositic plagioclase (Fig. 29) and its alteration with likely a Ca-poor pyroxene (Campbell 1996) crystallizing on top of the intrusion indicates either a new pulse of magma or that some Ca-rich melt lasted until the very end of the crystallization. On the other hand, the intrusions layering bears some resemblance to the 2.97 Ga Fiskenaesset Anorthosite-leucogabbro layered complex in Greenland (Windley et al. 1981, Ashwal et al. 1989 and Polat et al. 2012), where the bottom is composed of a mafic layer surrounded by gabbros overlain by leucogabbroic and anorthositic layers. The proposed layering of gabbroic rocks and accumulated plagioclase crystals surrounding the mafic layers indicates a possible basaltic inversion, which could further indicate a new magma pulse that was introduced into the intrusion or a highly tilted orientation which makes the assumption of the intrusion's original orientation undeterminable.

The crystallization of the intrusion likely formed three or four different layer groups with 1st mafic bottom of olivine-peridotite with cumulus spinel that transits into a more gabbroic layer that 2nd has convecting plagioclase crystallizing in it, until the very end of crystallization where Ca-rich anorthites formed an anorthositic layer on the intrusions

bottom (visible in DH 7). The 2nd layer is made of four cycles of plagioclase and gabbroic layers. The 3rd layer consist of ca-poor pyroxene and plagioclase that alter until the crystallizing systems energy balances between equilibrium. 4th layer is located beneath the 1st layer, but like the 2nd layer it has gabbroic rock and leucocratic gabbro roughly 50 meters thick that ends in multiple thin anorthositic layers. The PGE-minerals in the ultramafic layers probably formed during crystal compaction during the intrusions crystallization (Bourdeau and McCallum 1992) or a fluid transporting the sulfides during the metamorphic events, since the PGEs are usually found in the gabbroic rocks in the upper parts of these intrusions (Godel 2015).

Sulfide and PGE –formation on the very bottom and 'tail' parts of the intrusion are likely results in formation of mafic rocks, as well as possible fluid movement during the metamorphosis. This could also be resulted by hyper-aluminous magma proposed by plagioclase crystallization and multiple magma pulses (McCallum 1996).

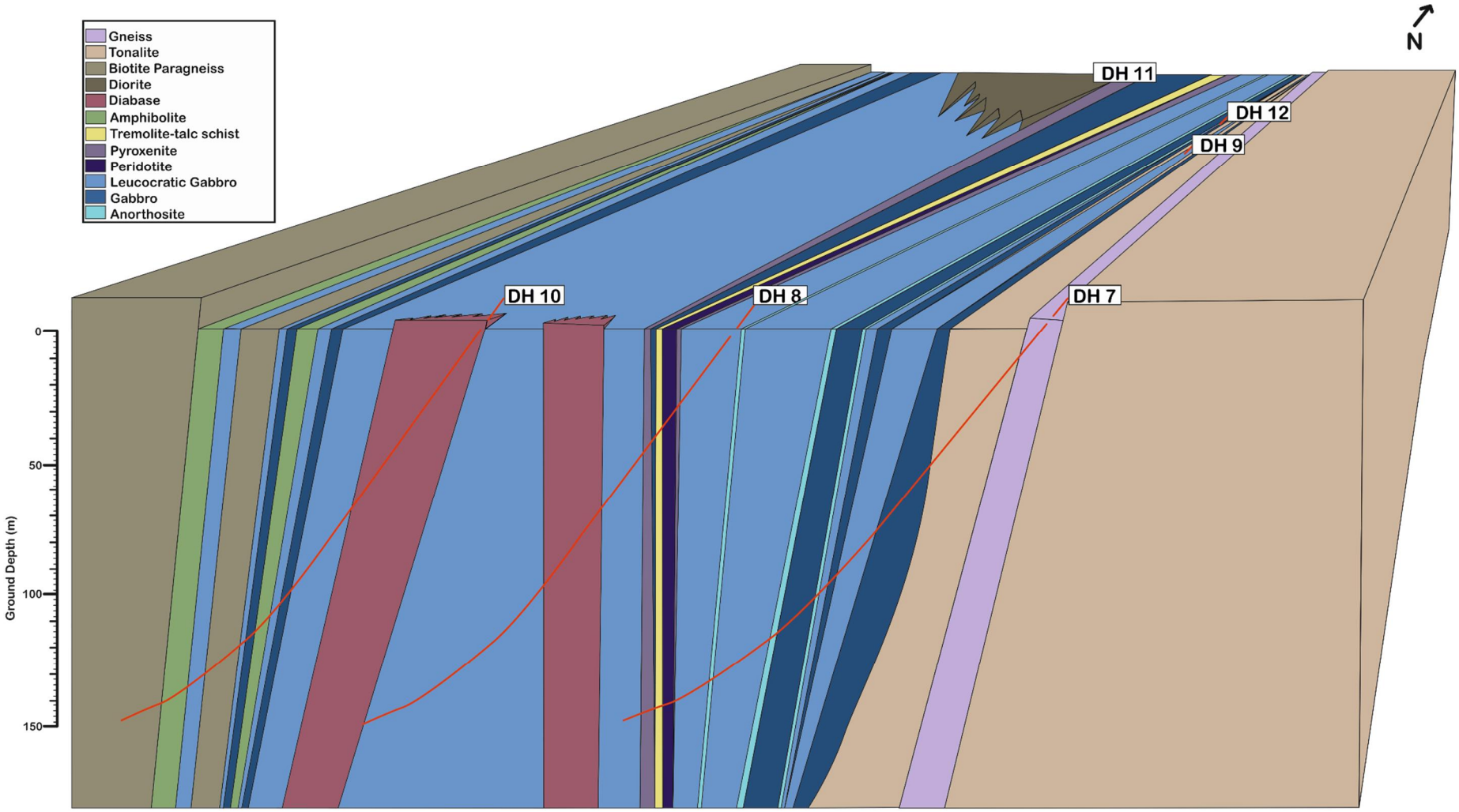

Figure 39. A schematic model of the Kuohatti mafic layered intrusion based on the drill core observations, petrography and geochemistry discussed in chapters 3 and 4. Drill cores are labeled accordingly and the red lines represent their directions and dips.

8.2 Petrology

When plotted to an AFM –diagram (Fig. 40, Irvine and Baragar 1971) the geochemistry of the Kuohattijärvi layered intrusion is seen as distinctive groups of the major rock types, as well as possible contamination within the two gabbros. Most notably gabbroic rocks form clear groups also on the CaO-MgO-Al_2O_3 –diagram (Fig. 41). The more differentiated leucocratic gabbros fall under the calc-alkaline field, whereas the other major rocks of the intrusion are tholeiitic. The two gabbros also overlap very slightly and might thus suggest the same origin for these rocks. The other primitive mafic rocks differ from the gabbros on both diagrams, which likely indicates the being crystallized before these gabbroic rocks as they should in a mineralogically layered intrusion (Hall 1996). A possible magmatic evolution indicated (Fig. 40 and 41) would likely be pyroxenite-peridotite-gabbro-leucocratic gabbro-anorthosite, where plagioclase cumulates formed in the gabbro either due to contamination or high amounts of plagioclase cumulates differentiating from the mafic magma.

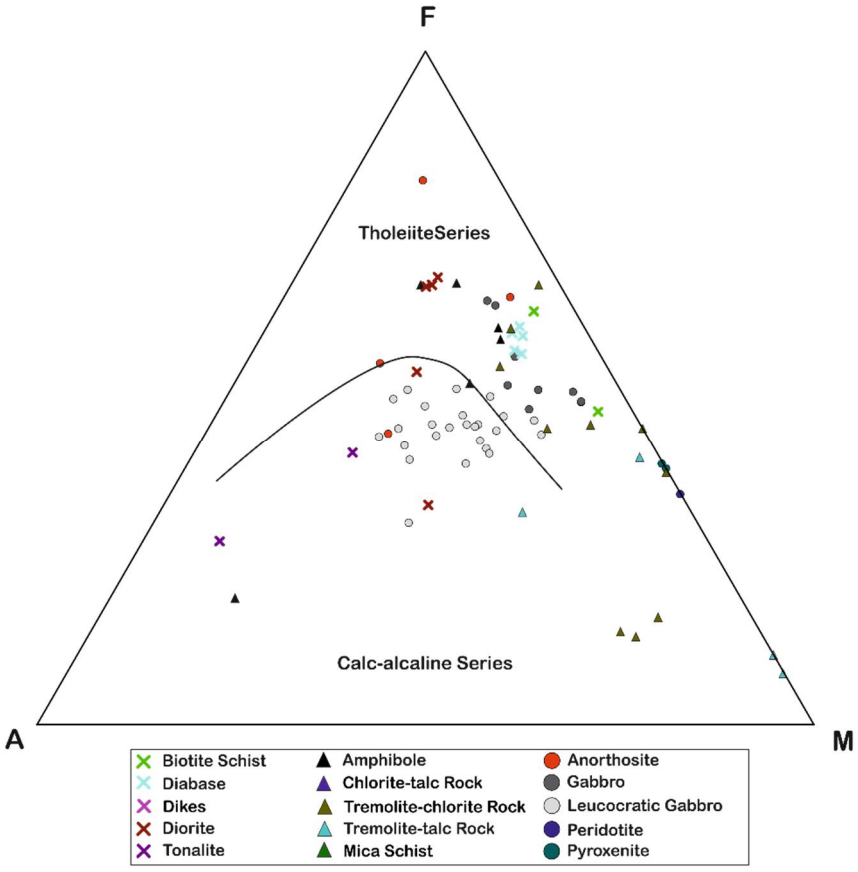

Figure 40. AFM-diagram for the major rock types of the Kuohatti mafic layered intrusion, after Irvine and Baragar (1971).

The higher degree of differentiation on the leucocratic gabbros might be due to plagioclase cumulates forming in the intrusion due to gravitational crystal floating (Ashwal 1993, Nashlund and McBirney 1996 and Campbell 1996). This would also explain the high Al_2O_3 content within these rocks as it would be a one typical for leucocratic gabbros filled with anorthosites (Ashwal 1993). The gabbros would then signify the likely composition for leucocratic gabbros before their differentiation during the formation of the layered intrusion. It could also be possible that the leucocratic gabbro differentiated from the melt due to some fraction of contamination as the original melt continued evolving and resulting as a more tholeiitic end-result. The rhythmic layering of the two gabbroic rocks also points out a possibility of multiple magma pulses that fed the convection and plagioclase crystallization with new aluminum-rich magma (McCallum 1996).

The anorthositic layers in the vicinity of these gabbroic rocks could be results from pressurized crystallization of fluctuation during possible lamination of the plagioclase crystals or the uppermost part of the fractionating crystals mush that crystallized on top of the leucocratic gabbro (Eales and Cawthorn 1996). The Ca-enrichment in plagioclase during the intrusion crystallization (Figs. 18–23) could also indicate the thermal changes within the intrusion as the more anorthositic plagioclase would need a degree of heat to crystallize, although this likely has been interrupted by metamorphosis and convection of the plagioclase crystals (Ashwal 1993, Eales and Cawthorn 1996).

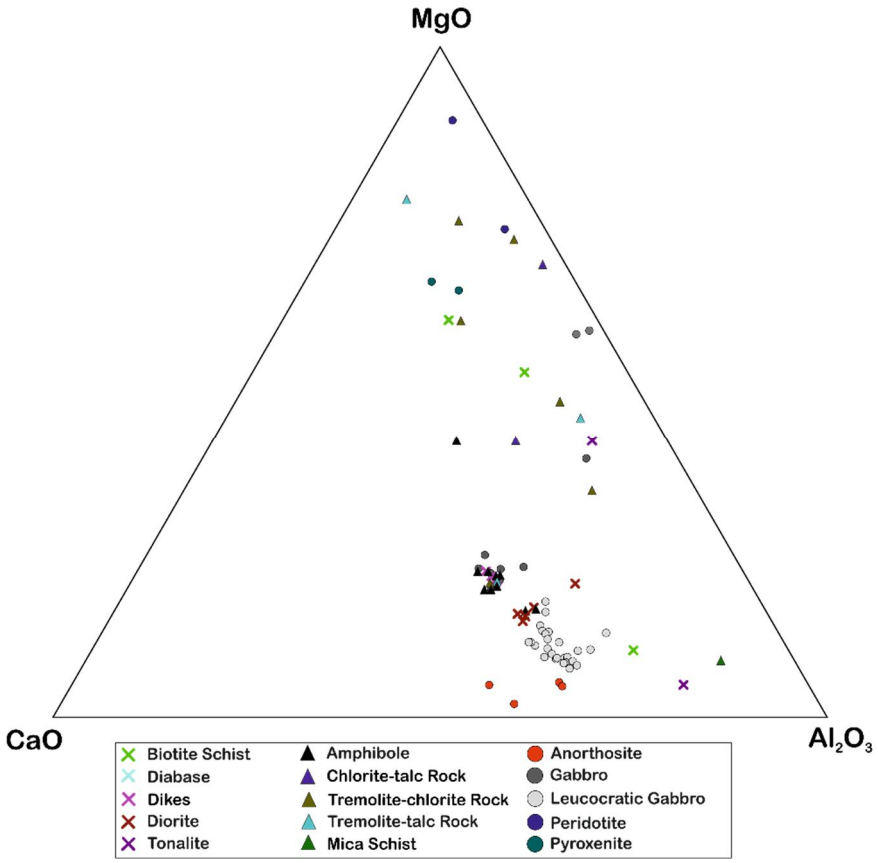

Figure 41. CaO-MgO-Al_2O_3-diagram for the major rock types of the Kuohatti mafic layered intrusion and other rock types within its vicinity.

Differentiation between different rock types can be noted from relative MgO contents (Fig. 42) with other elements, especially iron, chromium and calcium. These diagrams also show grouping of tremolite- and talc-based rocks with the pyroxenites and peridotites of the intrusion, signaling of a metamorphosis of at least granulite facies that resulted in metamorphic recrystallization within the most mafic rocks of the intrusion. Most of these metamorphosed mafic rocks as well as the remnants of pyroxenites and peridotite have crystallized on the lower parts of the intrusion. The metamorphic events at the Kuohatti area after the formation of the intrusion also seem to have impacted these mafic layers the most, which could be explained by the stability of these minerals on upper crust in the Bowen's series.

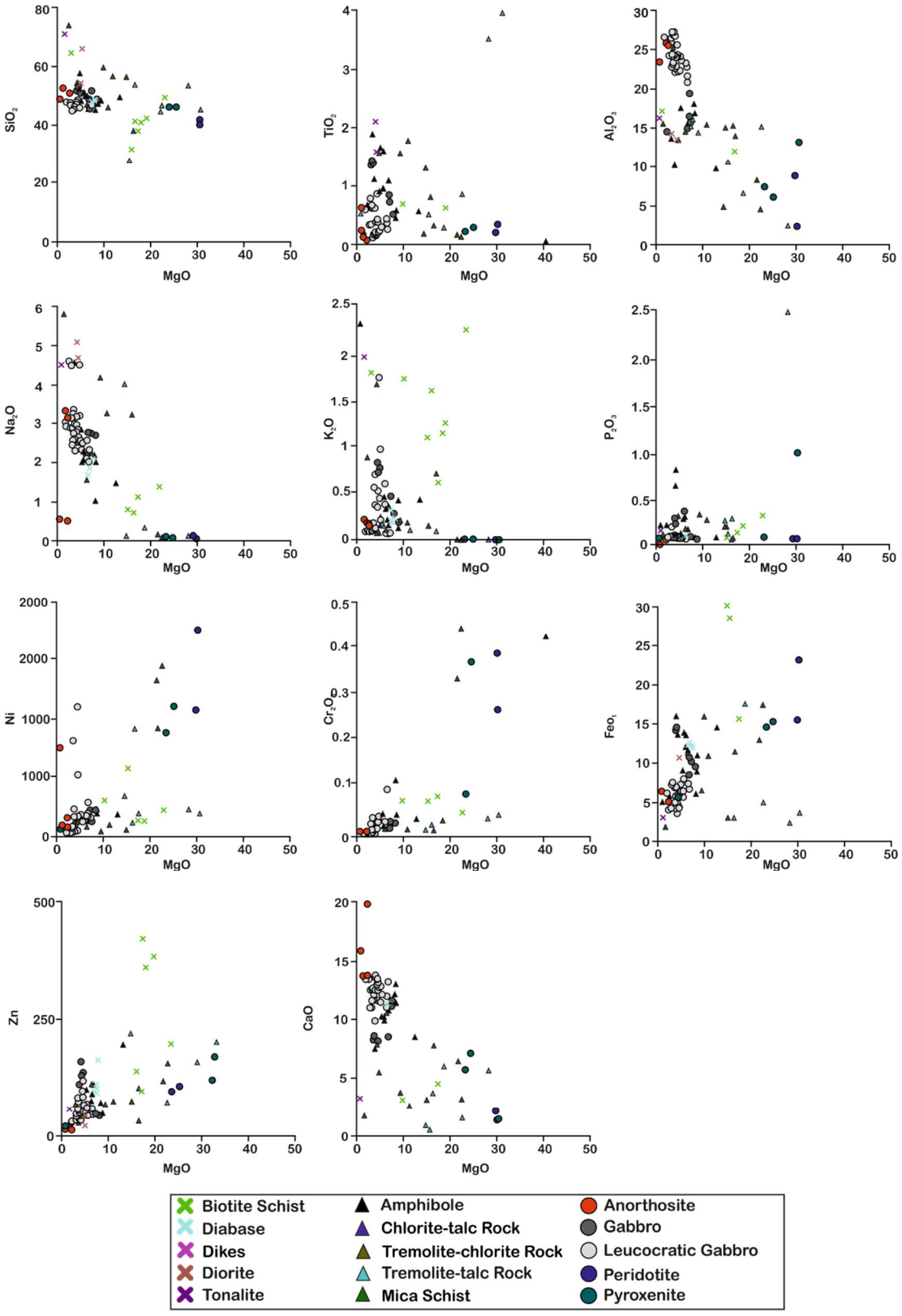

Figure 42. Multiple elements plotted relative to the MgO whole-rock composition of the Kuohatti mafic layered intrusion.

Chondrite-normalized REE patterns show correlation with each other (Fig. 26), although some anomalies within gabbroic rocks and tremolite-based schists vary slightly. The ultramafic rocks have slightly less differentiation from the average composition, whereas the gabbroic rocks are further from it. Eu-anomalies accompanied by enriched Light-REE (LREE) relate to plagioclase accumulation (Pettigrew and Hattori 2006), which suggest that the lack of Eu-anomalies on some gabbros suggest them to be crystallized with less or none plagioclase fractionation. The overall trend on these rocks is mainly LREE enriched, yet some mafic rocks in DH's 8, 9, 11 as well as the tonalite in DH 11 show an HREE depleting trend. One sample from the diabase cutting the intrusions shows a steeper HREE depleted trend, which matches with the ultramafic and mafic volcanic rocks analyzed from the surrounding areas (Mikkola et al. 2013)

The samples show change though, as the main minerals swap in CIPW-normative compositions between plagioclase-hypersthene-diopside and plagioclase-diopside-olivine or even plagioclase-hypersthene in one sample. This is neither observable as different layers between gabbros, which makes it more likely to a normative error. The gabbros also have more than twice the amount of magnetite, ilmenite and apatite.

The anorthosites (Fig. 8) on the other hand show way lower average An-component than the individual grains analyzed in chapter 6. The high An-component present in the chapter seems like a primal compositions as the metamorphic anorthosites (Mora et al. 2009) would be more ruptured and have higher An on their metamorphic rims (Steffen and Selverstone 2006). It is likely that the high amount of plagioclase and ilmenite cause distraction on the CIPW-normalization used here.

The tremolite- and talc-based rocks (Table 11) show an ultramafic origin, which is seen in some samples as extremely high amounts of calculated olivine and ca-poor pyroxenes, although some normative errors are plausible as these rocks are now highly altered. The olivine and orthopyroxene probably are the first minerals to be crystallized on the sequence within these ultramafic layers, then some diopside along with them.

8.3 Mineral phases and origins within the intrusion

8.3.1. Olivine

Analyzed olivine grains show a degree of variation in their MnO and Ni amounts, although the forsterite component has a very limited variance (Fig. 43 and 44). The likelihood of olivine being of metamorphic origin is very likely, as the grains are so fresh in contrast to the pyroxene grains. When the analyzed olivine samples are plotted with their forsterite component against MnO and Ni (Fig. 43 and 44), metamorphisism is even more likely. The olivine analyzes (Table 12) also match well with analyzes from other metamorphic olivines (Peltonen 1990) from Eastern Finland, although their SiO_2 content seem to be slightly higher and FeO lower.

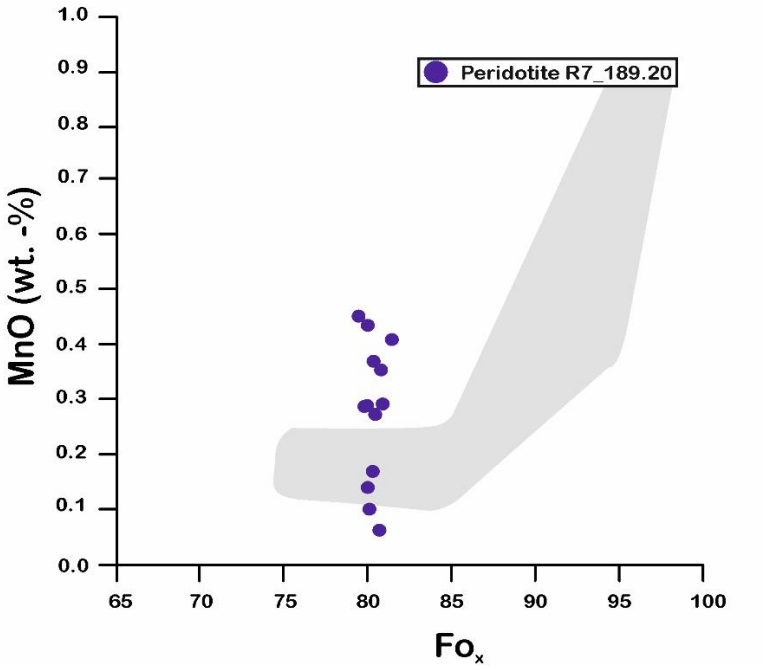

Figure 43. Analyzed olivine samples in respect of MnO (wt. -%) and Fo# (MgO/MgO+FeO). The grey are marks range for magmatic olivine (Blais 1989, Piquet 1982 and Peltonen 1990).

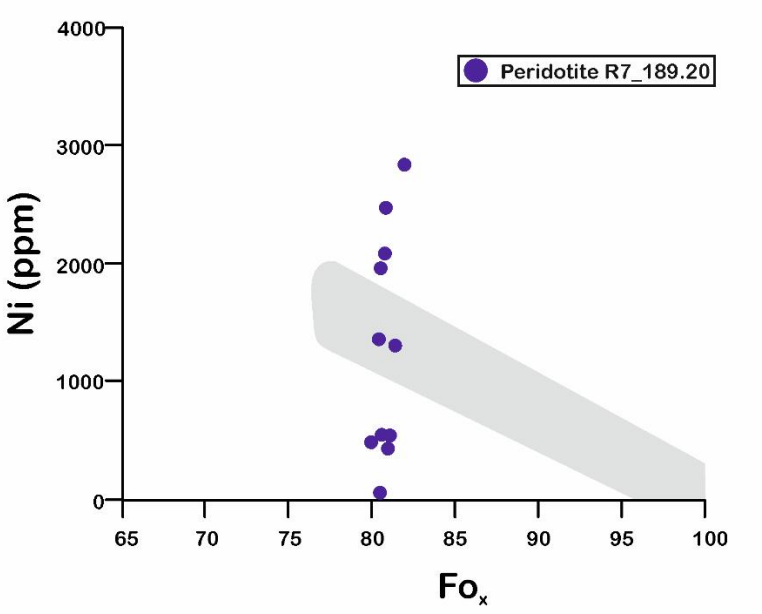

Figure 44. Analyzed olivine samples in respect of Ni (ppm) and Fo# (MgO/MgO+FeO). The grey area is the range of magmatic olivine (Blais 1989, Piquet 1982 and Peltonen (1990).

8.3.2. Pyroxene

The pyroxene samples analyzed seem to be orthopyroxene (Fig. 28), yet notably in sample R7_184.60 the analyzed pyroxenes here might well have a metamorphic origin (see also olivine 8.3.1). One the other hand, sample R7_83.05 likely represents remnants of a Ca-poor orthopyroxene formed during the later stages of crystallization along with plagioclase (Hall 1996).

8.3.3. Plagioclase

The analyzed plagioclase samples verify a strong fractionation between different layers and rock types (Fig. 29). This is likely a result of fractional crystallization and crystal floating, which strongly increases along with the minerals' grain size (Hall 1996). This is likely exactly what happened on the leucocratic gabbros on the uppermost parts of the intrusion and possibly with the anorthositic layers. More Na-rich plagioclase from the tremolite-talc schist could in addition indicate a mafic mineralization of Ca-rich pyroxene (Eales and Cawthorn 1996) and possible olivine, which caused a more Ca-poor plagioclase to crystallize. The anorthositic layers formed during the early stages of crystallization, possibly during or right after the ultramafic layers, and formed in situ on the bottom layers.

8.3.4. Amphiboles

Amphiboles from the pyroxenites and peridotite have compositions that set them into actinolite or tremolite of the actinolite-tremolite series (Fig. 30), although these end members are distributed between different samples and only the peridotitic samples have amphibolites from both end-members within the actinolite-tremolite series. The latter peridotite sample does in addition have some grains of magnesio-hornblende which could hypothetically be remnants of past olivine grains. The Ca-rich composition of these amphiboles suggests that they likely represent alternated past Ca-rich pyroxenes, which are now completely extinct from the intrusion (Table 9.) The analyzed amphiboles in table 13 also have compositions quite common to clinopyroxenes from other locations (Talousani et al. 2005), except for FeO and CaO that likely were taken elsewhere by possible hydrothermal alteration.

8.4. Age of the intrusion

The ruptured structure of the zircon grains (Figs 32 and 33) that bear more resemblance to the zircons' cores rather than those freshly crystallized from a magma in situ, arouse suspicions of their true origin. Only the leucocratic gabbro selected for analysis had enough visible zircons in thin section within the intrusion, yet the sample is located only 10 meters from the wallrock. There is also a lot of scattering within the resulted ages, as well as a Proterozoic affect, likely resulting in somewhat younger ages (See Fig 32 and 33) than their actual crystallization. The texture, resulted ages and lithological locations, selected for analysis (Chapter 7) lead to a conclusion that these zircons actually originated from the wallrock of the intrusion, and are placed wihin the intrusion during its crystallization and emplacement. In addition, the greenschist from the Kuohattijärvi suite is previously dated older than 2.7 Ga (Mikkola et al. 2013). The zircons analyzed here result in ages of 2.53–2.86 Ga for the rocks surrounding the intrusion, with most of the samples in either 2.70 Ga or 2.85 Ga. Their isotopic composition also matches with other Archean zircons from other layered intrusions (Korch and Gulson 1985, Arndt et al. 1991).

These Archean wallrocks went through multiple deformation events, most visible in the analyzed monazite grains (Fig 34), since monazite crystals are more likely to be affected by metamorphic events rather than zircons (Dahl 1997). The analyzed monazites result

in approximate age groups of 2.7–2.8 Ga, 2.4–2.5 Ga and 1.9 Ga, which correlate with the magmatic and metamorphic events on the Karelian craton. 2.7–2.8 Ga mark on the monazite is likely caused by the Archean magmatic events on the Karelian (Kontinen et al. 2007), whereas 2.4–2.5 Ga likely correlates with the mafic magmatism related to most of the Proterozoic layered intrusion in the vicinity of the study area. The grain at 1.9 Ga correlates with the Svecofennian orogeny and collision. It is also likely that the formation of the diabase dikes in the Eastern Finland (Vuollo et al. 1992, Vuollo and Huhma 2005, Mikkola et al. 2013) is visible in these monazite ages.

The age of the diabase sample (A2426) might be within the same age range of other diabase and diorite dikes from the area, analyzed by Vuollo and Huhma (2005) and Mikkola et al. (2013) from Eastern Finland and by Hanski et al. (2010) from layered intrusions in the Kuhmo district, but no distinctive age can be given for the diabase analyzed here. The resulted zircon ages also match the formation of tonalites in the Kuhmo area (Käpyaho et al. 2006, Käpyaho et al. 2007). Both the diabase and diorite dikes within the intrusions show almost no traces of metamorphic deformation and are likely lithlologically younger than any other rocks within the study area. The Sm-Nd composition of this diabase compiles with the other diabase dikes in the area (Vuollo and Huhma 2005, Mikkola et al. 2013). The difference between the diabase and Archean wall rock seems to be quite high (Table 16), which indicates a different origin for these two, which further supports the hypothesis that these diabase dikes are related to the previous ones noted from the area. The εNd of the wall rock seems to be quite high and due to the high level of alteration, these results must be approached cautiously as the actual Sm-Nd might be different.

Thus, the accurate age of the Kuohatti intrusion till remains unsolved and cannot be concluded from the data provided in this study. Further analysis is still needed, possibly from another, more zircon enriched location within the intrusion. Some careful age estimations can be made though, based on the fact that most of the deformation and magmatic events can be noted from the monazite analysis. The minimum age of 1.9 Ga is quite evident and the intrusion has to be formed during one of the events that left a mark on the monazite population. Other ruptured zircon grains, like the ones in this study, have previously been noted by Lauri et al. (2011) from the 2.4–2.5 Ga Proterozoic layered intrusions and zircon grains. The high amount of metamorphosis

would give an argument for the intrusion to be of Archean origin, as such intrusion have typically gone through high degrees of alteration and deformation (McCalum 1996, Mathison and Ahmat 1996), although this is the most unlikely scenario when concerning the data presented, yet still no definitive age can be given.

9. SUMMARY

The Kuohatti mafic layered intrusion has gone through multiple metamorphic events, notable on its structure and mineralization. Although highly altered due to these events, slight structural and cryptic layering are still visible and the intrusion is divided into 4 distinctive layers. The ultramafic rocks are strongly altered whereas the more shallow gabbroic rocks only have occasional metamorphic olivine and pyroxenites indicating a high-temperature medium-pressure metamorphic facies for the area. High amounts of plagioclase fractionation and occurrence in the intrusion are noteworthy as well as sulfide mineralization and possible magmatic events related to these events. The accurate age of the intrusion still remains unsolved in this work, although relative age for the Archean wall rock (2.6–2.8 Ga) and 2.4–2.5 Ga diabase dikes was confirmed. Multiple deformative events are visible on the monazites and zircons that originated from the surrounding rocks. One of these events is likely to present the age of the intrusion's formation, yet no further estimates can be made without further isotopic evidence.

10. ACKNOWLEDGEMENTS

Making this thesis was one of the best – although also the longest – things I did during my studies at the department of Geosciences. It was also very rewarding to take part in almost all analyzes used in this work. First I would like to thank both of my supervisors prof. Tapani Rämö and docent Tapio Halkoaho for being helpful and creative with the thesis. I also want to thank Pauli Saksa and Heli Kivisaari for giving a quick review on the work. Radoslaw Michallik was a huge help at the microprobe, thanks man! Everyone at the GTK, especially Maria Vuorio, Jenni Keränen, Hugh O'Brien and Hannu Huhma for being a huge help and having time for my questions. I had inspiring

conversations with Kirsi Larjamo, Henrik Kalliomäki and Jussi Heinonen at the University of Helsinki department of geosciences, big thanks to all of you! Riikka Fred gave a lot of support during rough times. Lastly I would like to thank my parents and sisters for being so supportive and understanding during my studies at the university, I wouldn't have made this without you!

11. REFERENCES

Alapieti, T., Filén, B., Lahtinen, J,. Lavrov, M., Smolkin, V. and Voitsekhovsky, S. 1990. Early Proterozoic Layered Intrusions in the Northeastern Part of the Fennoscandian Shield. Mineralogy and Petrology, 42. 1–22.

Andersen, T., Griffin, W., Jackson, S., Knudsen, T. and Pearson, N. 2004. Mid-Proterozoic Magmatic Arc Evolution at the Southwest Margin of the Baltic Shield. Lithos, 73. 289–318.

Arndt, N., Nelson, D., Compston, W., Trendall, A. and Thorne, A. 1991. The Age of the Fortescue Group, Hamersley Basin, Western Australia, from Ion Microprobe Zircon U-Pb Results. Australian Journal of Earth Sciences, 38. 261–281.

Ashwal, L., Jacobsen, S., Myers, J., Kalsbeek, F. and Goldstein, S. 1989. Sm-Nd age of the Fiskenaesset Anorthosite Complex, West Greenland. Earth and Planetary Science Letters, 91. 261–270.

Ashwal, L. 1993. Anorthosites. Springer-Verlag, Berlin. pp. 5–81.

Blais, S. 1989. Les Ceintures de Roches Vertes Archdennes de Finlande Orientale. Géologie, Pétrologie, Géochemie et Évolution Géodynamique. Centre Armoricain d'Etude Structurale des Socles, 22. 256 p.

Boynton, W. 1984. Cosmochemistry of the Rare Eart Elements: Meteorite Studies. In: Henderson, P., Rare Earth Element Geochemistry. Developments in Geochemistry, 2. pp. 63–114.

Campbell, I. 1996. Fluid Dynamic Processes in Basaltic Magma Chambers. Cawthorn, R. (editor), Layered Intrusions, Elsevier Science B.V. 45–76.

Dahl, P. 1997. A Crustal-chemical Basis for Pb Retention and Fission-track Annealing Systematic in U-bearing Minerals, with Implications for Geochronology. Earth and Planetary Science Letters, 150. 277–290.

DePaolo, D. 1981. Neodynium Isotopes in the Colorado Front Range and Crust-Mantle Evolution in the Proterozoic. Nature, 291. 193–196.

Deer, W., Howie, R. and Zussman, J. 1963a. Rock-Forming Minerals vol. 4 – Framework Silicates. Longmans, London.

Deer, W., Howie, R. and Zussman, J. 1963b. Rock-Forming Minerals vol. 2 – Chain Silicates. Longmans, London. pp. 1–161.

Eales, H. and Cawthorn, R. 1996. The Bushweld Complex. Cawthorn, R. (editor), Layered Intrusions, Elsevier Science B.V. 181–229.

Geological Survey of Finland. 2015. Bedrock of Finland 1:200 000. Geological Survey of Finland, Espoo.

Godel, B. 2015. Platinum-Group Element Edposits in Layered Intrusions: Recent Advances in the Understaindin of the Ore Formin Processes, In: Layered Intrusions, Charlier, B., Namur, O., Latypov, R. and Tegner, C. (editors). Springer Geology. pp. 379–434.

Halkoaho, T. and Niskanen, κ. 2012. New PGE-Cu-Ni Observations from the Early Paleoproterozoic Junttilanniemi Layered Intrusion, Paltamo, Eastern Finland. Geological Survey of Finland: Report of Investigation, 198. 29–33.

Hall, A. 1996. Igneous Petrology 2nd Edition. Longman Group Limited, Essex. 551p.

Hanski, E., Huhma, H. and Vuollo, J. 2010. SIMS Zircon Ages and Nd Isotope Systematic of the 2.2 Ga Mafic Intrusions in Northern and Eastern Finland. Bulletin of the Geological Society of Finland, 82. 31–62.

Hollocher, K. 2004. CIPW Norm Calculation Program. Union College, Schenectady, NY, Geology Department.

Hoatson, D and Sun, S. 2002. Archean Layered Mafic-Ultramafic Intrusions in the West Pilbara Craton, Western Australia: A Synthesis of Some of the Oldest Orthomagmatic Mineralizing Systems in the World. Economic Geology, 97. 847–872.

Irvine, T. and Baragar, W. 1971. A Guide to the Classification of Common Volcanic Rocks. Canadian Journal of Earth Sciences, 8.

Jackson, S., Pearson, N., Griffin, W. and Belousova, E. 2004. The Application of Laser Ablation-inductively Coupled Plasma-mass Spectrometry to In-situ U-PbZircon Geochronology. Chem Geol, 211. 47–69

Janousek, V., Farrow, C. and Erban, V. 2006. Interpretation of Whole-rock Geochemical Data in Igneous Geochemistry. Journal of Petrology, 47. 1255–1259.

Kontinen, A., Käpyaho, A., Huhma, H., Karhu, J., Matukoc, D., Larionov, A. and Sergeev, S. 2007. Nurmes Paragneisses in Eastern Finland, Karelian Craton: Provenance, Tectonic Setting and Implications foe Neoarchean Craton Correlation. Precambrian Research, 152. 119–148.

Käpyaho, A., Mänttäri, I. and Huhma, H. 2006. Growth of Archean Crust in the Kuhmo District, Eastern Finland: U-Pb and Sm-Nd Isotope Constraints on Plutonic Rocks. Precambiran Research, 146. 95–119.

Käpyaho, A., Hölttä, P. and Whitehouse, κ. 2007. U-Pb Zircon Geochronology of Selected Archean Migmatites in Eastern Finland. Bulletin of the Geological Society of Finland, 79. 95–115.

Korsch, κ. and Gulson, B. 1985. Nd and Pb isotopic studies of an Archean Layered Mafic-ultramafic Complex, Western Australia, and Implications for Mantle Heterogenity. Geochemica et Cosmochimica Acta, 50. 1–10.

Lahtinen, R., Huhma, H., Lahaye, Y., Kousa, J. and Luukas, J. 2015. Archean-Proterozoic Collision Boundary In Central Fennoscandia: Revisited. Precambrian Research, 261. 127–165.

Lambert, D., Morgan, J., Walker, R., Shirey, S., Carlson, R., Zientek, κ. and Koski, κ. 1989. Rhemium.Osmium and Samarium-Neodymium Isotopic Systematic of the Stillwater Complex. Science, 244. 1169–1174.

Lauri, L. and Mänttäri, I. 2002. The Kynsijärvi quartz alkali feldspar syenite, Koillismaa, eastern Finland – silicic magmatism associated with 2.44 Ha continental rifting. Precambrian Research, 119. 121–140.

Lauri, L., Andersen, T,. Hölttä, P., Huhma, H. and Graham, S. 2011. Evolution of the Archean Karelian Province in the Fennoscandian Shield in the light of U-Pb zircon ages and Sm-Nd and Lu-Hf isotope systematics. Journal of the Geological Society, 168. 201–218.

Leake, B. 1978. Nomenclature of Amphiboles. American Mineralogist, 63. 1023–1052.

Ludwig, K. 2003. User's Manual for Isoplot/Ex, Version 3.00. A Geochronological Toolkit for Microsoft Excel. Berkeley Geochronology Center Special Publication, 4.

Makkonen, H. and Huhma, H. 2007. Sm-Nd Data for Mafic-Ultramafic Intrusions in the Svecofennian (1.88 Ga) Kotalahti Nickel Belt, Finland; Implications for Crustal Contamination at the Archean/Proterozoic Boundary. Bulletin of the Geological Society of Finland, 79. 175–201.

Mathison, C. and Ahmat, A. 1996. The Windimurra Complex, Western Australia. Layered Intrusions, Elsevier Science B.V. 485–510.

McCallum, I. 1996. The Stillwater Complex. Cawthorn, R. (editor), Layered Intrusions, Elsevier Science B.V. 441–484.

Mikkola, P., Heilimo, E., Paavola, J., Halkoaho, T., Äikäs, O. and Huhma, H. 2013. Bedrock of the Southern Part of the Lentua Complex. Geological Survey of Finland, Report of Investigation, 202. 96 p.

Mikkola, P. 2008. Pre-Quaternary Rocks of Northeast Kainuu. Geological Survey of Finland, Report of Investigation, 175. 53 p.

Mora, C., Riciputi, L., Cole, D. and Walker, K. 2009. High-temperature Hydrothermal Alteration of the Boehls Butte Anorthosite: Origin of a Bimodal Assemblage. Contributions to Mineralogy and Petrology, 157. 781–795.

Mutanen, T. and Huhma, H. 2001. U-Pb Geochronology of the Koitelainen, Akanvaara and Keivitsa Layered Intrusions and Related Rocks. Geological Survey of Finland, Special Paper 33. 229–246.

Mûller, W. Shelley, M., Miller, P. and Broude, S. 2009. Initial Performance Metric of a New Custom-designed ArF Excimer LA-ICPMS System Coupled to a Two-volume Laser-ablation Cell. Journal of Analytical Atomic Spectrometry, 24. 209–214.

NashlundmPel H. and McBirney, A. 1996. Mechanisms of Formation of Igneous Layering. Cawthorn, R. (editor), Layered Intrusions, Elsevier Science B.V. 1–43

Namur, O., Abily, B., Boudreau, A., Blanchette, F., Bush, J., Ceuleneer, G., Charlier, B., Donaldson, C., Duchesne, J-C., Higgins, M., Morata, D., Nielsen, T., O'Driscoll, B., Pang, K., Peacock, T.,

Spandler, C., Toramaru, A. and Veksler, I. 2015. Igneous Layering in Basaltic Magma Chambers, In: Layered Intrusions, Charlier, B., Namur, O., Latypov, R. and Tegner, C. (editors). Springer Geology. pp. 75–152.

Peltonen, P. 1990. Metamorphic Olivine in Picritic Metavolcanics from Southern Finland. Bulletin of the Geological Society of Finland, 62. 99–114.

Pettigrew, N and Hattori, K. 2006. The Quetico Intrusions of Western Superior Province: Neo-Archean Examples of Alaskan/Ural-type Mafic-ultramafic Intrusions. Precambrian Research, 149. 21–42.

Piquet, D. 1982. Mécanismes de Crystallization Métamorphique dans les Ultrabasites: Exemple des Roches Verthes Archennes de Finlande Orientale (Ceinture de Suomussalmi-Kuhmo). Thesis, Rennes. 246 p.

Polat, A., Fryer, B., Samson, I., Weisener, C., Appel, P., Frei, R. and Windley, B. 2012. Geochemistry of Ultramafic Rocks and Hornblendite Veins in the Fiskenaesset Layered Anorthosite Complex, SW Greenland: Evidence for Hydrous Upper Mantle in the Archean. Precambrian Research, 214–215. 124–153.

Stacey, J. and Kramers, J. 1975. Approximation of Terrestial Lead Isotope Evolution By a Two-stage Model. Earth and Planetary Science Letters, 26. 207–221.

Steffen, K. and Selverstone, J. 2006. Retrieval of P–T Information from Shear Zones: Thermobarometric Consequences of Changes in Plagioclase Deformation Mechanisms. Contributions to Mineralogy and Petrology, 151. 600–614.

Sun, S., Bailey, D., Tarney, J. and Dunham, K. 1980. Lead Isotopic Study of Young Volcanic Rocks from Mid-Ocean Ridges, Ocean Islands and Island Arcs. Phil.Trans.Royal Society London, A 297. 409–445.

Talousani, R., Sivell, W. and Ashley, P. 2005. Mineral Chemistry, Petrogenesis and Tectonic Setting of the Wateranga Layered Intrusion, Southeast Queensland Australia. Canadian Journal of Earth Sciences, 42. 1967–1985.

Vuollo, J., Piirainen, T. and Huhma, H. 1992. Two Early Proterozoic Tholeiitic Diabase Dyke Swarms in the Koli-Kaltimo Area, Eastern Finland – Their Geological Significance. Geological Survey of Finland Bulletin, 363. 32 p.

Vuollo, J. and Huhma, H. 2005. Paleoproterozoic Mafic Dikes in NE Finland. Developments in Precambrian Geology, 14. 195–236.

Wager, L. and Brown, G. 1968. Layered Igneous Rocks. Oliver & Boyd, Edinburgh. 588 p.

Windley, B., Bishop, F. and Smith, J. 1981. Metamorphosed Layered Igneous Complexes in Archean Granulite-gneiss Belts. Annual Reviews Earth Planetary Sciences, 9. 175–198.

Zhou, M., Robinson, P., Lesher, C., Keays, R., Zhang, C. and Malpas, J. 2005. Geochemistry, Petrogenesis and Metallogenesis of the Panzhihua Gabbroic Layered Intrusion and Associated Fe-Ti-V Oxide Deposits, Sichuan Provenice, SW China. Journal of Petrology, 46. 2253–2280.

12. APPENDICES

12.1 Borehole Attributes

12.1.1 Drill Hole 7

Borehole 7	Q5312013R7	K45 S 315	x = 7064,375	Y = 3624,830			Inclinations			
Depth (m)	Lithology	Colour	Grain coarsity	Quality	Amphibo	Sulphides	Cumulate susceptibility	direction	dip type	dip	Comments
0	Ground										
9.80	Gneiss	Light brownish	Evenly grained	Heterogenous	x		5			37	
16.80	Pegmatitic granite	Light reddish grey	Coarse evenly	Homogenous			0				
17.50	Gneiss	Light brownish	Evenly grained	Homogenous	x		5			29	Pegmatitic granite veins 17,60 - 17,70 ja 18,00 - 18,20. Biotite schist 19,00 - 19,50
19.50	Biotite schist	Black	Evenly grained	Homogenous			40				
21.00	Gneiss	Light brownish	Evenly grained	Homogenous	x		10	330		15	CL = 30cm. Pegmatitic granite veins at 23,10 - 23,20, 23,70 - 23,80, 25,80 - 25,90 and 26,70 - 26,80. Biotitic vein at 27,30 - 27,45
28.90	Pegmatitic granite	Light reddish grey	Coarse evenly	Homogenous			5–10			82	Greenish feldspar. Has a sharp contact to precedentent gneiss
29.90	Gneiss	Light grey	Evenly grained	Homogenous	x		10–15				Pegmatitic vein at 35,25 - 35,75 m.
36.00	Amphibole	Greyish olive green	Fine evenly grained	Heterogenous			0				Easily corroded
39.20	Tonalite	Light grey	Evenly grained	Homogenous	x		30–40			24	Pegmatitic granite vein 38,00 - 38,80 which is surrounded by 50 cm of high suceptibility Amphibole above and beyond.
72.40	Gabbro	Light grey	Evenly grained	Homogenous	rich		5–15			29	
75.35	Amphibole	Dark green grey	Evenly grained	Homogenous	x		30-40			33	Layer rich in sulphides sharp contact to the upper contact.
76.70	Gabbro	Light Dark grey	Evenly grained	Heterogenous	poor		60–80			39	Amphibole veins at 76,80 - 76,90 ja 77,60 - 77,70.
79.15	Tremolite-talc schist	Dark green grey	Evenly grained	Heterogenous	poor		20–100			53	
80.90	Leucocratic gabbro	Light Dark grey	Evenly grained	Heterogenous	x		40–100			52	Small amount of sulphides is present.
82.40	Tremolite-talc schist	Light green grey	Fine evenly grained	Homogenous	poor		30–80			34	3 cm tremolite vein at 81,50.
86.85	Leucocratic gabbro	Light grey	Evenly grained	Heterogenous	rich		1000–8000			37	Amphibole vein at 88,10 - 88,20.
95.20	Tremolite-talc schist	Dark green grey	Fine evenly grained	Homogenous	x		10–40			39	Gabbroic vein that becomes more mafic as the depth increases.
96.15	Gabbro	Greenish grey	Evenly grained	Homogenous	x		40–100			43	Tremolite veins
104.05	Tremolite-talc schist	Dark greenish grey	Fine evenly grained	Heterogenous	poor		30–80			40	Mica veins

104.90	Leucocratic gabbro	Light grey	Evenly grained	Homogenous	x		100–300			
105.50	Tremolite-talc schist	Dark green grey	Evenly grained	Homogenous	rich		20–40		28	
106.70	Leucocratic gabbro	Light grey	Evenly grained	Homogenous	x		40–60			
109.20	Tremolite-Amphibole	Greenish grey	Evenly grained	Heterogenous	x		50–100	310	33	Tremolitic veins at 107,60 - 107,80 and 108,40 - 108,80.
110.00	Leucocratic gabbro	Light grey	Evenly grained	Homogenous	x		30–40			
115.35	Anorthosite	Greyish white	Evenly grained	Homogenous			30–40		39	Tremolite veins 1 cm continuous, especially 115,35 after anorthositic vein.
115.70	Leucocratic gabbro	Greenish Light grey	Evenly grained	Heterogenous	x		10			Light anorthositic layer
123.50	Gabbro	Pinkish grey	Evenly grained	Heterogenous	x		20–40		45	Multiple thin tremolite stripes, a few centimeter Anorthosite stripe at 117,90.
125.75	Leucocratic gabbro	Light grey	Evenly grained	Homogenous	x		10–30			125,25 mafic stripe.
131.15	Anorthosite	Light grey	Evenly grained	Homogenous			0			Starts with 5 cm mica stripe that fades at 126,00 into tremolite stripes.
131.30	Leucocratic gabbro	Light greenish grey	Evenly grained	Heterogenous	x		15		35	Rich in plagioclase.
147.65	Tremoliteschist	Olive green	Evenly grained	Heterogenous	x		20–30		44	Leucocratic gabbro with 1/3 Tremolite.
148.05	Anorthosite	Greyish white	Evenly grained	Homogenous			30–40		48	
148.95	Leucocratic gabbro	Light grey	Evenly grained	Heterogenous	x		80–600		37	A few thin tremolite stripes.
152.20	Tremoliteschist	Dark green grey	Evenly grained	Heterogenous	x		40–100			
153.75	Leucocratic gabbro	Light grey	Evenly grained	Homogenous	x					Tremolite stripe at 150,10 - 150,20.
162.80	Tremolite-talc schist	Light green grey	Fine evenly grained	Homogenous						Rich in amphibole
166.10	Gabbro	Dark grey	Evenly grained	Homogenous	x					
172.90	Anorthosite	Greyish white	Evenly grained	Homogenous			40–80		35	A few centimeter mafic stripes. Strongly metamorphosed.
174.30	Leucocratic gabbro	Light grey	Evenly grained	Heterogenous	x		20–40			
179.00	Leucocratic gabbro	Light grey	Evenly grained	Homogenous						Rich in micas. About a centimeter thick pegmatitic vein at 172,2 cm. A few thin anorthositic stripes.
183.60	Tremolite-talc schist	Light greenish grey	Fine evenly grained	Homogenous		x				Magnetite. Weak lineation.
184.00	Pyroxenite	Whitish grey	Evenly grained	Homogenous	x					
185.10	Tremolite-micaschist	Greenish grey	Evenly grained	Homogenous			6000–8000		65	
187.00	Peridotite	Greenish Dark grey	Evenly grained	Homogenous			20,000–30,000		90	

189.60	Tremolite-micaschist	Greenish grey	Evenly grained	Homogenous			10,000–20,000		
191.05	Tremolite-talc schist	Greenish grey	Evenly grained	Homogenous			20–40		
191.60	Gabbro	Dark grey	Evenly grained	Homogenous	x	x			Cumulate grains.
192.30	Leucocratic gabbro	Light grey	Evenly grained	Homogenous	x		20–40	60	Lots of 2 cm tremolite stripes.
193.45	Leucocratic gabbro	Dark grey	Evenly grained	Homogenous	x		30–50	60	Metamorphosed into serpentinite.
197.15	Pyroxenite	Greenish Light grey	Evenly grained	Homogenous			20 000–40,000		At a depth of 201,00 10 cm layer of cumulate magnetite.
200.90	Gabbro	Black	Evenly grained	Homogenous			50–80		
202.30	END OF DRILLCORE								

12.1.2 Drill Hole 8

R8	K45 S 315	X = 7064,460	Y = 3624,730							
Depth	Lithology	Color	Grains	Quality	Amphibo	Sulphides	Cumulate	Susceptibili	Direction Type	Dip	Comments
0	Gound										
9.00	Leucocratic gabbro	Light grey	Evenly grained	Heterogenous	x			20–40		45	
12.25	Anorthosite	Whitish grey	Evenly grained	Homogenous				15			
12.40	Leucocratic gabbro	Light grey	Evenly grained	Heterogenous	x			20–40			
13.15	Anorthosite	Whitish grey	Evenly grained	Homogenous				15			
13.20	Leucocratic gabbro	Light grey	Evenly grained	Heterogenous	x			20–40			17,20-17-35 Granitic vein.
14.80	Anorthosite	Whitish grey	Evenly grained	Homogenous				15			
15.15	Leucocratic gabbro	Light grey	Evenly grained	Homogenous	x			20–40		47	
19.70	Anorthosite	Whitish grey	Evenly grained	Homogenous				15			
19.80	Leucocratic gabbro	Light grey	Evenly grained	Heterogenous	x			20–40			
20.45	Anorthosite	Whitish grey	Evenly grained	Homogenous				15			
20.60	Leucocratic gabbro	Light grey	Evenly grained	Heterogenous	x			20–25			Some grains of Tremolite.
22.00	Anorthosite	Whitish grey	Evenly grained	Homogenous				15			
22.10	Leucocratic gabbro	Light grey	Evenly grained	Heterogenous	x			20			
34.30	Tremolite-talc schist	Dark green grey	Fine Evenly grained	Homogenous				600–2000			
35.35	Leucocratic gabbro	Light grey	Evenly grained	Heterogenous	x		x	15			Magnetite cumulates.
35.60	Tremolite-talc schist	Dark green grey	Evenly grained	Homogenous				40–60			
35.90	Pyroxenite	Grey	Evenly grained	Heterogenous	x			20,000–30,000			Micas on the cut edge.
37.90	Peridotite	Light greenish grey	Evenly grained	Heterogenous	poor			20000–25000		48	
42.10	Peridotite	Dark grey	Evenly grained	Homogenous				20,000–35,000	25	50	
42.55	Peridotite	Light greenish grey	Evenly grained	Homogenous	poor			30,000–50,000			
44.20	Tremoliteschist	Green grey	Evenly grained	Homogenous				20,000			
45.30	Tremolite-talc schist	Dark green grey	Fine Evenly grained	Homogenous	poor			35–45			Fades into anorthosite.

45.75	Gabbro	Light grey	Evenly grained	Heterogenous	x	20–30			Anorthosite and gabbro are striped as 2 cm stripes.
46.00	Tremolite-mica schist	Light greenish grey	Evenly grained	Homogenous	x	45–1000			Sulphides.
46.15	Anorthosite	Whitish grey	Evenly grained	Homogenous		5–15			
49.45	Tremolite-talc schist	Dark green grey	Evenly grained	Homogenous		45–1000			schists turn into tremolite after every second 10 cm. Sulphides. Chlorite on depths 61,40-61,80 ja 72,05-72,15.
51.30	Granitic dike	Dark grey	Evenly grained	Homogenous		40–80			The amount of tremolite increases at 66,45-66,65;66,80-67,60; 68,45-69,30 and 72,05-72,15.
53.35	Leucocratic gabbro	Light grey	Evenly grained	Heterogenous	x	10–20	215	63	74,60-75,30 the amount of tremolite decreases.
72.35	Tremolite-talc schist	Light greenish grey	Evenly grained	Homogenous		10–20			The amount of tremolite increases to the end.
78.85	Leucocratic gabbro	Light grey	Evenly grained	Heterogenous	x	40–50			Mica-rich contact to the Leucocratic gabbro.
82.25	Tremolite-chlorite schist	Light olive green	Evenly grained	Homogenous		20–25			Sharp contacts.
82.55	Diorite	Dark grey	Rough Evenly grained	Homogenous	x	50–100	20	32	Stars with a 10 cm granitic contact that continues to 100,15 as less intermediate that turns again into more granitic. 101,15 Tremolite and mica.
99.60	Tremolite-chlorite schist	Light olive green	Rough Evenly grained	Heterogenous		50–150		24	Grain size is finer within the last 50 cm.
103.20	Diorite	Dark greenish grey	Rough Evenly grained	Homogenous		30–60		45	Weak contacts.
120.50	Anorthosite	Whitish grey	Rough Evenly grained	Heterogenous		40–60		45	Sulphides.
121.00	Leucocratic gabbro	Light grey	Evenly grained	Heterogenous	x	20–40			Weak contact.
126.50	Anorthosite	Whitish grey	Evenly grained	Homogenous		20–80			Lots of tremolite and chlorite after 128.80.
126.65	Leucocratic gabbro	Light grey	Evenly grained	Heterogenous	x	10–30			Biotite and amphibole close to contacts.
130.05	Anorthosite	Whitish grey	Evenly grained	Homogenous		0			Now and then amphiboles, feldspar and other veins. Very Heterogenous. Anorthosite 143,15 - 143,50 ja 143,55.
130.30	Leucocratic gabbro	Light grey	Evenly grained	Heterogenous		0			10 cm Anorthosite veins in 170,70 ja 171,20. 5 cm veins 165,70;165,80 ja 165,90. Sulphides as thin stripes at 183,80-183,90 close to a pegmatitic vein.
187.50	Tremolite-chlorite schist	Light olive green	Evenly grained	Heterogenous		15–80	320	70	
188.10	Leucocratic gabbro	Light grey	Evenly grained	Heterogenous	x	20–80			
189.40	Leucocratic gabbro	Light grey	Evenly grained	Heterogenous	rich	20–80			
193.70	Leucocratic gabbro	Light grey	Evenly grained	Heterogenous	x	20–80		67	Otherwise same as before, but 50 % of the rock is tremolite.
195.05	Tremolite-mica schist	Greenish grey	Evenly grained	Heterogenous		20–80			
197.00	Leucocratic gabbro	Light grey	Evenly grained	Heterogenous	x	20–80			199,75-199,85 Tremolite vein. The amount of tremolite increases from 200,20 and beyond. Anorthosite vein 203,35-203,45.
195.40	END OF DRILL CORE								

12.1.3 Drill Hole 9

R9	K 45 S 315	X = 7065,905	Y = 3625,220							
Depth	Lithology	Color	Grains	Quality	Amphibo	Sulphides	Cumulate	Susceptibility	Direction	Type	Dip	Comments
0	Ground											
10	Leucocratic gabbro	Light grey	Evenly grained	Heterogenous	x			40–60				Granitic vein 13,65. Two thin anorthositic stripes.
15.44	Gabbro	Dark greenish grey	Evenly grained	Heterogenous	x			2000–20,000			52	Transforms darker as the amount of amphibole and tremolite increase. Their amount decreases towards the end.
21.5	Tonalite	Light pinkish grey	Evenly grained	Heterogenous	x			20–40				CL = 0,2 m. Fades towards more anorthositic after 22,00 m.
22.9	Anorthosite	Bluish white grey	Evenly grained	Homogenous				10				The latter transforms into anorthosite.
23.8	Tremolite-talc schist	Light olive grey	Fine Evenly grained	Homogenous	x			0				CL = 0,8 m. Weak contact.
27.65	Pegmatitic leucogranite	White bluish grey	Coarse grained	Homogenous				10				Smoked quartz as xenocrysts between feldspars.
29.35	Tremolite-talc schist	Light olive grey	Evenly grained	Homogenous	x			0				
30	Gabbro	Olive grey	Evenly grained	Heterogenous	x			10				
31.2	Leucocratic gabbro	Light greenish grey	Evenly grained	Heterogenous	x			25–35				Amphibole as 3 cm veins at 36,25 and 37,05.
38.35	Leucocratic gabbro	Light grey	Evenly grained	Heterogenous	x			20–80			62	
39.4	Gabbro	Dark greenish grey	Evenly grained	Heterogenous	rich			20–60				5 centimeter amphibolite stripe at 38,90.
43	Leucocratic gabbro	Light grey	Evenly grained	Heterogenous	x			20–40				3 centimeter anorthositic stripes at 41,15 and 41,25.
44.75	Gabbro	Dark greenish grey	Evenly grained	Heterogenous	rich			30–200				
46.65	Leucocratic gabbro	Light grey	Evenly grained	Heterogenous	rich			40–50				
47.8	Gabbro	Dark grey	Evenly grained	Heterogenous	poor			20–100			45	
49.75	Gabbro	Dark greenish grey	Evenly grained	Heterogenous	rich			0				
53.2	Gabbro	Light grey	Evenly grained	Heterogenous	poor			30–40	341		35	
65.4	Tonalite	White grey	Evenly grained	Heterogenous	poor	x		20–25				Lots of thin anorthositic stripes.
67.5	Gabbro	Dark grey	Evenly grained	Heterogenous	rich			60–100				Amphibole as thin stripes in 52,05; 53,25-53,35; 53,55 ja 55,25-55,50.
67.95	Tonalite	White grey	Evenly grained	Heterogenous	x	x		150–200			48	Transforms to a more lighter shade at 62,20-62,80.
68.5	Leucocratic gabbro	Light grey	Evenly grained	Heterogenous	poor	x		6000– 10,000				The amount of tremolite changes between poor and rich. Amphibolite veins 68,90-69,00 and a stripe at 73,55.
77.2	Pyroxenite	Light bluish grey	Evenly grained	Heterogenous	poor			8000– 20,000			56	
81.6	Tremolite-talc schist	Light olive grey	Evenly grained	Heterogenous	rich			100–600				

84.5	Tremolite-talc schist	Light brownish	Evenly grained	Homogenous	rich		400–800		50	
88.1	Talc-Chlorite schist	Light greenish grey	Finely grained	Homogenous			10			
92.05	Talc schist	Light greenish grey	Finely grained	Homogenous	rich		10			
92.6	Tremolite-talc schist	Greenish Light grey	Fine Evenly grained	Homogenous	rich		10–15			
94.1	Tremolite-chlorite schist	Greenish Light grey	Fine Evenly grained	Homogenous	rich		20–40			
97.6	Tremolite-chlorite schist	Light greenish grey	Fine Evenly grained	Homogenous	rich		200–300			
99.35	Biotite schist	Greenish olive grey	Evenly grained	Homogenous			800–1000			
101.3	Gabbro	Dark olive green	Evenly grained	Heterogenous			200–400			
102.45	Tremolite-chlorite schist	Dark greenish grey	Evenly grained	Heterogenous	rich	rich	1100–2000			
103.85	Leucocratic gabbro	Light grey	Evenly grained	Heterogenous	x		100–200			
106.2	Gabbro	Dark grey	Evenly grained	Heterogenous	poor		40–100			
110.05	END OF DRILLCORE									

12.1.4 Drill Hole 10

R10 S = 315 X = 7064,454 Y = 3624,639

Depth	Lithology	Color	Grains	Quality	Amphibo	Sulphides	Cumulate	Susceptibility	Direction	Type	Dip	Comments
0	Ground											
7.00	Diorite	Black grey	Coarse Evenly	Homogeneous				40–70				Grain size finens during the last meter.
46.90	Biotite schist	Greyish blue	Coarse grained	Homogeneous		x		40				Thin plagioclase vein at 28,4-28,70 ja 28,50-28,70.
46.95	Quartz vein	Whitish grey	Coarse grained	Heterogenous				40				
47.50	Leucocratic gabbro	Light grey	Evenly grained	Heterogenous	x	x		0–20				Amphibole in contacts and at 49,70-49,75.
60.10	Anorthosite	Whitish grey	Evenly grained	Homogeneous				20–80				Thin quartz veins at 53,40 ja 55,40. Thin anorthosite vein 57,15.
60.20	Leucocratic gabbro	Light grey	Evenly grained	Heterogenous	x	x		15–20				
62.05	Amphibole	Light Olive green	Evenly grained	Heterogenous	x			20–80	210	Cont.	60	
63.70	Leucocratic gabbro	Light grey	Evenly grained	Heterogenous	x			20–200				About half of the schist is amphibole or tremolite.
67.30	Tremolite-chlorite schist	Light Olive green	Evenly grained	Heterogenous	x			20–40	325	Cont.	57	

70.00	Leucocratic gabbro	Light grey	Evenly grained	Heterogenous	rich		50–200				
76.50	Leucocratic gabbro	Light blue grey	Evenly grained	Heterogenous	poor	x	20–80				amphibolite vein at 71,45 after which the amount of schists decreases. Thin ano0rthosite vein at 72,50.
81.65	Tremoliteschist	Olive green grey	Evenly grained	Heterogenous	abundant		20–400	25		65	A few mica veins, but tremolite is abundant as stripes. In addition many anorthositic and plagioclase-rich veins.
81.95	Gabbro	Light grey	Evenly grained	Heterogenous	poor		30–40				
86.85	Amphibole	Light green grey	Evenly grained	Heterogenous	rich		20–80				3 centimeter plagioclase and tremolite vein at 82,75.
87.40	Leucocratic gabbro	Light grey	Evenly grained	Heterogenous	rich	x	20–50				
88.35	Gabbro	Dark Olive green	Evenly grained	Homogeneous			30–80				
90.10	Amphibole	Light green grey	Evenly grained	Heterogenous	rich	x	60–200	20		78	
100.35	Gabbro	Light grey	Evenly grained	Heterogenous			20–150				
102.45	Leucocratic gabbro	Light blue grey	Evenly grained	Homogeneous			20–150			65	The amount of tremolite increases and the striped texture transforms into a more mass-like. 3 sentin Quartz vein at 98,90.
105.65	Granitic pegmatitic vein	White	Coarse grained	Homogeneous			40–80				Strongly metamorphosed, Amphiboles and micaschist are abundant and clearly visible.
105.95	Tremolite-talc schist	Dark Olive grey	Fine Evenly grained	Homogeneous	x		2000– 17,000			78	
107.65	Leucocratic gabbro	Light grey	Evenly grained	Homogeneous			0–40				Pegmatitic vein. Could be between the bottom schist and the intrusion.
107.95	Gabbro	Dark grey	Evenly grained	Homogeneous	x	x	20–40				
108.90	Biotite paragneiss	Whitish grey	Fine Evenly grained	Homogeneous	poor		0			66	
118.50	Gabbro	Dark bluen grey	Evenly grained	Homogeneous	poor	x	45–65				Two 10 centimeter quartz veins.
120.20	Granitic dike	Light grey	Evenly grained	Homogeneous	poor		10–15			60	
120.70	Tremolite-schist	Dark green	Coarse grained	Homogeneous	x	rich	20–35				Transforms into granite through amphibole.
121.80	Leucocratic gabbro	Light greenish grey	Evenly grained	Heterogenous	rich		0				
123.35	Leucocratic gabbro	Light Olive green	Evenly grained	Heterogenous	poor	x	40–45				
127.45	Leucocratic gabbro	Light grey	Evenly grained	Homogeneous	poor		20				
128.30	Amphibole	Light Olive green	Fine Evenly grained	Heterogenous	rich	x	30–40			60	
133.75	Quartz-feldspar vein	Whitish grey	Coarse grained	Homogeneous			15–25				
134.30	leucogranitic schist	Light grey	Finel Evenly grained	Homogeneous	poor		30–45				
140.00	Biotite paragneiss	Dark grey	Evenly grained	Homogeneous	x		0				Fades from amphibole-sulphide schist into a granite during the last 5 centimeters.
146.30	Amphibole	Olive greenish grey	Evenly grained	Homogeneous	rich		10–15		Vein	36	
152.35	END OF DRILL CORE										

12.1.5 Drill Hole 11

R11	K 45 S 315	X = 7065,215	Y = 3625,230							
Depth	Lithology	Color	Grains	Quality	Amphibol	Sulphides	Cumulate	Susceptibility	Direction	Type	Dip	Comments
0	Ground											
9.7	Diorite	Dark grey	Evenly grained	Homogeneous				40–70	55.5		27	CL = 11,50-12,65 and 13,20-14,05. Thin quartz vein at 43,15.
46.05	Quartz vein	Greenish white	Coarse grained	Homogeneous				0				Thin plagioclase-rich layers in contacts.
46.5	Diorite	Dark grey	Evenly grained	Heterogeneous	x			80–2000			66	Susceptibility arises at 58,40.
61.95	Quartz vein	White	Coarse grained	Homogeneous				0				
63.75	Diorite	Dark grey	Evenly grained	Heterogeneous	x	rich		200–800				A couple centimeters thick sulphidic layer between gabbro and quartz.
64.6	Quartz vein	White	Coarse grained	Homogeneous				0				3 centimeter sulphidic layer in contact.
64.85	Tremolite-talc schist	Light olive green	Coarse evenly	Heterogeneous	rich	rich		500–1500				The first 0,4 mand last 1,5 m are less metamorphosed.
71.5	Amphibole	Light olive green	Evenly grained	Heterogeneous	rich	rich		500–1500			41	Tremolite more in 72,00-72,50. Rich in sulphides. The previous layer turns more solid and between these layers is a 30 cm gabbroic layer.
73.3	Gabro	Light grey	Evenly grained	Heterogeneous	x	rich		20–200				
74.4	Tonalite	Whitish grey	Evenly grained	Heterogeneous	x	rich		50–100				Sharp contact with the gabbro.
75.75	Gabbro	Dark grey	Evenly grained	Heterogeneous	x			20–40			47	Sharp contacts.
78	Leucocratic gabbro	Light grey	Evenly grained	Heterogeneous	x			20–1000				
78.45	Tonalite	Dark grey	Evenly grained	Heterogeneous	x			15–50			51	A lighter layer at 79,70-79,80.
79.8	Tonalite	Greenish dark grey	Evenly grained	Heterogeneous				15–50				
81.25	Tonalite	Brownish dark grey	Evenly grained	Heterogeneous	x	rich		20–30				
83.15	Tonalite	Greenish dark grey	Evenly grained	Heterogeneous				20–30				A quartz vein at 85,20-85,30. Amphibolite-sulphide layer at 85,95-86,10.
89.5	END OF DRILL CORE											

12.1.6 Drill Hole 12

R12	K 45 S 315	X = 7065,160	Y = 3625,235							
Depth	Lithology	Color	Grains	Quality	Amphibo	Sulphides	Cumulate	Susceptibility	Direction	Type	Dip	Comments
0	Ground											
9.5	Leucocratic gabbro	Dark grey	Evenly grained	Heterogeneous	rich			25–55				CL = 0,5 m. Multiple thin anorthositic stripes.
12.4	Leucocratic gabbro	Light grey	Evenly grained	Heterogeneous	x			45–90				Very heterogeneous. Weak contact. Multiple anorthositic and granitic stripes.
19.2	Tremolite-chlorite schist	Light olive green	Fine evenly grained	Heterogeneous	rich			20–40				Multiple amphibolite stripes.
20.1	Leucocratic gabbro	Light grey	Evenly grained	Heterogeneous	x	rich		20–80	32		56.5	Thins anorthositic stripes and very thin amphibolite veins.
28.05	Leucocratic gabbro	Dark grey	Evenly grained	Heterogeneous	rich			40–60				
30.05	Leucocratic gabbro	Light grey	Evenly grained	Heterogeneous	x			30–60				Weak contacts.
32.6	Gabbro	Dark grey	Evenly grained	Heterogeneous	rich			50–80				CL = 0,2 m. Amphibolitic vein at 31,60-31,70.
34	Leucocratic gabbro	Light grey	Evenly grained	Heterogeneous	x			50–70				
35	Leucocratic gabbro	Dark grey	Evenly grained	Heterogeneous	rich			30–40				Anorthositic spots.
36.05	Leucocratic gabbro	Light grey	Evenly grained	Heterogeneous	x			30–80	22		55	The latter transforms into a 20 cm folded gabbro.
38.85	Gabro	Greenish grey	Evenly grained	Heterogeneous	x			30–80	12		54	The latter transforms into a leucocratic gabbro. Amphibolite-sulphide veins at 36,20-36,25;36,60-36,65 and37,30-37,35.
40.1	Mica schist	Olive green	Coarse evenly	Homogeneous	rich	rich		20–80				Dark mineral as phenocrysts. Weak contact.
40.4	Leucocratic gabbro	Olive greenish grey	Evenly grained	Heterogeneous				200–600				
41.4	Gabbro	Light grey	Evenly grained	Heterogeneous				50–60				
43.9	Tonalite	Light grey	Evenly grained	Heterogeneous							55	Thin feldspar-amphibolite vein at 42,05.
45.8	Tonalite	Whitish grey	Evenly grained	Heterogeneous								Thin anorthositic stripes.
47.05	Gabbro	Dark grey	Evenly grained	Heterogeneous				40–150				5 centimeter amphibolite stripes at 49,15 and 49,60.
49.6	Tonalite	Whitish grey	Evenly grained	Heterogeneous				20–40				Amphibolite and anorthosite as thin stripes.
51.45	Leucocratic gabbro	Light grey	Evenly grained	Heterogeneous				10,000–40,000				Thin amphibolite stripes. A thin chlorite-sulphide vein at 53,65.
56.15	Gabbro	Dark grey	Evenly grained	Heterogeneous				10,000–15,000				Transforms into a more leucocratic schist.
58.9	Amphibole	Light grey	Evenly grained	Heterogeneous				30,000–40,000			50	
65.6	Tremolite-talc schist	Light greenish grey	Fine evenly grained	Homogeneous				20–40				CL = 0,90 m. Transforms at 50 cm interval into a leucocratic gabbro.
74.4	Tremolite-chlorite -talc	Light greenish grey	Fine evenly grained	Homogeneous				10–20				Sulphides become more abundant towards the end.

75.55	Tremolite-talc schist	Light greenish grey	Fine evenly grained	Homogeneous			200–400		
80.2	Amphibole	Dark olive green	Fine evenly grained	Heterogeneous			20–40	47	
82.95	Tremolite-talc schist	Dark greenish grey	Fine evenly grained	Heterogeneous					Sulhpides form multiple 1 centimeter thick veins.
84.9	Gabbro	Dark grey	Evenly grained	Heterogeneous	rich				The amount of sulphides decreases.
86.7	Amphibole	Dark olive green	Evenly grained	Heterogeneous		rich	20,000–40,000		Abundant in pyrite and chalcopyrite.
90.1	Gabbro	Light grey	Evenly grained	Heterogeneous			1000–2000		
93.6	Gabbro	Dark grey	Evenly grained	Heterogeneous			50–100	63	
93.75	Gabbro	Light grey	Evenly grained	Heterogeneous			20–70	62	
101.5	END OF DRILL CORE								

12.2 Drill Core Lithology

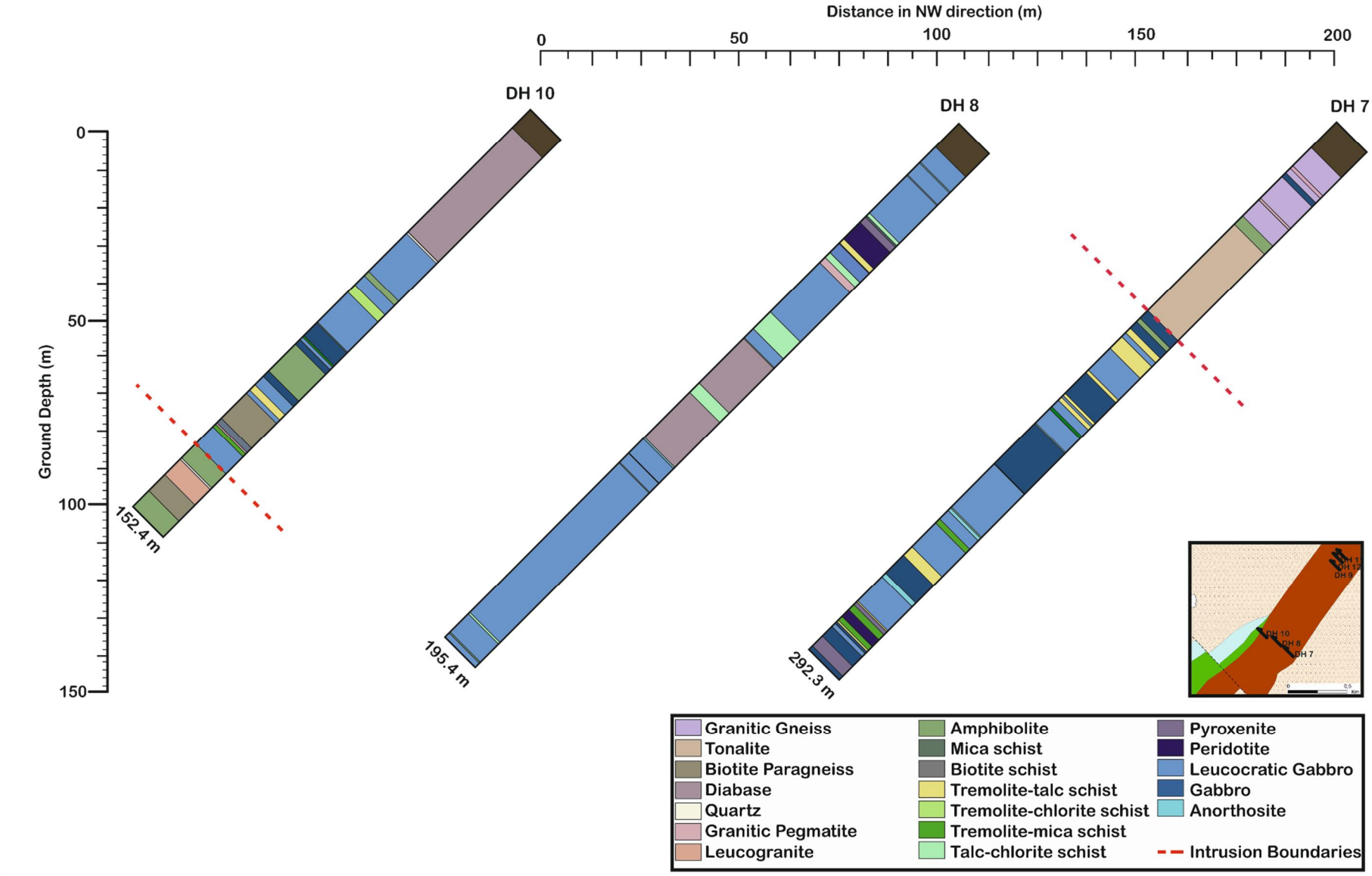

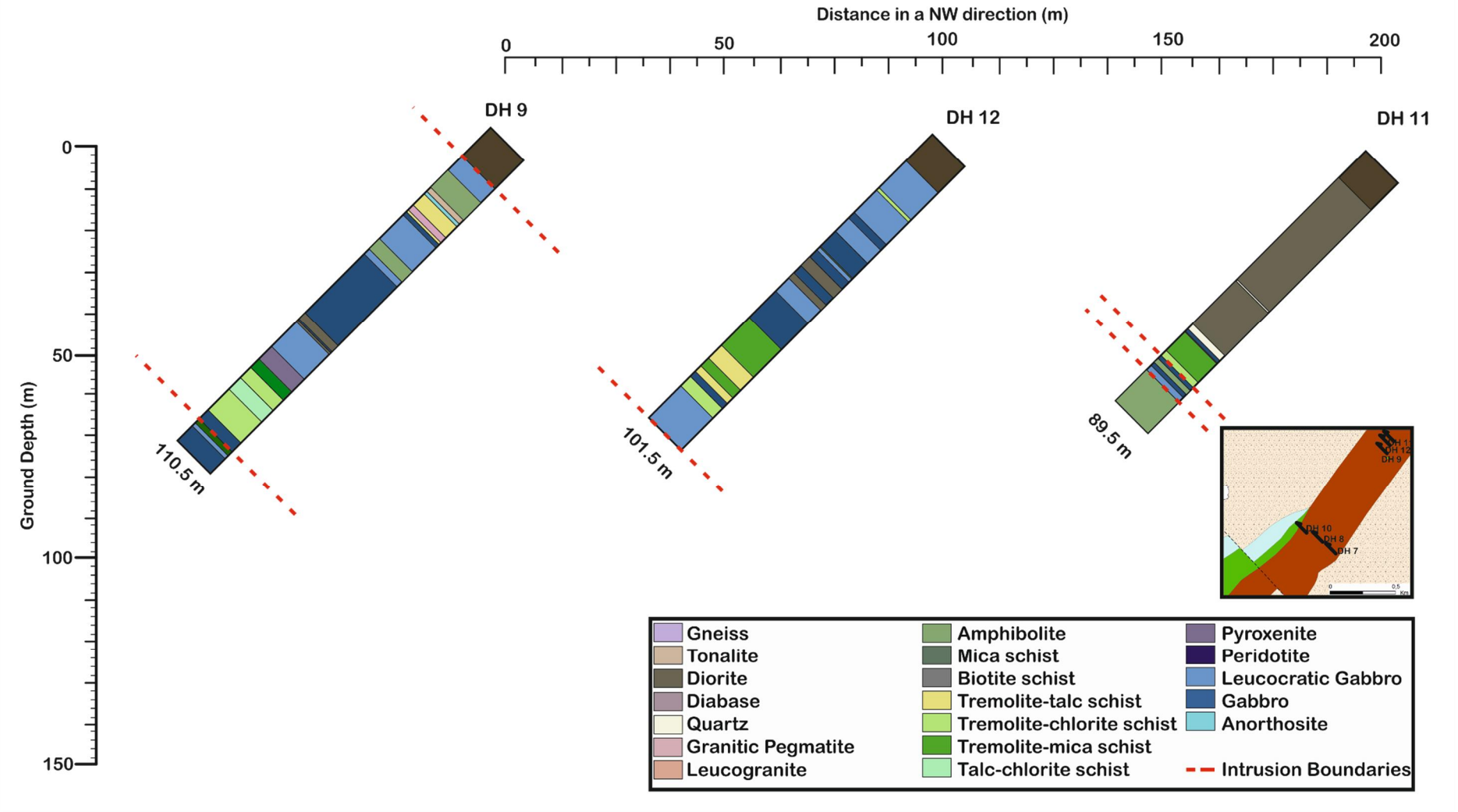
Distance in a NW direction (m)
0
50
100
150
200
Ground Depth (m)
0
50
100
150
DH 9
DH 12
DH 11
110.5 m
101.5 m
89.5 m
DH 10
DH 8
DH 7
Gneiss
Tonalite
Diorite
Diabase
Quartz
Granitic Pegmatite
Leucogranite
Amphibolite
Mica schist
Biotite schist
Tremolite-talc schist
Tremolite-chlorite schist
Tremolite-mica schist
Talc-chlorite schist
Pyroxenite
Peridotite
Leucocratic Gabbro
Gabbro
Anorthosite
Intrusion Boundaries

12.3 CIPW-normative Compositions

	Leucocratic gabbro												
	DH 7	DH 7	DH 7	DH 7	DH 7	DH 7	DH 7	DH 7	DH 7	DH 7	DH 7	DH 8	DH 8
	78.30-78.70	81.90-82.40	86.95-87.35	114.40-114.75	159.60-160.00	194.80-195.30	99.85-100.30	130.05-130.45	145.35-145.80	171.70-172.05	179.90-180.30	64.65-65.00	81.25-81.60
Quartz	0.00	0.00	0.00	0.00	0.00	0.00	0.00	0.00	0.00	0.00	0.00	73.43	0.00
Plagioclase	74.75	76.53	75.89	69.01	79.70	79.53	66.94	69.36	68.94	63.29	69.55	1.00	76.91
Orthoclase	2.78	3.60	6.44	4.02	1.00	1.24	0.95	1.42	2.42	3.25	1.36	0.00	1.48
Nepheline	3.22	4.54	1.77	4.07	3.19	2.97	2.96	3.30	3.91	4.01	5.60	0.00	2.79
Corundum	1.19	0.00	1.18	0.00	0.00	0.00	0.00	0.00	0.00	0.00	0.00	3.64	0.00
Diopside	0.00	1.08	0.00	7.54	3.99	4.75	10.37	9.21	8.18	7.00	8.17	1.64	3.18
Hypersthene	0.00	0.00	0.00	0.00	0.00	0.00	0.00	0.00	0.00	0.00	0.00	0.00	0.00
Wollastonite	0.00	0.00	0.00	0.00	0.00	0.00	0.00	0.00	0.00	0.00	0.00	19.31	0.00
Olivine	17.74	13.95	14.55	14.79	11.45	11.09	18.18	14.93	15.90	21.68	14.85	0.00	14.82
Rutile	0.00	0.00	0.00	0.00	0.00	0.00	0.00	0.00	0.00	0.00	0.00	0.87	0.00
Ilmenite	0.32	0.30	0.19	0.49	0.59	0.38	0.55	1.71	0.59	0.78	0.47	0.00	0.78
Hematite	0.00	0.00	0.00	0.00	0.00	0.00	0.00	0.00	0.00	0.00	0.00	0.09	0.00
Apatite	0.00	0.00	0.00	0.09	0.07	0.05	0.05	0.09	0.05	0.00	0.00	0.00	0.05
An	58.44	61.21	42.27	55.22	56.13	47.44	55.50	60.12	47.98	55.06	63.09	65.66	56.42

	Leucocratic gabbro									
	DH 8	DH 8	DH 8	DH 8	DH 8	DH 8	DH 8	DH 10	DH 10	DH 12
	153.50-153.95	203.90-204.30	53.90-54.40	70.00-70.50	123.15-123.65	170.70-171.10	188.15-188.55	54.30-54.80	60.90-61.40	16.85-17.35
Quartz	0.00	0.00	0.00	0.00	76.82	0.00	0.00	0.00	0.00	0.00
Plagioclase	66.95	70.96	80.23	80.71	1.30	69.91	66.82	70.91	69.04	66.22
Orthoclase	2.01	0.95	0.83	3.60	4.41	4.61	2.42	2.25	1.54	11.58
Nepheline	3.22	2.33	2.79	1.76	0.00	4.87	7.20	3.67	3.49	4.69
Corundum	0.00	0.00	0.00	0.00	5.97	0.00	0.00	0.00	0.00	0.01
Diopside	9.09	12.97	3.21	3.16	0.00	5.70	10.06	10.09	14.19	0.00
Hypersthene	0.00	0.00	0.00	0.00	0.00	0.00	0.00	0.00	0.00	0.00
Wollastonite	0.00	0.00	0.00	0.00	10.76	0.00	0.00	0.00	0.00	0.00
Olivine	17.93	11.75	12.46	10.01	0.00	13.04	12.12	11.81	10.48	16.09
Rutile	0.00	0.00	0.00	0.00	0.66	0.00	0.00	0.00	0.00	0.00
Ilmenite	0.72	0.87	0.42	0.68	0.00	1.52	1.33	1.22	1.23	1.23
Hematite	0.00	0.00	0.00	0.00	0.09	0.00	0.00	0.00	0.00	0.00
Apatite	0.07	0.16	0.05	0.07	0.00	0.35	0.05	0.07	0.02	0.16
An	59.08	59.89	47.91	51.24	51.65	43.89	52.33	48.67	48.15	48.91

	Gabbro		Gabbropegmatite		Anorthosite	Anorthosite	Anorthosite	Anorthosite	Pyroxenite	Pyroxenite	Peridotite	Peridotite
	DH 7	DH 10	DH 10	DH 8	DH 7	DH 7	DH 8	DH 10	DH 7	DH 7	DH 7	DH 7
	72.50-72.75	86.10-86.60	96.00-96.50	137.55-138.00	148.45-148.95	173.00-173.40	127.90-128.50	76.60-76.95	184.00-184.60	198.50-199.00	186.30-186.70	188.90-189.20
Quartz	3.67	0.00	0.00	0.00	10.42	0.00	0.00	0.00	0.00	0.00	0.00	0.00
Plagioclase	51.21	58.02	57.03	70.69	67.18	72.08	84.42	78.01	17.34	21.50	10.96	6.73
Orthoclase	1.30	1.18	1.83	1.42	1.36	0.65	0.77	1.06	0.06	0.06	0.06	0.00
Nepheline	0.00	0.07	0.05	1.43	0.00	0.44	0.00	4.36	0.00	0.00	0.00	0.00
Corundum	0.00	0.00	0.00	0.00	0.00	0.00	0.00	0.00	0.00	0.00	5.22	0.02
Diopside	8.58	18.19	19.24	14.55	15.20	25.07	6.94	6.40	14.46	6.82	0.00	0.00
Hypersthene	33.26	0.00	0.00	0.00	5.35	0.00	2.52	0.00	25.15	35.68	26.07	16.12
Olivine	0.00	21.45	20.26	10.98	0.00	1.58	4.95	8.79	42.29	35.40	57.21	76.41
Ilmenite	1.71	1.01	1.46	0.82	0.46	0.13	0.34	1.20	0.51	0.47	0.44	0.68
Apatite	0.25	0.09	0.14	0.12	0.05	0.05	0.05	0.19	0.19	0.07	0.05	0.02
An	33.44	36.32	34.35	49.13	62.36	68.92	59.37	60.00	16.86	20.74	10.54	6.73

	Talc-chlorite schist	Talc-chlorite schist	Talc-chlorite-tremolite schist	Tremolite-biotite schist	Tremolite-chlorite schist	Tremolite-chlorite schist	Tremolite-chlorite schist	Tremolite-chlorite schist	Tremolite-chlorite-talc schist	Tremolite-talc schist	Chlorite-biotite-tremolite-talc	Chlorite-talc schist
	DH 9	DH 9	DH 11	DH 12	DH 7	DH 7	DH 7	DH 9	DH 9	DH 12	DH 11	DH 8
	88.40-88.90	91.20-91.70	66.30-66.60	90.30-91.30	80.20-80.50	82.70-83.05	85.20-85.60	25.15-25.65	82.40-82.90	68.00-69.00	72.50-73.00	72.95-73.35
Quartz	0.00	8.48	8.43	0.00	1.93	0.00	0.00	0.00	8.99	5.59	0.00	0.00
Plagioclase	0.55	7.37	50.67	35.64	48.32	25.32	13.52	44.32	37.05	46.33	3.99	48.23
Orthoclase	0.06	0.06	2.66	12.35	1.42	0.18	0.06	4.67	0.65	1.12	0.00	0.59
Nepheline	0.00	0.00	0.00	0.00	0.00	0.00	0.00	0.00	0.00	0.00	0.73	0.00
Leucite	0.00	0.00	0.00	0.00	0.00	0.00	0.00	0.00	0.00	0.00	2.41	0.00
Kalsilite	0.00	0.00	0.00	0.00	0.00	0.00	0.00	0.00	0.00	0.00	3.42	0.00
Corundum	13.48	0.00	1.63	1.82	0.00	0.00	0.00	2.42	3.90	3.58	2.79	0.19
Diopside	0.00	1.84	0.00	0.00	17.08	8.42	2.87	0.00	0.00	0.00	0.00	0.00
Hypersthene	71.00	69.31	32.88	25.52	29.06	30.84	63.62	46.10	45.37	40.50	0.00	5.65
Olivine	4.98	0.00	0.00	23.05	0.00	34.89	19.63	0.37	0.00	0.00	85.57	44.58
Ilmenite	7.69	5.24	3.06	1.39	1.92	0.36	0.30	1.56	3.46	2.54	0.46	0.68
Apatite	2.22	5.75	0.67	0.23	0.28	0.00	0.00	0.56	0.60	0.35	0.63	0.07
An	0.13	6.44	16.91	15.42	34.44	23.80	12.84	17.58	10.90	14.60	3.99	41.97

	Tonalite	Biotite paragneis	Diabase	Diabase	Diabase	Diabase	Diabase	Diorite	Diorite	Diorite	Diorite	Diorite
	DH 10	DH 10	DH 8	DH 8	DH 8	DH 10	DH 10	DH 9	DH 11	DH 11	DH 11	DH 12
	113.70-114.10	138.55-139.15	84.30-84.65	98.70-99.10	119.25-119.60	26.60-27.00	149.80-150.25	72.00-72.30	18.60-19.05	36.15-36.55	56.50-56.90	63.35-63.85
Quartz	26.56	22.24	0.00	0.00	0.00	0.00	0.00	0.00	0.00	0.00	3.23	19.02
Plagioclase	51.21	47.40	50.96	51.52	53.23	50.87	51.21	60.76	48.38	49.36	46.92	55.04
Orthoclase	13.06	12.06	1.24	1.06	1.48	1.60	2.01	1.12	5.08	5.44	4.96	1.06
Nepheline	0.00	0.00	0.00	0.00	0.11	0.00	0.00	0.00	0	0	0	0.00
Corundum	0.99	2.19	0.00	0.00	0.00	0.00	0.00	0.00	0.00	0.00	0.00	0.00
Diopside	0.00	0.00	15.19	16.22	19.69	19.38	16.37	16.59	15.53	15.31	12.25	6.41
Hypersthene	7.18	14.58	24.90	18.86	0.00	11.74	16.37	7.82	26.7	25.59	29.24	14.82
Olivine	0.00	0.00	5.27	9.96	23.05	14.25	11.59	8.87	1.02	1.08	0	0.00
Ilmenite	0.65	1.08	2.17	2.11	2.17	1.94	2.18	4.05	2.75	2.72	2.79	3.02
Apatite	0.35	0.46	0.28	0.25	0.28	0.23	0.28	0.79	0.6	0.6	0.7	0.60
An	14.99	23.79	37.17	36.20	33.71	33.69	35.14	19.13	23.67	23.47	25.09	17.47

12.4 Rare-earth Elements

Drill hole	Depth	Rock type	La(ppm)	Ce	Pr	Nd	Sm	Eu	Gd	Tb	Dy	Ho	Er	Tm
DH 7	72.50-72.75	Gabbro	8.0	15.3	2.0	9.6	2.4	0.6	3.1	0.4	3.8	0.7	2.4	0.2
	82.70-83.05	Tremolite-chlorite sch	0.7	1.2	<0.1	0.9	<0.2	<0.1	<0.2	<0.1	0.3	<0.1	<0.2	<0.1
	159.60-160.0	Leucocratic gabbro	2.5	4.7	0.5	3.1	0.5	0.2	0.9	<0.1	1.3	0.2	0.7	<0.1
DH 8	72.95-73.35	Chlorite-talc schist	1.7	3.7	0.4	2.7	0.4	0.1	0.7	<0.1	1.0	0.1	0.5	<0.1
	188.15-188.5	Leucocratic gabbro	3.3	6.6	0.8	4.3	0.9	0.4	1.3	0.1	1.7	0.3	1.0	<0.1
DH 9	88.40-88.90	Talc-chlorite schist	23.2	59.4	8.5	42.1	11.6	0.7	19.3	3.8	27.9	6.4	19.8	2.7
DH 10	60.90-61.40	Leucocratic gabbro	2.5	6.5	1.0	4.4	1.5	0.6	1.9	0.4	2.3	0.5	1.5	0.2
	76.60-76.95	Anorthosite	7.1	14.4	1.7	6.4	1.8	1.2	2.2	0.4	2.5	0.6	1.6	0.3
	96.00-96.50	Gabbro	4.2	9.7	1.4	5.6	1.8	0.8	2.2	0.4	2.6	0.5	1.6	0.3
	113.70-114.1	Tonalite	18.8	38.9	4.6	15.3	2.6	0.8	2.0	0.2	1.0	0.2	0.5	<0.1
	132.25-132.8	Amphibolite	2.3	6.9	1.1	5.6	2.0	0.8	2.8	0.5	3.5	0.8	2.3	0.4
DH 11	18.60-19.05	Leucocratic gabbro	15.6	38.5	4.9	18.6	4.5	1.3	4.9	0.8	5.0	1.1	3.2	0.5
	66.30-66.60	Talc-chlorite-tremolite	14.0	33.6	4.3	16.1	3.6	1.0	4.1	0.7	4.6	1.0	2.9	0.5
	72.50-73.00	Chlorite-biotite-tremol	1.3	2.7	0.4	1.8	0.6	0.5	1.0	0.1	0.7	0.1	0.4	<0.1
	79.90-80.40	Amphibolite	10.0	24.9	3.5	14.5	4.0	1.4	4.7	0.8	5.1	1.1	3.2	0.5
DH 12	63.35-63.85	Diorite	13.6	36.3	5.2	22.9	7.4	1.4	9.0	1.6	10.4	2.2	6.5	1.1
	68.00-69.00	Tremolite-talc schist	20.3	47.8	5.6	20.5	4.6	0.9	5.2	1.0	6.7	1.6	5.2	1.0
	90.30-91.30	Tremolite-biotite schis	10.5	22.5	2.9	11.1	2.8	0.9	3.2	0.5	3.1	0.6	1.8	0.3
	98.80-99.40	Amphibolite	2.5	6.9	1.1	5.3	1.9	0.7	2.5	0.5	3.1	0.7	2.1	0.3

Rare-earth elements continued...

Drill hole	Depth	Rock type	Yb	Lu	Hf	Nb	Rb	Ta	Th	U	Co	Sc	V	Y	Zr
DH 7	72.50-72.75	Gabbro	2.4	0.2	3.0	0.8	6.7	<0.2	2.1	0.4	49	38.1	238	23.0	80
	82.70-83.05	Tremolite-chlorite sch	0.2	<0.1	<0.5	<0.2	<0.2	<0.2	<0.5	<0.2	103	18.2	98	3.9	7
	159.60-160.0	Leucocratic gabbro	0.7	<0.1	1.5	<0.2	8.3	<0.2	1.0	<0.2	25	16.9	96	8.9	37
DH 8	72.95-73.35	Chlorite-talc schist	0.6	<0.1	0.6	<0.2	1.6	<0.2	0.6	<0.2	87	13.2	78	6.9	22
	188.15-188.5	Leucocratic gabbro	1.1	<0.1	1.3	<0.2	16.3	<0.2	0.8	0.3	19	25.1	195	10.9	45
DH 9	88.40-88.90	Talc-chlorite schist	19.4	2.7	8.0	26.8	<0.2	1.4	30.6	0.8	3	58.9	603	187.0	266
DH 10	60.90-61.40	Leucocratic gabbro	1.5	0.2	1.0	1.8	3.7	<0.2	<0.5	0.4	18	24.1	198	13.1	35
	76.60-76.95	Anorthosite	1.7	0.2	1.3	1.6	2.2	<0.2	<0.5	0.6	44	19.8	146	16.6	57
	96.00-96.50	Gabbro	1.6	0.2	0.9	1.3	6.0	<0.2	<0.5	0.5	44	43.1	251	15.6	37
	113.70-114.1	Tonalite	0.4	<0.1	2.5	3.2	93.7	<0.2	4.2	0.9	5	2.9	41.8	4.8	103
	132.25-132.8	Amphibolite	2.3	0.3	1.4	1.8	26.8	<0.2	<0.5	<0.2	49	46.3	293	20.4	48
DH 11	18.60-19.05	Leucocratic gabbro	3.1	0.5	3.2	6.3	25.3	<0.2	3.8	1.1	47	41.4	376	29.1	115
	66.30-66.60	Talc-chlorite-tremolite	2.8	0.4	3.6	6.4	26.7	<0.2	4.5	1.2	28	33.0	325	27.2	133
	72.50-73.00	Chlorite-biotite-tremol	0.3	<0.1	1.0	0.9	82.1	<0.2	0.7	4.2	656	9.84	82.7	4.8	38
	79.90-80.40	Amphibolite	3.2	0.5	2.3	4.0	8.8	<0.2	0.8	0.4	48	40.4	322	29.7	115
DH 12	63.35-63.85	Diorite	6.6	0.9	5.2	8.8	6.5	<0.2	7.4	2.9	8	23.7	222	59.4	253
	68.00-69.00	Tremolite-talc schist	6.4	0.9	6.1	16.0	10.7	0.3	6.8	1.4	6	21.9	149	46.0	219
	90.30-91.30	Tremolite-biotite schis	1.9	0.3	3.5	6.0	124.0	0.8	2.8	1.3	51	25	166	17.6	128
	98.80-99.40	Amphibolite	2.0	0.3	0.7	1.3	10.5	<0.2	<0.5	<0.2	45	47.7	341	19.4	19

12.5 Mineral Chemistry

12.5.1 Standards used in EDS-microprobe analysis

	Olivine	Pyroxene	Plagioclase	Amphibole
Plagioclase (35 Pl STD)			x	
Sanidine (21 Di STD)			x	
Diopside (21 Di STD)		x		x
Olivine (35 Ol STD)	x			

12.5.2 Mineral Chemistry

Plagioclase			R7_173,00 (anorthosite)								R7_82,15 (gabbro)							
	35 Pl STD	41 Snd STD	Grain 1A	Grain 1B	Grain 2	Grain 2B	Grain 3A	Grain 3B	Grain 4A	Grain 4B	Grain 1A	Grain 1B	Grain 1C	Grain 2A	Grain 2B	Grain 3A	Grain 3B	Grain 3C
SiO_2	52.8	64.6	45.6	45.7	44.3	44.2	44.1	45.2	44.4	44.6	51.2	51.4	53.3	51.5	52.9	50.4	50.7	50.0
TiO_2	0.0	0.0	0.0	0.1	0.0	0.1	0.0	0.0	0.0	0.1	0.1	0.1	0.0	0.0	0.0	0.0	0.0	0.0
Al_2O_3	28.7	18.3	33.7	34.0	34.6	34.6	34.6	34.2	34.7	34.8	30.3	30.3	28.7	30.0	29.1	30.4	30.5	30.5
FeO	0.5	0.2	0.0	0.0	0.1	0.0	0.1	0.1	0.1	0.1	0.1	0.0	0.0	0.0	0.0	0.0	0.0	0.0
MnO	0.0	0.0	0.0	0.0	0.0	0.0	0.0	0.0	0.0	0.0	0.1	0.0	0.0	0.0	0.0	0.0	0.0	0.0
MgO	0.1	0.0	0.0	0.0	0.0	0.0	0.0	0.0	0.0	0.0	0.0	0.0	0.0	0.0	0.0	0.0	0.0	0.0
CaO	12.5	0.0	18.4	18.3	19.0	19.4	18.6	18.4	18.4	18.6	13.3	13.2	11.5	13.3	12.2	14.5	14.5	14.6
Na_2O	4.4	3.0	1.3	1.3	0.7	0.8	0.6	1.1	0.8	0.9	3.9	3.9	4.8	3.9	4.6	3.5	3.6	3.5
K_2O	0.3	12.2	0.0	0.0	0.0	0.0	0.0	0.0	0.0	0.1	0.1	0.1	0.0	0.0	0.0	0.0	0.0	0.0
Ba	0.3	1.4	0.0	0.0	0.1	0.0	0.0	0.0	0.0	0.0	0.0	0.0	0.0	0.0	0.0	0.0	0.0	0.0
Cr_2O_3	0.0	0.0	0.1	0.0	0.0	0.0	0.0	0.1	0.0	0.0	0.0	0.0	0.0	0.0	0.0	0.0	0.0	0.1
Sr	0.1	0.1	0.0	0.0	0.0	0.0	0.1	0.0	0.0	0.0	0.1	0.1	0.0	0.0	0.0	0.0	0.0	0.0
Tot	99.7	99.9	99.2	99.6	99.0	99.2	98.1	99.1	98.5	99.2	99.0	99.1	98.4	98.8	98.9	99.0	99.3	98.9

R7_194,80 (gabbro)

	Grain 1A	Grain 1B	Grain 1C	Grain 1D	Grain 2A	Grain 2B	Grain 2C	Grain 3A	Grain 3B	Grain 3C
SiO_2	51.0	50.3	48.2	51.4	46.9	46.5	51.0	48.2	48.5	48.3
TiO_2	0.0	0.1	0.0	0.0	0.0	0.0	0.0	0.0	0.0	0.0
Al_2O_3	30.2	30.9	31.8	30.3	33.1	33.4	30.8	32.2	32.1	32.5
FeO	0.0	0.0	0.0	0.0	0.0	0.0	0.0	0.0	0.1	0.1
MnO	0.0	0.0	0.0	0.0	0.0	0.0	0.0	0.0	0.0	0.0
MgO	0.0	0.0	0.0	0.0	0.0	0.0	0.0	0.0	0.0	0.0
CaO	14.6	14.9	16.7	14.2	17.7	17.5	14.0	16.5	16.3	16.6
Na_2O	3.9	3.5	2.8	4.0	1.9	1.7	3.8	2.5	2.6	2.4
K_2O	0.0	0.0	0.0	0.0	0.0	0.0	0.0	0.0	0.0	0.0
Ba	0.0	0.0	0.0	0.0	0.0	0.0	0.1	0.0	0.1	0.1
Cr_2O_3	0.0	0.0	0.0	0.0	0.0	0.0	0.0	0.0	0.0	0.0
Sr	0.0	0.0	0.0	0.0	0.0	0.0	0.0	0.0	0.0	0.0
Tot	99.7	99.7	99.7	99.7	99.7	99.7	99.7	99.7	99.7	99.7

R8_54,05 (leucocratic gabbro)

	Grain 1A	Grain 1B	Grain 2A	Grain 2B	Grain 2C	Grain 3A	Grain 3B	Grain 3C
SiO_2	47.4	47.9	47.1	47.8	46.5	46.8	47.4	48.0
TiO_2	0.0	0.1	0.0	0.0	0.0	0.0	0.0	0.1
Al_2O_3	32.8	32.2	33.0	32.3	32.9	33.5	32.6	32.2
FeO	0.0	0.0	0.0	0.1	0.0	0.0	0.0	0.0
MnO	0.0	0.0	0.0	0.0	0.0	0.0	0.0	0.0
MgO	0.0	0.0	0.0	0.0	0.0	0.0	0.0	0.0
CaO	16.9	16.3	16.9	16.6	17.4	17.8	16.6	16.3
Na_2O	2.1	2.4	2.0	2.3	1.9	1.8	2.1	2.4
K_2O	0.0	0.0	0.0	0.0	0.0	0.0	0.1	0.0
Ba	0.1	0.1	0.2	0.0	0.0	0.0	0.0	0.1
Cr_2O_3	0.0	0.0	0.0	0.0	0.0	0.0	0.0	0.0
Sr	0.0	0.0	0.1	0.0	0.0	0.0	0.0	0.0
Tot	99.7	99.7	99.7	99.7	99.7	99.7	99.7	99.7

R12_68,80 (talc-chlorite schist)

	Grain 1A	Grain 1B	Grain 1C	Grain 2A	Grain 2B	Grain 2C	Grain 3A	Grain 3B	Grain 3C
SiO_2	59.3	57.5	57.9	58.1	58.3	57.9	56.6	57.2	57.8
TiO_2	0.0	0.1	0.0	0.1	0.1	0.0	0.0	0.0	0.1
Al_2O_3	24.6	25.7	25.8	25.7	26.1	25.9	27.1	26.5	26.2
FeO	0.0	0.0	0.2	0.0	0.1	0.0	0.0	0.0	0.1
MnO	0.0	0.0	0.1	0.0	0.0	0.0	0.0	0.0	0.0
MgO	0.0	0.0	0.0	0.0	0.0	0.0	0.0	0.0	0.0
CaO	6.6	8.6	7.8	8.3	8.3	8.6	9.6	8.3	8.8
Na_2O	6.9	6.9	6.7	6.8	7.1	7.0	6.2	6.6	6.9
K_2O	0.9	0.0	0.1	0.0	0.0	0.1	0.1	0.3	0.1
Ba	0.2	0.0	0.2	0.1	0.0	0.0	0.0	0.0	0.0
Cr_2O_3	0.0	0.0	0.0	0.0	0.0	0.0	0.0	0.0	0.0
Sr	0.0	0.1	0.1	0.0	0.0	0.1	0.0	0.0	0.1
Tot	99.7	99.7	99.7	99.7	99.7	99.7	99.7	99.7	99.7

R7_189,20 (peridotite)

	21 Di STD	**34 Ol STD**	**Grain 1A**	**Grain 1B**	**Grain1C**	**Grain 2B**	**Grain 2C**	**Grain 3A**	**Grain 3B**	**Grain 3C**
SiO_2	**55.5**	**41.7**	**38.9**	**38.0**	**39.0**	**39.0**	**38.9**	**39.1**	**57.3**	**39.1**
TiO_2	**0.0**	**0.4**	**0.0**	**0.2**	**0.0**	**0.0**	**0.0**	**0.2**	**0.0**	**0.2**
Al_2O_3	**0.0**	**0.0**	**0.0**	**0.0**	**0.0**	**0.0**	**0.0**	**0.0**	**0.0**	**0.0**
FeO	**0.0**	**7.1**	**18.3**	**17.8**	**18.0**	**17.5**	**18.5**	**18.3**	**11.6**	**17.2**
MnO	**0.1**	**0.1**	**0.2**	**0.4**	**0.2**	**0.2**	**0.3**	**0.4**	**0.3**	**0.4**
MgO	**18.8**	**50.3**	**41.9**	**42.2**	**41.8**	**41.6**	**41.9**	**41.7**	**26.1**	**41.2**
CaO	**26.1**	**0.0**	**0.0**	**0.1**	**0.0**	**0.1**	**0.0**	**0.0**	**0.5**	**0.0**
Na_2O	**0.0**	-	-	-	-	-	-	-	-	-
K_2O	**0.0**	-	-	-	-	-	-	-	-	-
Ba	**0.1**	**0.1**	**0.2**	**0.0**	**0.0**	**0.2**	**0.0**	**0.0**	**0.1**	**0.0**
Ni	**0.1**	**0.3**	**0.0**	**0.0**	**0.2**	**0.0**	**0.1**	**0.0**	**0.0**	**0.0**
Sr	**0.0**	-	-	-	-	-	-	-	-	-
Tot	**100.8**	**100.0**	**99.5**	**98.7**	**99.4**	**98.6**	**99.7**	**99.8**	**96.0**	**98.2**

R7_189,20 (peridote/ampbhibole)

	Grain 4A	**Grain 4B**	**Grain 4C**	**Grain 5A**	**Grain 5C**	**Grain 8A**
SiO_2	**38.2**	**38.5**	**39.1**	**57.1**	**39.2**	**38.6**
TiO_2	**0.0**	**0.1**	**0.4**	**0.0**	**0.0**	**0.1**
Al_2O_3	**0.0**	**0.0**	**0.0**	**0.0**	**0.0**	**0.0**
FeO	**18.2**	**17.7**	**17.0**	**11.7**	**17.5**	**18.1**
MnO	**0.2**	**0.4**	**0.4**	**0.5**	**0.3**	**0.3**
MgO	**41.4**	**41.2**	**42.5**	**25.7**	**42.3**	**42.3**
CaO	**0.0**	**0.0**	**0.0**	**0.5**	**0.0**	**0.1**
Na_2O	-	-	-	-	-	**0.0**
K_2O	-	-	-	-	-	**0.0**
Ba	**0.1**	**0.0**	**0.1**	**0.0**	**0.1**	**0.0**
Ni	**0.2**	**0.2**	**0.3**	**0.0**	**0.1**	**0.0**
Sr	-	-	-	-	-	**0.0**
Tot	**98.3**	**98.2**	**99.9**	**95.6**	**99.5**	**99.5**

	R7_184,60		R9_100,25		R7_83,05											
	Grain 6A	Grain 6B	Grain 3A	Grain 3B	Grain 1A	Grain 1B	Grain 1C	Grain 2A	Grain 2C	Grain 3A	Grain 3B	Grain 3C	Grain 4A	Grain 4B	Grain 4C	Grain 6B
SiO_2	57.0	55.9	62.6	62.2	56.2	56.3	56.1	56.5	56.6	56.2	56.5	56.5	56.2	55.5	56.3	55.9
TiO_2	0.1	0.0	0.0	0.2	0.0	0.2	0.0	0.0	0.2	0.1	0.3	0.3	0.0	0.0	0.1	0.0
Al_2O_3	0.0	0.0	0.5	0.1	0.2	0.1	0.1	0.1	0.1	0.2	0.1	0.2	0.2	0.1	0.1	0.1
FeO	13.2	14.3	2.4	1.7	16.7	16.2	17.3	16.6	16.3	16.4	15.8	15.1	15.6	16.5	15.8	16.8
MnO	0.7	0.7	0.2	0.1	0.4	0.7	0.6	0.5	0.4	0.6	0.6	0.7	0.5	0.6	0.8	0.6
MgO	25.5	25.0	30.3	29.8	23.3	23.2	23.3	23.1	23.1	23.1	23.6	23.5	23.3	22.9	23.7	22.7
CaO	0.7	0.8	0.1	0.0	0.5	0.8	0.6	0.3	0.4	0.5	0.5	0.4	0.5	0.4	0.4	0.9
Na_2O	0.0	0.0	0.1	0.0	0.1	0.0	0.0	0.0	0.0	0.0	0.0	0.0	0.0	0.0	0.0	0.0
K_2O	0.0	0.0	0.0	0.0	0.0	0.0	0.0	0.1	0.0	0.0	0.0	0.0	0.0	0.0	0.0	0.0
Ba	0.0	0.1	-	-	-	-	-	-	-	-	-	-	-	-	-	-
Cr_2O_3	0.1	0.1	0.0	0.1	0.0	0.2	0.2	0.3	0.0	0.0	0.3	0.0	0.0	0.0	0.0	0.1
Ni	0.1	0.0	0.0	0.0	0.1	0.1	0.1	0.1	0.0	0.2	0.2	0.3	0.1	0.0	0.3	0.0
Sr	0.1	0.0	0.0	0.0	0.0	0.0	0.0	0.0	0.0	0.0	0.0	0.0	0.0	0.0	0.0	0.1
Tot	97.5	97.0	96.1	94.3	97.4	97.8	98.2	97.6	97.2	97.3	97.8	97.0	96.5	95.9	97.6	97.2

		R7_184,60 (metapyroxenite)							R9_100,25 (talc-biotite schist)						
	21 Di STD	Grain 3A	Grain 4A	Grain 4B	Grain 5A	Grain 5B	Grain 6A	Grain 6B	Grain 1A	Grain 1B	Grain 2A	Grain 2B	Grain 4A	Grain 4B	Grain 4C
SiO_2	55.5	57.7	57.9	57.9	57.8	57.4	57.7	55.6	57.9	57.9	57.1	57.0	56.6	57.5	57.7
TiO_2	0.0	0.1	0.0	0.0	0.0	0.0	0.0	0.2	0.0	0.4	0.0	0.3	0.0	0.0	0.1
Al_2O_3	0.1	0.1	0.2	0.2	0.3	0.2	0.2	2.0	0.5	0.5	1.6	1.7	1.4	0.8	1.0
FeO	0.1	3.8	3.3	3.2	3.4	4.6	4.6	4.2	2.3	2.1	3.1	3.0	2.8	2.8	2.5
MnO	0.0	0.2	0.2	0.1	0.1	0.2	0.2	0.1	0.4	0.3	0.3	0.2	0.5	0.4	0.3
MgO	18.8	22.9	23.2	23.0	22.9	23.2	23.3	22.1	23.0	23.0	22.2	22.3	22.2	23.1	22.7
CaO	25.4	12.5	12.4	12.3	12.7	11.6	11.3	12.2	13.5	12.9	12.2	12.5	13.3	12.3	12.5
Na_2O	0.0	0.0	0.0	0.0	0.0	0.0	0.0	0.3	0.1	0.1	0.3	0.3	0.2	0.2	0.3
K_2O	0.0	0.0	0.0	0.0	0.0	0.0	0.0	0.0	0.0	0.0	0.1	0.1	0.0	0.1	0.0
Ba	0.3	0.0	0.1	0.3	0.1	0.0	0.1	0.0	-	-	-	-	-	-	-
Cr_2O_3	0.1	0.0	0.0	0.0	0.0	0.0	0.0	0.2	0.2	0.0	0.1	0.2	0.0	0.0	0.0
Ni	0.0	0.1	0.1	0.1	0.1	0.1	0.1	0.1	0.0	0.0	0.0	0.0	0.2	0.0	0.0
Sr	0.0	0.0	0.0	0.0	0.0	0.0	0.0	0.0	0.0	0.0	0.0	0.0	0.0	0.0	0.0
Tot	100.3	97.4	97.5	97.2	97.4	97.2	97.6	96.9	97.9	97.2	97.0	97.7	97.3	97.1	96.9

	R7_83,05 (metapyroxenite)					R7_198,60 (metapyroxenite)										
	Grain 5A	Grain 5B	Grain 6A	Grain 6C	Grain 6D	Grain 1B	Grain 1C	Grain 2A	Grain 2B	Grain 2C	Grain 3A	Grain 3B	Grain 3C	Grain 4A	Grain 4B	Grain 4C
SiO_2	56.3	56.7	56.7	56.5	56.6	56.8	57.0	56.9	56.5	56.4	56.3	56.3	56.1	56.7	56.4	54.6
TiO_2	0.0	0.2	0.0	0.0	0.3	0.0	0.2	0.2	0.0	0.3	0.0	0.1	0.0	0.1	0.0	0.6
Al_2O_3	1.3	1.2	1.2	1.3	1.1	0.6	0.7	0.7	0.7	1.1	0.7	0.8	0.4	0.8	0.5	2.0
FeO	5.8	6.1	6.2	6.3	7.2	8.8	6.9	6.6	6.0	6.7	6.3	8.6	9.1	6.3	10.6	10.5
MnO	0.2	0.3	0.2	0.2	0.4	0.3	0.2	0.3	0.1	0.2	0.1	0.4	0.4	0.3	0.5	0.6
MgO	20.9	21.1	21.3	21.2	21.2	21.4	21.2	21.1	20.6	20.5	20.7	20.7	20.7	20.6	21.3	20.2
CaO	11.9	11.7	11.9	11.9	11.1	9.3	11.8	11.4	12.1	11.8	12.1	9.8	9.3	12.4	8.2	7.6
Na_2O	0.1	0.2	0.1	0.2	0.1	0.1	0.1	0.1	0.1	0.1	0.1	0.1	0.0	0.1	0.1	0.3
K_2O	0.0	0.0	0.0	0.0	0.0	0.0	0.0	0.0	0.0	0.0	0.0	0.0	0.0	0.0	0.0	0.0
Ba	-	-	-	-	-	-	-	-	-	-	-	-	-	-	-	-
Cr_2O_3	0.2	0.0	0.0	0.0	0.1	0.1	0.0	0.2	0.0	0.1	0.0	0.0	0.3	0.0	0.0	0.0
Ni	0.1	0.2	0.0	0.0	0.0	0.0	0.0	0.1	0.0	0.2	0.1	0.0	0.0	0.0	0.2	0.1
Sr	0.0	0.0	0.0	0.0	0.0	0.0	0.0	0.0	0.0	0.0	0.0	0.0	0.0	0.0	0.0	0.0
Tot	96.9	97.6	97.7	97.7	98.1	97.4	98.1	97.6	96.1	97.5	96.4	96.8	96.4	97.3	97.7	96.6

	R7_189,20 (peridotite/amphibole)							
	Grain 6A	**Grain 6B**	**Grain 6C**	**Grain 7A**	**Grain 7B**	**Grain 7**	**Grain 8**	**Grain 8**
SiO_2	**56.5**	**57.1**	**55.3**	**57.9**	**58.1**	**57.9**	**55.3**	**57.8**
TiO_2	**0.0**	**0.0**	**0.3**	**0.0**	**0.0**	**0.1**	**0.3**	**0.0**
Al_2O_3	**0.1**	**0.6**	**2.4**	**0.1**	**0.1**	**0.1**	**2.1**	**0.0**
FeO	**6.8**	**4.2**	**5.0**	**2.9**	**4.7**	**3.5**	**4.3**	**6.7**
MnO	**0.5**	**0.0**	**0.1**	**0.2**	**0.1**	**0.3**	**0.0**	**0.3**
MgO	**24.0**	**23.0**	**22.5**	**23.8**	**24.1**	**23.6**	**22.3**	**24.8**
CaO	**7.7**	**11.2**	**11.0**	**11.4**	**10.0**	**11.0**	**11.2**	**7.7**
Na_2O	**0.0**	**0.1**	**0.4**	**0.0**	**0.0**	**0.0**	**0.3**	**0.0**
K_2O	**0.0**	**0.1**	**0.0**	**0.0**	**0.1**	**0.1**	**0.0**	**0.0**
Ba	-	-	-	-	-	-	-	-
Cr_2O_3	**0.0**	**0.2**	**0.2**	**0.0**	**0.0**	**0.2**	**0.3**	**0.0**
Ni	**0.1**	**0.0**	**0.1**	**0.2**	**0.0**	**0.0**	**0.0**	**0.1**
Sr	**0.0**	**0.0**	**0.0**	**0.0**	**0.0**	**0.0**	**0.0**	**0.0**
Tot	**0.0**	**0.0**	**0.0**	**0.0**	**0.0**	**0.0**	**0.0**	**0.0**

12.6 U-Pb Isotope Geochemistry

12.6.1 A2427

	ppm			Ratios								Discordance		Ages								
Name	U	^{206}Pb	$^{206}Pb_c$(%)	206/204	$^{207}Pb/^{206}Pb$	1SE	$^{207}Pb/^{235}U^*$	1SE	$^{206}Pb/^{238}U^*$	1SE	Rho	Central (%	Minimum rim (%)	207/206	1s	207/235	1s	206/238	1s	from	to	Time
A2427-1	42	33.2	0.00E+00	34119	0.21359	0.00343	14.246	0.78418	0.48374	0.02547	0.956	-16	-12	2933	25	2766	52	2544	111	49	67	34
A2427-2	30	23	0.00E+00	41946	0.20422	0.0032	13.3678	0.74395	0.47475	0.02535	0.960	-15	-11	2860	24	2706	53	2504	111	44	63	38
A2427-3	31	23.5	0.00E+00	35388	0.20416	0.00302	13.1633	0.61144	0.46763	0.02059	0.948	-16.2	-12.5	2860	22	2691	44	2473	90	34	63	43
A2427-4	24	20.5	0.00E+00	39032	0.20486	0.00307	14.7979	0.79365	0.5239	0.02698	0.96	-6.4	-2.2	2865	23	2802	51	2716	114	41	63	48
A2427-5	28	23	0.00E+00	6112	0.20303	0.00301	14.3409	0.69401	0.51229	0.0236	0.952	-7.9	-3.8	2851	24	2773	46	2666	101	34	63	51
A2427-6	20	17	0.00E+00	18242	0.20044	0.00307	14.4077	0.70515	0.52134	0.02423	0.95	-5.4	-1	2830	25	2777	46	2705	103	34	63	52
A2427-7	81	62.9	0.00E+00	45729	0.1979	0.00277	13.1722	0.62324	0.48272	0.02182	0.955	-11.6	-7.8	2809	22	2692	45	2539	95	34	63	53
A2427-9	30	28.6	0.00E+00	55362	0.20437	0.00337	16.7035	0.89037	0.59277	0.03005	0.951	6.1	.	2861	26	2918	51	3001	122	34	63	58
A2427-10	94	73.2	0.00E+00	38492	0.1922	0.00277	13.0532	0.61993	0.49255	0.02229	0.953	-7.9	-3.8	2761	23	2684	45	2582	96	34	63	60
A2427-11	44	34.8	0.00E+00	26534	0.20901	0.00314	14.3581	0.73684	0.49823	0.02445	0.956	-12.2	-8.3	2898	24	2774	49	2606	105	37	68	61
A2427-12	42	32.4	0.00E+00	16840	0.19541	0.00316	13.2052	0.6222	0.49012	0.02169	0.939	-9.4	-5	2788	26	2694	44	2571	94	34	63	62
A2427-13	36	28.1	0.00E+00	23188	0.20779	0.00325	14.319	0.68665	0.49979	0.02265	0.945	-11.6	-7.4	2888	24	2771	46	2613	97	34	63	84
A2427-14	39	31	0.00E+00	62726	0.20416	0.00312	14.4811	0.68169	0.51444	0.02291	0.946	-7.9	-3.6	2860	23	2782	45	2676	98	34	63	85
A2427-15	42	33.5	0.00E+00	39027	0.20793	0.00335	14.6584	0.70005	0.5113	0.02298	0.941	-9.6	-5.2	2889	25	2793	45	2662	98	34	63	88
A2427-16	29	22.5	0.00E+00	23751	0.20439	0.00311	14.2541	0.67262	0.50581	0.0226	0.947	-9.5	-5.3	2862	23	2767	45	2639	97	34	63	89
A2427-17	29	22.5	0.00E+00	28122	0.20973	0.00429	15.2155	0.77592	0.52616	0.02458	0.916	-7.5	-1.9	2903	33	2829	49	2725	104	32	49	91
A2427-18	33	28.3	0.00E+00	7633	0.20539	0.00315	15.4352	0.74337	0.54504	0.02488	0.948	-2.8	.	2870	24	2842	46	2805	104	34	63	92
A2427-19	26	21	0.00E+00	24276	0.21556	0.00327	15.9132	0.75768	0.53541	0.02417	0.948	-7.7	-3.5	2948	24	2872	45	2764	101	29	62	96
A2427-20	38	27.9	0.00E+00	20053	0.20519	0.00316	13.7194	0.61814	0.48493	0.02053	0.940	-13.5	-9.4	2868	24	2731	43	2549	89	34	63	97
A2427-21	36	27.4	0.00E+00	44027	0.20234	0.00316	13.9431	0.6498	0.49979	0.02195	0.942	-9.9	-5.7	2845	25	2746	44	2613	94	34	63	99
A2427-22	51	35.3	0.00E+00	61356	0.18344	0.0029	11.6048	0.51557	0.45883	0.01905	0.935	-11.2	-6.8	2684	25	2573	42	2434	84	34	63	100
A2427-23	37	28.5	0.00E+00	37576	0.20582	0.00365	14.7248	0.68549	0.51887	0.02234	0.925	-7.6	-2.7	2873	28	2798	44	2694	95	34	63	124
A2427-24	48	34.2	0.00E+00	71234	0.19554	0.00278	12.8797	0.56079	0.47771	0.01966	0.945	-11.8	-7.9	2789	23	2671	41	2517	86	34	63	125
A2427-25	35	28.5	0.00E+00	52161	0.20365	0.00309	15.3572	0.71747	0.54693	0.02416	0.946	-1.9	.	2856	25	2838	45	2812	101	34	63	127
A2427-26	26	16.7	0.00E+00	38117	0.19514	0.00348	11.8269	0.51367	0.43956	0.01741	0.912	-18.7	-14.3	2786	28	2591	41	2349	78	34	63	129
A2427-27	55	29	0.00E+00	37970	0.21962	0.00443	11.062	0.49075	0.36532	0.01443	0.891	-37.8	-34.2	2978	31	2528	41	2007	68	34	63	130
A2427-8N	153	114.3	0.00E+00	144103	0.18037	0.0024	11.6932	0.53134	0.47018	0.02043	0.956	-7.8	-4	2656	21	2580	43	2484	90	34	63	57

	Internal precision (percent standard error from counting statistics only)						Relative error on regression line (%)			Tera-Wasserburg output for 3D regression						Signal (volts)				Observed correlation coefficient for raw data
Name	U	^{206}Pb	206/204	$^{207}Pb/^{206}Pb$	$^{207}Pb/^{235}U$	$^{206}Pb/^{238}U$*	$^{207}Pb/^{206}Pb$	$^{207}Pb/^{235}U$	$^{206}Pb/^{238}U$*	$^{238}U/^{206}Pb$	1s	$^{207}Pb/^{206}Pb$	1s	$^{204}Pb/^{206}Pb$	1s	204	206	207	238	
A2427-1	1.1	23.66	32.96	1.13	0.95	0.84	0.49	1.49	2.01	2.067	0.109	0.21359	0.00343	2.9E-05	9.7E-06	84.6643	103555	22298.3	169180	0.239
A2427-2	0.85	29.18	20.33	1.05	1.11	1.04	0.53	1.63	2.1	2.106	0.112	0.20422	0.0032	2.4E-05	4.8E-06	45.4865	74601.8	15327.4	126040	0.521
A2427-3	0.76	24.48	19.9	0.75	0.71	0.61	0.6	1.43	1.86	2.138	0.094	0.20416	0.00302	2.8E-05	5.6E-06	44.9653	79229.5	16225.4	138302	0.355
A2427-4	1.26	26.45	18.24	0.91	0.86	1.09	0.56	1.36	1.81	1.909	0.098	0.20486	0.00307	2.6E-05	4.7E-06	36.5081	67551.2	13943.4	103835	0.623
A2427-5	2.82	12.5	61.25	0.76	0.85	0.64	0.61	1.32	1.7	1.952	0.09	0.20303	0.00301	0.00016	0.0001	163.526	77696.3	15824.3	123722	0.498
A2427-6	0.74	20.63	26.17	0.86	0.81	0.61	0.62	1.31	1.67	1.918	0.089	0.20044	0.00307	5.5E-05	1.4E-05	80.0652	57593.4	11583.3	89818.3	0.277
A2427-7	1.54	15.65	35.26	0.62	1.33	1.18	0.62	1.43	1.8	2.072	0.094	0.1979	0.00277	2.2E-05	7.7E-06	142.225	212639	42244.4	360586	0.881
A2427-9	1.61	27.1	15.98	1.03	0.96	0.83	0.6	1.13	1.47	1.687	0.086	0.20437	0.00337	1.8E-05	2.9E-06	52.2526	96743	19846.9	131197	0.334
A2427-10	1.71	17.29	39.04	0.73	1.5	1.14	0.64	1.45	1.77	2.03	0.092	0.1922	0.00277	2.6E-05	1E-05	150.158	247372	47693.4	415861	0.885
A2427-11	2.41	17.95	30.7	0.93	1.48	1.5	0.52	1.41	1.79	2.007	0.098	0.20901	0.00314	3.8E-05	1.2E-05	106.391	113652	23910.1	188749	0.809
A2427-12	2.07	20.39	36.12	1.02	0.86	0.66	0.63	1.43	1.78	2.04	0.09	0.19541	0.00316	5.9E-05	2.1E-05	114.038	109520	21530.4	185502	0.126
A2427-13	2.95	17.75	31.87	0.86	1.33	1.51	0.59	1.32	1.74	2.001	0.091	0.20779	0.00325	4.3E-05	1.4E-05	105.569	94822.5	19800.7	162039	0.822
A2427-14	2.22	26.43	19.22	0.81	1.01	0.79	0.6	1.3	1.69	1.944	0.087	0.20416	0.00312	1.6E-05	3.1E-06	60.1573	104724	21438.2	171457	0.615
A2427-15	2.25	17.86	25.11	0.94	1.31	1.2	0.59	1.29	1.7	1.956	0.088	0.20793	0.00335	2.6E-05	6.4E-06	79.4531	113087	23608.5	188258	0.729
A2427-16	2.28	21.27	26.46	0.79	1.42	1.21	0.6	1.32	1.72	1.977	0.088	0.20439	0.00311	4.2E-05	1.1E-05	67.979	76041.4	15579.5	128286	0.848
A2427-17	1.34	30.51	31.79	1.28	1.45	0.87	0.69	1.34	1.67	1.901	0.089	0.20973	0.00429	3.6E-05	1.1E-05	63.1301	81003.3	16995.7	132626	0.472
A2427-18	1.09	15.03	53.57	0.81	0.9	0.7	0.6	1.22	1.6	1.835	0.084	0.20539	0.00315	0.00013	7E-05	130.234	95557.6	19678.4	147818	0.511
A2427-19	1.25	18.67	24.11	0.87	1.03	0.8	0.53	1.22	1.63	1.868	0.084	0.21556	0.00327	4.1E-05	9.9E-06	79.8889	72430.1	15665.5	115904	0.575
A2427-20	0.47	17.5	35.09	0.82	0.87	0.62	0.6	1.38	1.79	2.062	0.087	0.20519	0.00316	0.00005	1.8E-05	144.677	94327.7	19406.7	166913	0.446
A2427-21	3.47	25.63	20.26	0.86	1.38	1.19	0.61	1.35	1.74	2.001	0.088	0.20234	0.00316	2.3E-05	4.6E-06	58.4492	92485.9	18753.7	160019	0.789
A2427-22	2.35	28.72	17.82	0.97	0.97	0.93	0.67	1.63	1.9	2.179	0.091	0.18344	0.0029	1.6E-05	2.9E-06	48.0925	119137	21945.8	225367	0.485
A2427-23	1.3	27.07	22.57	1.16	1.09	0.76	0.6	1.28	1.68	1.927	0.083	0.20582	0.00365	2.7E-05	6E-06	67.1922	96122.5	19855.9	162212	0.247
A2427-24	1.59	25.25	14.67	0.58	0.73	0.71	0.63	1.47	1.82	2.093	0.086	0.19554	0.00278	1.4E-05	2.1E-06	34.1063	115489	22665.2	213851	0.683
A2427-25	0.58	28.69	16.71	0.74	0.6	0.72	0.61	1.23	1.59	1.828	0.081	0.20365	0.00309	1.9E-05	3.2E-06	60.1116	96154.8	19643.2	153316	0.396
A2427-26	1.5	31.35	12.96	1.21	1.08	0.76	0.63	1.6	1.98	2.275	0.09	0.19514	0.00348	2.6E-05	3.4E-06	36.2517	56487.3	11069.9	114677	0.215
A2427-27	1.09	24.73	22.18	1.46	2.96	1.66	0.56	1.71	2.38	2.737	0.108	0.21962	0.00443	2.6E-05	5.8E-06	105.939	98001.7	21588	243531	0.88
A2427-8M	2.14	22.65	23.64	0.58	0.6	0.63	0.68	1.61	1.85	2.127	0.092	0.18037	0.0024	7E-06	1.6E-06	96.6767	386233	70011.8	681019	0.574

12.6.2 A2444

	ppm			Ratios								Discordance			Ages				
Name	U	^{206}Pb	$^{206}Pb_c$(%)	206/204	$^{207}Pb/^{206}Pb$	1SE	$^{207}Pb/^{235}U^*$	1SE	$^{206}Pb/^{238}U^*$	1SE	Rho	Central (%	Minimum rim (%)		207/206	1s	207/235	1s	Th/U
A2444-3	2.39	300	300	324	0.2036	0.0006	16.7956	0.2480	0.5984	0.0087	0.98	103	2855	5	2923	14	3023	35	0.93
A2444-6	0.34	69	134	76	0.2028	0.0006	16.4758	0.2437	0.5893	0.0086	0.98	104	2849	5	2905	14	2987	35	1.77
A2444-1	1.00	45	90	52	0.2024	0.0006	14.1177	0.2092	0.5058	0.0074	0.98	92	2846	5	2758	14	2639	31	1.73
A2444-10	0.03	7	7	12	0.2024	0.0010	12.5366	0.1910	0.4492	0.0066	0.95	84	2846	8	2645	14	2392	29	0.54
A2444-16	0.00	156	391	135	0.2023	0.0005	16.9987	0.2505	0.6094	0.0089	0.98	108	2845	4	2935	14	3068	35	2.89
A2444-4	0.11	215	650	203	0.2014	0.0005	15.2744	0.2247	0.5502	0.0080	0.98	99	2837	4	2833	14	2826	33	3.21
A2444-22	0.56	60	71	72	0.2008	0.0007	16.5105	0.2458	0.5962	0.0087	0.97	106	2833	6	2907	14	3015	35	0.99
A2444-7	0.95	32	34	41	0.2007	0.0006	15.6426	0.2318	0.5652	0.0082	0.98	101	2832	5	2855	14	2888	34	0.84
A2444-15	0.00	171	446	170	0.2006	0.0005	15.9865	0.2357	0.5780	0.0084	0.98	104	2831	4	2876	14	2940	34	2.63
A2444-13b	0.21	116	215	126	0.2004	0.0005	16.3948	0.2416	0.5935	0.0086	0.98	106	2829	4	2900	14	3003	35	1.71
A2444-19	0.00	113	102	169	0.1992	0.0005	15.3517	0.2262	0.5589	0.0081	0.98	102	2820	4	2837	14	2862	34	0.60
A2444-5	0.21	104	139	131	0.1990	0.0005	16.0843	0.2369	0.5861	0.0085	0.98	105	2818	4	2882	14	2974	35	1.06
A2444-12	0.83	73	99	98	0.1972	0.0006	14.3859	0.2125	0.5290	0.0077	0.98	97	2803	5	2775	14	2737	32	1.01
A2444-24	0.38	127	176	166	0.1969	0.0005	15.6819	0.2312	0.5776	0.0084	0.98	104	2801	4	2858	14	2939	34	1.06
A2444-26	0.80	80	144	93	0.1967	0.0007	15.6479	0.2325	0.5769	0.0084	0.97	104	2799	5	2856	14	2936	34	1.55
A2444-23	0.34	52	82	70	0.1938	0.0006	14.0150	0.2083	0.5244	0.0076	0.97	97	2775	5	2751	14	2718	32	1.17
A2444-20	1.12	241	1055	202	0.1931	0.0006	14.1751	0.2102	0.5323	0.0078	0.98	98	2769	5	2761	14	2751	33	5.23
A2444-13a	0.89	247	772	234	0.1931	0.0005	14.3673	0.2116	0.5396	0.0078	0.98	99	2769	4	2774	14	2782	33	3.31
A2444-2	0.00	58	71	84	0.1926	0.0006	14.1141	0.2088	0.5316	0.0077	0.98	99	2764	5	2757	14	2748	33	0.85
A2444-21	0.29	187	193	292	0.1901	0.0005	13.2810	0.1961	0.5068	0.0074	0.98	96	2743	5	2700	14	2643	31	0.66
A2444-9	0.13	363	572	437	0.1891	0.0005	15.8666	0.2333	0.6086	0.0088	0.99	112	2734	4	2869	14	3064	35	1.31
A2444-11	0.60	346	762	476	0.1865	0.0005	13.1438	0.1943	0.5111	0.0074	0.98	97	2712	5	2690	14	2661	32	1.60
A2444-14	0.20	219	275	332	0.1862	0.0005	13.6355	0.2007	0.5312	0.0077	0.98	101	2708	4	2725	14	2747	32	0.83
A2444-25	0.75	162	185	212	0.1860	0.0005	15.4156	0.2271	0.6011	0.0087	0.98	111	2707	4	2841	14	3034	35	0.88
A2444-18	0.15	208	242	352	0.1768	0.0005	12.4696	0.1836	0.5114	0.0074	0.98	101	2623	4	2640	14	2663	32	0.69
A2444-8	0.33	274	579	419	0.1746	0.0004	13.1097	0.1928	0.5446	0.0079	0.99	107	2602	4	2688	14	2803	33	1.38
A2444-17	0.23	292	347	434	0.1675	0.0005	12.5968	0.1857	0.5454	0.0079	0.98	110	2533	5	2650	14	2806	33	0.80

12.6.3 A2427 Monazites

	ppm			Ratios								Discordance			Ages				
Name	U	^{206}Pb	$^{206}Pb_c$(%)	206/204	$^{207}Pb/^{206}Pb$	1SE	$^{207}Pb/^{235}U^*$	1SE	$^{206}Pb/^{238}U^*$	1SE	Rho	Central (%	Minimum rim (%)		207/206	1s	207/235	1s	Th/U
A2427Zr-1	0.02	141	910	31	0.2086	0.0011	14.9302	0.2159	0.5192	0.0072	0.93	93	2894	9	2811	14	2696	31	29.12
A2427Zr-19	0.03	337	2473	20	0.2085	0.0013	15.8179	0.2349	0.5504	0.0077	0.90	98	2894	10	2866	14	2827	32	121.51
A2427Zr-13	0.02	127	796	31	0.2073	0.0012	13.8952	0.2024	0.4861	0.0068	0.92	89	2885	9	2743	14	2554	29	25.55
A2427Zr-11	0.02	428	2935	30	0.2069	0.0011	15.4823	0.2241	0.5427	0.0076	0.93	97	2882	9	2845	14	2795	32	96.44
A2427Zr-4	0.03	297	2111	19	0.2063	0.0013	15.2174	0.2262	0.5350	0.0075	0.90	96	2877	10	2829	14	2762	32	109.68
A2427Zr-17	0.02	93	634	25	0.2058	0.0012	14.9224	0.2193	0.5258	0.0074	0.91	95	2873	10	2810	14	2724	31	25.23
A2427Zr-23	0.02	140	975	28	0.2051	0.0012	15.1889	0.2227	0.5370	0.0075	0.92	97	2868	10	2827	14	2771	31	34.47
A2427Zr-2	0.02	127	848	26	0.2048	0.0012	13.2901	0.1951	0.4706	0.0066	0.91	87	2865	10	2700	14	2486	29	32.74
A2427Zr-14	0.02	139	858	33	0.2046	0.0011	14.3216	0.2077	0.5077	0.0071	0.93	92	2863	9	2771	14	2647	30	25.82
A2427Zr-15	0.02	102	634	30	0.2044	0.0011	15.2893	0.2223	0.5424	0.0076	0.92	98	2862	9	2833	14	2794	32	21.12
A2427Zr-3	0.02	97	614	28	0.2035	0.0012	13.0674	0.1913	0.4658	0.0065	0.91	86	2854	10	2685	14	2465	29	22.22
A2427Zr-16	0.02	269	1963	25	0.2032	0.0013	14.0967	0.2080	0.5030	0.0070	0.91	92	2852	10	2756	14	2627	30	79.72
A2427Zr-25	0.02	137	970	30	0.2031	0.0012	15.1362	0.2214	0.5405	0.0075	0.92	98	2851	9	2824	14	2786	31	31.86
A2427Zr-9	0.02	130	795	27	0.2022	0.0011	16.8516	0.2446	0.6044	0.0084	0.93	107	2844	9	2926	14	3048	34	29.99
A2427Zr-21	0.02	79	502	32	0.2015	0.0012	13.8747	0.2024	0.4993	0.0070	0.92	92	2839	9	2741	14	2611	30	15.82
A2427Zr-27	2.03	153	1141	49	0.1995	0.0013	7.8232	0.1148	0.2845	0.0040	0.90	56	2822	11	2211	13	1614	20	23.21
A2427Zr-18	1.22	135	977	30	0.1959	0.0012	14.5770	0.2122	0.5397	0.0076	0.92	98	2792	10	2788	14	2782	32	32.99
A2427Zr-24	0.02	72	462	38	0.1958	0.0011	12.8488	0.1871	0.4758	0.0066	0.92	90	2792	9	2669	14	2509	29	12.08
A2427Zr-26	0.03	94	670	24	0.1948	0.0014	11.0769	0.1673	0.4124	0.0058	0.89	80	2783	11	2530	14	2226	26	27.86
A2427Zr-20	2.42	125	942	31	0.1910	0.0012	12.8712	0.1877	0.4888	0.0069	0.91	90	2751	10	2670	14	2566	30	30.41
A2427Zr-22	0.02	52	288	36	0.1899	0.0011	12.3290	0.1798	0.4708	0.0066	0.92	91	2742	9	2630	14	2487	29	8.05
A2427Zr-7	1.23	101	492	71	0.1887	0.0009	12.4043	0.1753	0.4767	0.0067	0.95	90	2731	8	2636	13	2513	29	6.88
A2427Zr-10	1.10	145	787	86	0.1867	0.0008	12.7289	0.1792	0.4945	0.0069	0.95	94	2713	7	2660	13	2590	30	9.17
A2427Zr-12	1.59	106	674	36	0.1864	0.0011	12.4052	0.1795	0.4827	0.0068	0.92	91	2710	9	2636	14	2539	29	18.96
A2427Zr-6	1.91	112	655	18	0.1845	0.0013	13.3113	0.1997	0.5233	0.0075	0.88	98	2694	12	2702	14	2713	32	37.02
A2427Zr-5	2.88	167	1101	24	0.1833	0.0012	12.5560	0.1846	0.4967	0.0071	0.89	93	2683	11	2647	14	2600	31	45.75

12.7 Sm-Nd Isotope Geochemistry

Sample	Location/min	Rock type	Sm (ppm)	Nd (ppm)	$^{147}Sm/^{144}Nd$ ± 0.4% 0.0040		$^{143}Nd/^{144}Nd$ 2se		T (Ma)	eps(T)	T-DM De Paolo (1981)
A2426	Kuohatti 1 Nurmes	Gabbro	4.92	20.58	0.1444	0.0006	0.511676	0.000030	2400	-2.7	3045
A2427	Kuohatti 2 Nurmes	Talc chlorite rock	14.44	36.36	0.2401	0.0010	0.513185	0.000030	2400	-2.8	